Geoarchaeological prospection with multi-coil electromagnetic induction sensors

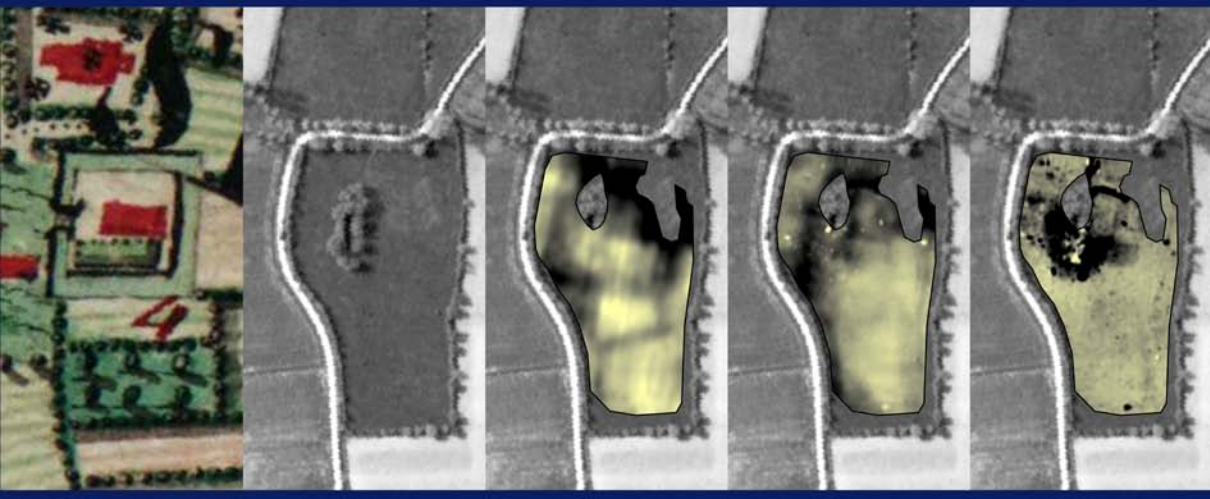

David Simpson

UNIVERSITEIT GENT

FACULTEIT BIO-INGENIEURSWETENSCHAPPEN

Promoter:	Prof. dr. ir. Marc Van Meirvenne Department of Soil Management, Faculty of Bioscience Engineering, Ghent University
Supervisor:	Prof. dr. Jean Bourgeois Department of Archaeology and Ancient History of Europe, Faculty of Arts and Philosophy, Ghent University
Dean:	Prof. dr. ir. Guido Van Huylenbroeck
Rector:	Prof. dr. Paul Van Cauwenberge

David Simpson

GEOARCHAEOLOGICAL PROSPECTION WITH MULTI-COIL ELECTROMAGNETIC INDUCTION SENSORS

Thesis submitted in fulfillment of the requirements
for the degree of Doctor (PhD) in Applied Biological Sciences:
Land and Forestry Management

Dutch translation of the title:

GEOARCHEOLOGISCHE PROSPECTIE DOOR ELEKTROMAGNETISCHE INDUCTIESENSOREN MET MEERDVOUDIGE SPOELEN

Illustrations on the cover:
The abandoned village of Sint-Rijkers, close to Alveringem (West-Flanders, Belgium). From left to right: (a) map of Ferraris (1771-1778), showing a square ditch surrounding a house with a garden, probably inhabitated by the priest of the village church at the other side of the road; (b) aerial photograph taken during World War II (the 9th of May, 1944; copyright: Keele University); (c) altitude map interpolated from GPS positions; (d) sensor map of the soil electrical conductivity and (e) of the soil magnetic susceptibility (see Chapter 7).

Citation:
Simpson D 2009. Geoarchaeological prospection with multi-coil electromagnetic induction sensors, PhD thesis, Ghent University.

ISBN-number: 978-90-5989-344-3

Dankwoord

Met voldoening kijk ik terug op de voorbije vier jaren. Dit heb ik in de eerste plaats te danken aan mijn promotor Marc, die me zowel de vrijheid heeft gegeven als de nodige begeleiding om dit doctoraat tot een goed einde te brengen. Ik denk dat weinig doctoraatsstudenten de luxe hadden zoals ik om op eender welk moment advies te kunnen vragen bij hun promotor. Op de tweede, eervolle plaats staat Jean, die ondanks zijn drukke agenda toch tijd wist vrij te maken, vooral nadat ik ontdekte dat bellen op zijn GSM veel effectiever was dan het sturen van een e-mail!

Erika, despite the fact you were not officially a promoter of my PhD, I think you surely played this role. I felt immediately welcome in Potsdam, also thanks to your colleagues Robin, Jörg, Ute and Marko.

Een grote luxe voor mijn werk was de constante beschikbaarheid van bekwame technische ondersteuning, door opeenvolgend Mike, Hans en Valentijn. Met hen heb ik soms zware dagen op het veld beleefd, maar door de goede sfeer verliep alles toch vlot. Ook op de vakgroep was er een aangename sfeer dankzij de (ex-)collega's van ORBit: Maarten, Liesbet, Sam, Meklit, Udaya, Timothy, Islam, Gonzalo en Karl en dankzij de andere collega's van de vakgroep. Ik denk dat we er in geslaagd zijn een goede samenwerking te hebben in plaats van interne concurrentie, ondanks de A1-druk.

De archeologen van de Blandijnberg moeten zeker niet onderdoen voor de bodemkundigen, wat betreft de goede sfeer en samenwerking. Enkele mensen in het bijzonder hebben me goed geholpen: Lieven met de sensorvergelijkingen en de interessante geofysische discussies; Jacky, Birger en Wouter met hun luchtfoto-expertise.

Alexander en Harry, het duo van ter Duinen, ben ik zeer dankbaar voor hun geloof dat geofysische technieken een belangrijke bijdrage kunnen leveren voor archeologisch onderzoek. Zonder Alexander was het veldwerk zeker trager van start gegaan en was ik nooit in Zeeuws-

Vlaanderen verzeild geraakt. Nog andere “gelovigen” wens ik te danken: de mensen van de VLM-West Vlaanderen, het VIOE-Maritiem Erfgoed en de Hogeschool Gent-BIOT.

Enkele personen hebben me geholpen om essentiële vragen in verband met o.a. elektromagnetische inductie en bodemkunde te beantwoorden: Alain Tabbagh, Roger Langohr, Jurgen de Zaeytijd, Scott Holladay en Mike Catalano. Een andere groep ben ik erkentelijk voor de toegang te verlenen tot hun eigendom en interesse te tonen voor het onderzoek: de landbouwers van de vele percelen die we opgemeten hebben.

Naast het werk wens ik ook enkele mensen te bedanken die gezorgd hebben voor de nodige ondersteuning en ontspanning. De land- en bossers voor de leuke studententijd en de moeite om regelmatig eens samen te komen. Het Outland Rafting Team zal ik niet vergeten omwille van o.a. het ijsbrekervaren, de slalomkoers en allerhande verfrissingen. Doe zo voort gasten en tot de volgende! Natuurlijk kan ik ook de Antwerpse collegemoate niet vergeten, die ondertussen al uitgebreid zijn met Nieuwkerkse inwijkelingen. Dankzij hen ben ik mijn puberjaren (en daarna) veilig doorgekomen. Dan zijn er nog enkele vrienden die ondanks de uitdrukking uit het oog uit het hart, er toch nog in slagen om contact te houden: Nina en Stan, nog veel genot van de Zweedse bossen; Alexander, Michiel, Niels en Pieter.

Ik prijs me zeer gelukkig met mijn familie, waarmee ik met de jaren een steeds sterkere band heb. Ma en pa, bedankt voor de jarenlange zorgen en voor de gezellige tijd samen (en pa ook voor de thesistekst na te kijken). Olijfje, bedankt voor je bezorgdheid en de leuke (sport-) activiteiten. Nicky, merci voor de ontgroening en de gratis consultancy. Hilde en Katleen, ik ben zeer blij dat jullie ook deel van het gezin zijn. Também agradeço à minha familia de Portugal, por ter aceitado de braços abertos um estrangeiro em casa.

Door een bovennatuurlijk toeval is Bona in mijn leven gekomen, die me elke dag verrast en waarnaar ik elke dag uitkijk. Dank je voor de vier jaren in België en voor het uitzicht op een warme toekomst!

Table of contents

Samenvatting

Archeologische prospectie heeft tot doel de archeologisch waardevolle resten van een site in te schatten, om vervolgens de inhoud te kunnen onderzoeken, te beschermen of te bewaren. Geoarcheologie past technieken toe uit de aardwetenschappen om het paleomilieu van een archeologische site beter te vatten en extra informatie te verschaffen via ecofacts (vb. graankorrels, pollen). Geofysische methoden, voornamelijk ontwikkeld in de aardwetenschappen, werden al in het begin van de 20ste eeuw toegepast voor archeologische prospectie. Daarbij worden bodemsensors gebruikt die bepaalde fysische eigenschappen van de bodem meten zoals de elektrische geleidbaarheid. Deze fysische eigenschappen worden beïnvloed door bodemkarakteristieken zoals het kleigehalte en het vochtgehalte, waardoor deze sensors in staat zijn de natuurlijke bodemvariabiliteit in kaart te brengen. Archeologische sporen kunnen een verandering veroorzaken van deze natuurlijke achtergrondwaarden, wat zichtbaar is als een lokale anomalie.

De drie meest gebruikte sensortypes in archeologische prospectie zijn de magnetometer, de elektrische weerstandssensor en de bodemradar. Elektromagnetische inductie, gebruik makend van laagfrequente elektromagnetische golven opgewekt door spoelen, is minder vaak toegepast ondanks de voordelen die deze methode biedt. Het belangrijkste voordeel is de simultane meting van twee fysische eigenschappen, de elektrische geleidbaarheid en de magnetische susceptibiliteit. Een bijkomend voordeel van dit sensortype is dat geen contact met het bodemoppervlak vereist is wat metingen over ruwe bodemoppervlakken vergemakkelijkt.

Sommige studies tonen zwakke resultaten van elektromagnetische inductieprospecties, maar zonder een duidelijke oorzaak te geven. In de meeste gevallen wordt de sensor niet met zijn volledig potentieel gebruikt, waardoor algemene conclusies worden getrokken die niet volledig juist zijn. De gevoeligheid van zowel de geleidbaarheid- als de susceptibiliteitmeting zijn sterk afhankelijk van de sensorhoogte boven het bo-

demoppervlak, de afstand tussen de sensorspoelen en de oriëntatie van de sensorspoelen. In de voorbije jaren werden sensors uitgebracht met meerdere spoelconfiguraties die een groter gevoeligheidsbereik hebben en daardoor ook een beter detectieniveau kunnen behalen dan sensors met één enkele spoelconfiguratie. Het doel van dit doctoraatsonderzoek was om het potentieel van deze elektromagnetische inductiesensors met meervoudige spoelconfiguraties te testen voor geoarcheologische prospectie.

Een gemotorizeerd sensorplatform werd ontwikkeld om grote oppervlaktes in een hoge resolutie te kunnen opmeten. Sledes zonder enig metaal werden ontworpen om de sensors te trekken achter een terreinvoertuig dat werd uitgerust met een differentiële GPS. Met behulp van een begeleidingssysteem gestuurd door de GPS, vooraan gemonteerd op het terreinvoertuig, kon op lijnen met een tussenafstand van 0.4 m gereden worden. Het effect van de rijsnelheid op de gegevenskwaliteit werd getest. De resultaten toonden een daling van de maximale uitwijking en een vergroting van de anomaliebreedte in de rijrichting. Daarom is het aangewezen om de rijsnelheid voldoende laag te houden (< 5 km h^{-1}) om het detectieniveau te vergroten wanneer gedetailleerde archeologische prospectiemetingen worden uitgevoerd.

Een ander belangrijk punt was de precisie van de meetposities. Tussen de GPS-antenne en de centrumlocatie van de sensor is een vaste afstand, die verdubbelt als de meting in twee rijrichtingen uitgevoerd wordt. Deze positiefout werd gecorrigeerd door elk punt een vaste afstand in de rijrichting op te schuiven. Ondanks dat elke elektromagnetische inductiesensor een interne elektronische temperatuurscompensatie bevat, vertoonden alle sensors in dit onderzoek drift van de meetwaarden in de tijd. Tijdsdrift kan dikwijls lokale anomalieën verdoezelen, vooral in langdurige prospecties. Een unieke procedure werd ontwikkeld om de drift te registreren en te corrigeren, gebruik makend van een kalibratielijn opgemeten voor de eigenlijke prospectie. De drift werd gemodelleerd met een functie bestaande uit meerdere derdegraad-polynomen. Het aantal polynoomfuncties werd door de gebruiker bepaald. Een volgende stap in de verwerking was het identificeren en verwijderen van lokale, extreme meetwaarden, meestal ten gevolge van metalen voorwerpen. Dit werd bewerkstelligd door binnen een lokaal venster metingen met een uitwijking boven een grenswaarde te elimineren. Ten slotte werd een procedure

getest om de onregelmatig verspreide gegevens te interpoleren naar een raster. Een lokaal krigingprogramma werd geschreven dat gebruikt maakt van een lineair variogrammodel, waarmee verscheidene sensormetingen kunnen geïnterpoleerd worden zonder het variogram handmatig te modelleren. Het grootste voordeel van kriging ten opzicht van bijvoorbeeld inverse afstandsweging was dat metingen dichtbij elkaar minder gewicht krijgen dan verspreide metingen. De keuze van het lineair variogram zonder een sill was verantwoord omdat de straal van het zoekvenster klein genoeg gekozen was zodat het variogram op de meeste locaties een lineair verloop heeft.

Om de respons van de verschillende spoelconfiguraties beter te begrijpen werd hun gevoeligheid getest voor een gelaagde bodem en voor kleine, driedimensionale structuren. Daarvoor werd een experimentele site ingericht met ingegraven structuren die archeologische resten nabootsten. De metingen op deze site toonden een goede overeenkomst met de theoretische gelaagde modellen, op basis van de lage inductienummerbenadering. Dus het was verantwoord om deze theoretische modellen toe te passen om de geleidbaarheid en susceptibiliteit van het bodemprofiel te reconstrueren. De spoeloriëntaties reageerden zeer verschillend ten aanzien van de kleine, driedimensionale structuren. Over het algemeen gaven de spoeloriëntaties met de ondiepste gevoeligheid de sterkste geleidbaarheidsanomalieën. Wat betreft de susceptibiliteitsmeting, hier bleken de spoelconfiguraties 1.1 m PERP, 2 m HCP en 2.1 m PERP een sterkere uitwijking te geven dan de andere configuraties. Maar de 2.1 m PERP toonde wel een complex anomaliepatroon met zowel positieve als negatieve uitwijkingen, met een veel grotere horizontale dimensie dan de structuren. De VCP-anomalieën waren iets minder sterk, maar waren zeer compact boven de magnetische structuren en geheel positief. De 1 m HCP anomalie was relatief zwak vergeleken met de andere spoelconfiguraties, waarschijnlijk doordat de respons van teken verandert op geringe diepte. Een verhoging van de sensor boven het bodemoppervlak had een algemene verlaging van de signaalsterkte tot gevolg.

De geleidbaarheidsrespons van de elektromagnetische inductiesensor werd vergeleken met elektrische weerstandsmetingen en de susceptibiliteitsrespons met magnetische gradiometermetingen. De susceptibiliteitsanomalieën kwamen goed overeen met de gradiometeranomalieën, maar de graad van overeenkomst was sterk afhankelijk van de spoelcon-

figuratie. De 1 m HCP, een veelgebruikte spoelconfiguratie in archeologische prospectie, was eigenlijk zeer zwak in vergelijking met de gradiometer. Dit kwam overeen met de resultaten van de gevoeligheidstesten. De magnetische gradiometer gaf sterke uitwijkingen en een scherp beeld van de anomalieën, maar was ook gecompliceerd door de typische bipolaire respons. De geleidbaarheidsmeting met elektromagnetische inductie was gevoeliger voor hoge geleidbaarheidsvariaties dan voor lage geleidbaarheidsintervallen, waar dit voor de elektrische weerstandsmeting juist omgekeerd is. Dit was voornamelijk te wijten aan het ruisniveau dat verschillend is bij de twee methoden. Daarnaast hadden ook de spoelconfiguraties en de electrodeconfiguraties een invloed op de gevoeligheid voor lokale geleidbaarheidsveranderingen. Een voordeel van de elektrische weerstandsmethode is dat er inversieprogramma's beschikbaar zijn, die tweedimensionale en zelfs driedimensionale structuren kunnen modelleren gebaseerd op oppervlaktemetingen. Voorlopig kunnen enkel ééndimensionale structuren zoals gelaagde bodems gemakkelijk gereconstrueerd worden met elektromagnetische inductiemetingen.

Verscheidene archeologische sites op verschillende locaties werden opgemeten met de elektromagnetische inductiesensor om hun potentieel te testen voor verschillende veldomstandigheden. Twee soorten sites werden gekozen: Middeleeuwse sites met duidelijke sporen zoals bakstenen funderingen, en Bronstijdsites met voornamelijk opgevulde grachten die moeilijker detecteerbaar zijn. De metingen op de Middeleeuwse sites toonden duidelijke, complementaire anomalieën van de geleidbaarheid en de susceptibiliteit. De Bronstijd grachten werden niet altijd goed gedetecteerd, en de detectie was sterk afhankelijk van de bodem waarin de grachten werden gegraven en de resterende omvang van de opgevulde grachten. Ze werden het duidelijkst gedetecteerd door de geleidbaarheidsmeting van spoelconfiguraties met een ondiepe gevoeligheid. De susceptibiliteitsmetingen gaven in de meeste gevallen vrijwel geen respons. Tot slot werd ook een procedure uitgetest om de sensoranomalieën te verifiëren met boorobservaties langsheen transecten. Deze methode bleek succesvol, op voorwaarde dat voldoende boringen werden geplaatst, waarvan de locatie geselecteerd werd op basis van de sensormetingen en uitgevoerd door een persoon die de sensoranomalieën begrijpt.

Om te besluiten toonde dit onderzoek duidelijk het potentieel aan van elektromagnetische inductiesensors met meerdere spoelconfiguraties

voor geoarcheologische prospectie. Maar voor een goed resultaat moet er meer aandacht besteedt worden aan de prospectiestrategie en de dataverwerking dan tot nu toe door de meeste uitvoerders wordt gedaan. In bepaalde situaties kan elektromagnetische inductie meer informatie bieden dan andere sensors dankzij de simultane meting van de geleidbaarheid en de susceptibiliteit en de metaalgevoeligheid, en ook dankzij de verschillende dieptegevoeligheid van de meerdere spoelconfiguraties.

Summary

Archaeological prospection aims at estimating the archaeologically valuable remains of a site, in order to investigate, preserve or conserve its contents. Geoarchaeology applies techniques that were mostly adopted from earth sciences, to understand better the paleoenvironmental context of an archaeological site and to provide additional evidence of human occupation in the form of ecofacts (e.g. grains, pollen). Geophysical exploration methods used in earth science were applied in archaeological prospection since the beginning of the 20th century. These methods use soil sensors, measuring physical properties of the earth such as the electrical conductivity. These physical properties are influenced by soil characteristics such as the clay content or the moisture content; therefore these sensors can actually map the natural soil variability of an area. Archaeological traces can cause a change in these natural background values, which is then visible as a local anomaly.

The three most common sensor types used in archaeological prospection are the magnetometer, the electrical resistivity sensor and ground-penetrating radar. Electromagnetic induction, using low frequency electromagnetic waves generated by coils, is less often used in spite of its apparent advantages. Its main advantage is the simultaneous measurement of two physical properties, the electrical conductivity and the magnetic susceptibility. A second advantage is the fact that it does not require any contact with the soil surface, facilitating the application of this sensor on rough terrain.

Some studies have indicated poor results from electromagnetic induction sensors, but it is often not clear why. In most case studies the full potential of these sensors is not used and general conclusions are drawn that are not entirely correct. The sensitivity of both the conductivity and the susceptibility measurement is strongly dependant on three aspects: the height of the sensor above the soil surface, the coil separation and the coil orientation. In recent years, multi-coil sensors have been developed that

are able to measure simultaneously multiple coil configurations. These instruments could offer a greater sensitivity range than previously developed single-coil sensors. The goal of this doctoral research was to evaluate the potential of these multi-coil electromagnetic induction sensors for geoarchaeological prospection.

A motorized sensor platform was developed to carry the electromagnetic induction sensor, allowing the measurement of large areas in high resolution. Custom-made, non-metallic sleds were designed to pull the sensors behind an all-terrain vehicle equipped with a differential GPS. With the aid of a lightbar guidance system linked to the GPS, it was possible to operate the platform at 0.4 m cross-line distance. The effect of the driving speed on the data quality was tested. The results indicate a decrease of the maximum value and a widening of the local anomalies in the driving direction for higher speeds. Therefore, the speed should remain low ($< 5\ \mathrm{km\ h^{-1}}$) to enhance the detection level of the sensor for detailed archaeological prospection.

Another important issue was the accuracy of the measurement positions. The spatial offset between the GPS antenna and the centre locations of the sensor was corrected using a fixed spatial shift in the direction of the survey line. Drift of the measurements in time can often obscure local anomalies, especially for long duration surveys. A unique procedure was developed to monitor and correct the drift, using a calibration line recorded before the actual survey starts. The drift was modelled best with a piecewise polynomial function, with a user-defined number of functions. Local extreme measurements, often caused by small metallic objects, can also disturb other, nearby anomalies. These extremes were removed using a user-defined threshold of deviation within a search window. The final step in the data processing was the interpolation of the irregularly spaced data to a grid. A local kriging program was written using a linear model, enabling the multiple sensors outputs to be interpolated without variogram modelling. The main advantage of the kriging algorithm over inverse distance weighting was the reduced weighting of clustered measurements. The choice of a linear model without a sill was justified because the chosen search radius was small enough, resulting in a variogram that was approximately linear at most locations.

In order to understand the response of the different coil configurations their sensitivity was tested for a layered soil and for small, three-

dimensional structures. For this purpose, an experimental site was constructed with self-made structures, simulating real archaeological remains. The field measurements corresponded well with the theoretical models based on the low-induction-number approximation for layered soils. This justified the use of layered models to reconstruct the soil profile conductivity and susceptibility. The coil configurations reacted very differently to the small, three-dimensional structures. In general, the coil configuration with a high sensitivity at shallow depths produced stronger conductivity anomalies. The coil configurations 1.1 m PERP, 2 m HCP and 2.1 m PERP produced a stronger susceptibility anomaly than the other configurations. The 2.1 m PERP, however, displayed a complex pattern of positive and negative susceptibility responses, which were also a lot larger than the size of the structures. The susceptibility anomalies of the VCP orientation were less strong, but were very compact and entirely positive to high magnetic structures. The susceptibility anomaly of the 1 m HCP configuration was surprisingly weak compared to the other configurations. This was attributed to the change in sign at a shallow depth. An increase of the sensor height above the soil surface resulted in a decrease of the signal-to-noise.

The next step was to compare the conductivity response with the electrical resistivity sensor measurements and the magnetic susceptibility with the magnetic gradiometer data. The magnetic susceptibility map of the electromagnetic induction sensor corresponded well with the magnetic gradiometer map, but this correspondence showed a large variation between the different coil configurations. The 1 m HCP configuration, often used in archaeological prospection, was actually very poor in comparison to the gradiometer; this was to be expected based on the sensitivity results. Although the magnetic gradiometer seemed to be very sensitive to small structures and produced crisp images, its anomalies were more complicated than some electromagnetic induction anomalies due to the typical bipolar response. The electrical conductivity measurements of the electromagnetic induction sensor were more sensitive to high conductivity variations than to low ones, while this was the opposite for electrical resistivity measurements. This was mainly due to the high noise level of the electromagnetic induction sensor in the low conductivity range. However, the detection of small conductivity changes also depended largely on the coil configuration, or electrode arrangement in the case of

the electrical resistivity method. An advantage of the electrical resistivity method is the availability of inversion programs that can model two-dimensional, and even three-dimensional, structures based on surface measurements. Until now, only simple, one-dimensional models can be inverted using electromagnetic induction measurements

Several archaeological sites at different locations were surveyed with the electromagnetic induction sensors to evaluate their potential in real site conditions. Two types of sites were selected: Medieval Age sites with clear structures such as brick foundations and Bronze Age sites with small ditches that are more difficult to detect. The Medieval sites showed clear, complementary anomalies of conductivity and susceptibility. The detection of the Bronze Age ditches was more difficult and dependant mostly on the soil type where the ditches were dug and the remaining size of the filled ditches. They were most clearly detected by a change in electrical conductivity for the coil configurations, which have a high sensitivity to shallow soil layers. The magnetic anomalies of the studied ditches were either very weak or nonexistent. Finally, a procedure was tested to see whether the sensor anomalies using soil auger observations on transects could be verified. This methodology proved successful, providing that a sufficient number of observations was taken, directed by the sensor maps and with a high qualitative interpretation by a person who understands the sensor anomalies.

To conclude, this research showed the potential of using electromagnetic induction sensors with multiple coil configurations for geoarchaeological prospection. However, in order to obtain good results, the survey strategy and the data processing requires more thought than most surveyors apply at present. In certain cases, electromagnetic induction sensors can offer more information than other sensors due to its simultaneous measurement of conductivity and susceptibility, due to its sensitivity to metal, and due to the different depth sensitivities of the multiple coil configurations.

List of figures

List of tables

List of abbreviations

ATV	all-terrain-vehicle
DEM	digital elevation model
ER	electrical resistivity, refers to the geophysical method
FDEM	frequency-domain electromagnetic induction
GIS	geographical information system
GPR	ground-penetrating radar
(d)GPS	(differential) global positioning system
HCP	horizontal coplanar (coil orientation)
IP	in-phase (frequency-domain response)
LIDAR	light detection and ranging
LIN	low induction number
NAP	normaal Amsterdams peil (Dutch)
PERP	perpendicular (coil orientation)
QP	quadrature-phase (frequency-domain response)
RTK	real time kinematic
SD	standard deviation
TAW	tweede algemene waterpassing (Dutch)
TDEM	time-domain electromagnetic induction
UXO	unexploded ordnance
VCP	vertical coplanar (coil orientation)

Chapter 1

Introduction

1.1 Geoarchaeological Prospection

1.1.1 Need for archaeological prospection

Archaeological investigation is a very important instrument in reconstructing the history of mankind. Apart from other evidence such as standing structures (e.g. the Pyramids of Egypt) or writings (e.g. the Bible), most of the facts gathered about history were discovered in the soil. Most people regard the soil as a garbage bin, where useless material can be stored that will eventually "disappear". This behaviour is advantagous for archaeologists because the rubble does not disintegrate immediately and, if read in the appropriate way, the soil layers act like the pages of a history book. The industrial and green revolutions initiated in the 19th Century, and the consequent dramatic population growth, led to an alarming increase of soil disturbance. Apart from the other problems this causes, such as the loss of food production or environmental functions, we risk loosing vital historical evidence forever. The destruction of archaeological evidence can be compared with burning down libraries. Especially in a country like Belgium, the risk of loss is higher due to the high population density and a high resource use per capita combined with a richness of archaeological evidence of practically all historical periods.

For these reasons, there is a great need to protect the archaeological evidence, in the first place by detecting its mere existence and secondly by preservation or conservation. The first step is known as archaeological prospection.

1.1.2 Archaeological prospection methods

The aim of archaeological prospection methods is to sample or scan a part of the soil volume in order to estimate quantitatively the archaeologi-

cal content of the total soil body, and to analyse or interpret this data qualitatively. The interpolation of samples to deduce the complete archaeological content of a site is inherently subject to uncertainties, which is dependent on the choice of method and nature of the site. Archaeological prospection sampling methods can be divided in two categories: one, where a direct view of the material is collected (e.g. pottery sherds on the soil surface or soil samples) and two, where indirect information is obtained (e.g. crop marks on aerial photographs or topographical maps). Direct methods have the advantage over indirect methods in that the interpretation of the material is uniquely determined but they have the disadvantage of being destructive.

A first direct sampling method is the collection of all artefacts lying on the surface of a site. The area can be entirely scanned or only for a certain percentage. Often a site is divided into, for example, 10 by 10 m blocks. When an artefact is discovered it is noted in which block it has been found. This provides a spatial distribution of artefacts over blocks, which can be subject to further quantitative and qualitative analyis. The sampled volume of soil is entirely covered in the horizontal plane but it is by definition restricted to the upper surface in the vertical direction. The time of the surface collection is very important, certainly on sites with agricultural management. After the winter, many archaeological remains are upheaved by frost and are thus more abundantly present at the soil surface. Ploughing can also lift objects to the surface. A second direct sampling method is core drilling (or augering), whereby a vertical core of soil is sampled at discrete positions in the horizontal plane. This method is more useful when the artefacts are expected at deeper layers, such as at paleolithic sites in alluvial plains. A third direct method is the opening of trenches with a mechnical digger, guided by an experienced archaeologist who analyses the trench for valuable remains. The trenches can be organised at fixed distances of for example 10 m or at specific locations based on other information. In Belgium, the custom is to open 10 % of the site. Although this method offers a good insight both in the horizontal plane and in depth, it is very destructive. A fourth method, which is situated in between core drilling and trenching is opening a pit of typically 1 by 1 by 1 m, which is comparable to a profile pit used in soil classification.

Apart from other techniques, such as map and landscape analysis, the two main indirect prospection methods are both remote sensing tech-

niques, which means that information about the soil volume is obtained from a distance using sensor technology. The first method is based on images (photographs or scans) of the soil surface captured from a platform above the earth (air balloon, airplane, satellite). Differences in soil material are often visible on these images as changes in crop vigour or soil colour. A second indirect method is geophysical prospection, where sensors on the soil surface detect physical properties of the soil such as the electrical conductivity, which can indicate the presence of anthropogenic material. Geophysical sensors were developed mostly for geological exploration (electrical resistivity for mining) or for military purposes (Fluxgate magnetometer for submarine detection, radar for airplane detection). They were adapted to investigate the shallow soil layer where the archaeological remains are located. Although the term “near-surface geophysics” is often used, this term also includes applications down to tens of meters deep. In this thesis, the term “soil sensing” is preferred, which focuses on the soil that is roughly 2 m deep, and which distinguishes it from airborne or satellite remote sensing. However, deeper geological layers are sometimes mapped with geophysical sensors in order to understand the paleolandscape.

1.1.3 Geoarchaeological prospection

Apart from looking just at artefacts, archaeologists are becoming more and more aware that the environment itself in which the artefacts are embedded contains valuable information. To capture this information, an array of techniques were adopted from geosciences, such as geochemical analysis and micromorphology, and applied in archaeological prospection so that a new discipline emerged called Geoarchaeology [1, 2]. In this discipline, for example, geological maps are used in combination with dating techniques for paleoenvironmental reconstruction. Archaeological prospection techniques that also focus on mapping the environment are categorized under geoarchaeological prospection. Soil sensing is a very useful, non-destructive method in the geoarchaeological prospection toolbox.

1.2 General objectives

1.2.1 Goal

Archaeological studies increasingly incorporate geophysical prospection in their strategy. A qualitative geophysical survey requires a thorough knowledge of the capabilities and limits of the available sensors. Although frequency-domain electromagnetic induction (FDEM) sensors have been used for decades in archaeological studies, questions still remain about their effectiveness to detect archaeological traces [3]. Also, the recent development of multi-coil instruments could improve the detection and interpretation of certain traces. Therefore, the general goal of this thesis was to evaluate the potential of multi-coil FDEM sensors for geoarchaeological prospection. Specifically, the following objectives were investigated.

1.2.2 Development of a sensor platform and processing software

Archaeological features are very small and located close to the soil surface compared to common targets in other geophysical applications, such as geological layers. A high number of data samples per unit area is required to capture the targets, but this increases the survey time. Often the surveyor has to compromise between the area covered and the sampling density. For geoarchaeological studies, larger areas than for common archaeological sites need to be covered in order to map the landscape setting. For this purpose, it was necessary to construct a sensor platform that was able to measure large areas (several hectares/day) in high resolution and with a high positioning accuracy.

The character of the measured anomalies, often weak and relatively small, requires special data handling. Issues such as spatial accuracy of the data positions and drift of the sensor values in time need to be controlled. The irregularly spaced measurements should be interpolated to a grid without loosing the detail of the small anomalies. Therefore, the first objective was to develop a sensor platform and write software to process the data.

1.2.3 Sensitivity testing of electrical conductivity and magnetic susceptibility measurements

In the past, the output of an FDEM sensor was often a single value of either apparent electrical conductivity (σ_a) or magnetic susceptibility (χ_a) in one coil configuration. New FDEM-instruments measure both properties simultaneously in multiple coil configurations. The extended range of output values increase the capabilities of the sensor but also complicate the interpretation of the measurements. Thus, there is a need to understand what the benefit of this extra output really is. To address this issue, it is important to know first the spatial sensitivity of the different configurations. Although the sensitivity of several coil configurations was evaluated by [4] with computer models, experimental field test were not conducted due to the lack of available sensors. Therefore, the second objective was to conduct field experiments over several structures with known properties, evaluating the sensitivity for both the electrical and magnetic response.

1.2.4 Comparison with other geophysical sensors

Case studies such as [5] revealed the strong correlation between the conductivity and susceptibility values measured with FDEM sensors on one hand and with ER sensors and magnetometers on the other hand. However, FDEM sensors can produce very different anomalies depending on which coil configuration is used. The degree of correspondence between FDEM-sensor maps and other geophysical maps is for this reason dependent on the position and nature of the archaeological structure and the spatial sensitivity of the coil configuration. The third objective of this doctoral research was to compare the measurements of several coil configurations of FDEM sensors with ER sensors and magnetometers.

1.2.5 Evaluation on archaeological sites

The nature of archaeological features varies between very small, weak differences in soil material such as postholes and large, unnatural soil material such as wall foundations. Over time, archaeological sites can be eroded or covered by sediments or degraded by physical, chemical or biological processes. The soil environment can also differ from heavy clay in former tidal areas to aeolian sand deposits. All these factors have an influence on the detection level of geophysical sensors. Thus, the fourth

objective was to evaluate the FDEM sensor on different archaeological sites with varying soil material and anthropogenic disturbances.

1.3 Overview of the thesis

The thesis is divided in nine chapters (Figure 1.1). The second chapter explains the principles of FDEM sensors, their spatial sensitivity and what physical properties they measure. The third chapter deals with (a) the adaptations necessary to conduct high definition measurements, (b) the control of time drift, (c) the removal of extreme values and (d) interpolation. Chapter 4 presents controlled field experiments with buried structures to test the sensitivity of the magnetic susceptibility response for different coil configurations. In chapter 5, the susceptibility response for two coil orientations was compared with magnetic gradiometer measurements on an existing archaeological site containing the remains of a late Medieval castle. Chapter 6 describes the electrical conductivity response for different coil configurations on known structures and compares it with electrical resistivity sensor measurements with varying electrode separations. This chapter describes also how the electrical conductivity responses were evaluated on two sites with circular ditches surrounding former Bronze Age burial mounds. In chapter 7, the full potential of multi-coil FDEM sensors was tested on the remains of a late Medieval house, using the maps to reconstruct the natural soil profile and to evaluate the complementarity of the maps. Chapter 8 presents a geoarchaeological case study, where the FDEM sensor maps were verified with soil auger observations. Finally, chapter 9 summarizes the thesis in general discussions and conclusions.

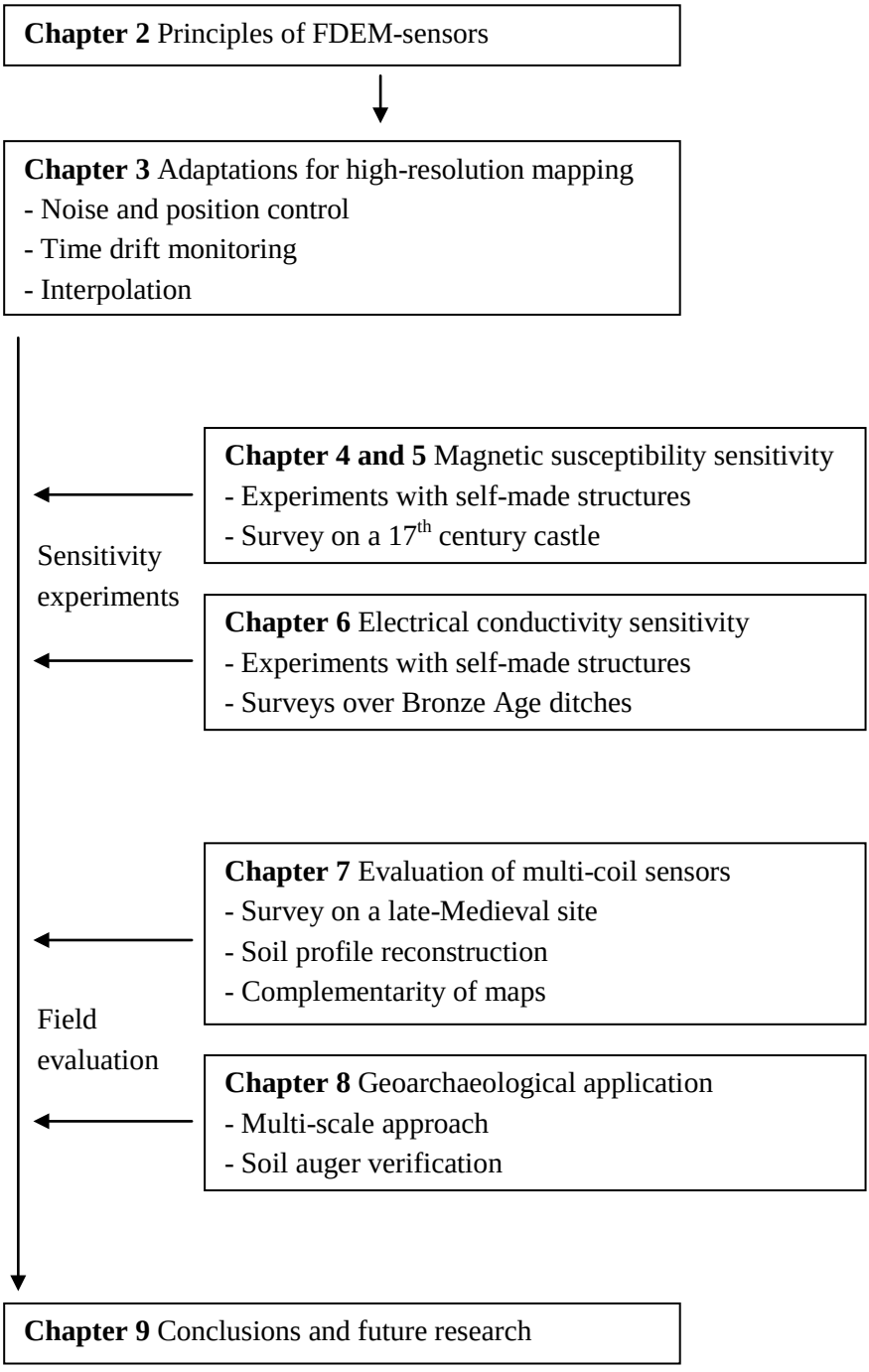

Figure 1.1 Schematic overview of the thesis.

Chapter 2

Principles of FDEM sensors

2.1 Electrical conductivity and magnetic susceptibility of soils and artefacts

2.1.1 Electrical conductivity

If a potential difference ΔV exists between the ends of a wire, causing a current with strength I to flow through it, then Ohm's Law states:

$$R = \frac{\Delta V}{I}. \tag{2.1}$$

R is the electrical resistance of the wire, which depends of its cross-sectional area A and its length l. The electrical resistivity ρ is independant of the dimensions of the material and is given by:

$$\rho = \frac{AR}{l}. \tag{2.2}$$

The reciprocal of ρ ($1/\rho$) is the electrical conductivity σ. Ohm's law for the potential difference along a wire can be generalised to any form of material. Therefore, the electrical conductivity[1] is a measure of how easily electrical current flows through a material. The SI-unit is S m^{-1} but the range of values commonly measured in soils is better displayed in mS m^{-1}. Some typical values of conductivities are given in Table 2.1.

In the soil, electrical current mainly flows in the water-filled pores [6]. Hence, the current is electrolytic, meaning that ions (salts) are transported in a fluid (soil water). The solid particles of the soil (made of quartz, feldspars...) and the air in the soil pores have a very low conductivity. Thus, the factors related to the electrolytic conduction will influ-

[1]In the manuscript, "electrical" will be sometimes omitted from the terms "electrical conductivity/resistivity" to improve the readability.

ence the bulk conductivity of the soil, which were classified by [7] in four categories: nature and arrangement of the soil constituents, water content, pore fluid composition and temperature.

Table 2.1 Typical conductivity values of some minerals and rocks, adopted from [8].

Type	σ (mS m^{-1})
quartz	2.5×10^{-8}-5×10^{-11}
granite rock	0.001-4.5
soil water	10
clays	10-1000
sea water	5000
Iron (pure)	1.044×10^{4}

First, the clay content is the most important soil constituent playing a role in the conductivity. Clay particles usually have a net negative charge at their surface due to isomorphic substitutions of ions in the mineral lattice with another charge [9]. This negative charge attracts positive ions to the clay surface. Therefore, clay particles have a large capacity to retain ions, contrary to sand or silt particles. These ions can be used for the electric current flow in the soil, so a higher clay content is associated with an increase in conductivity. The arrangement of the soil constituents is determined by the geometry of the pores, their form and distribution. Large macropores are in general less conductive than smaller mesopores, and connected pores conduct better than closed pore distributions.

Second, an increase in water content opens more pathways for the current to flow and hence the conductivity will increase. It is important to note that there is a positive interaction between clay content and moisture content. The increase of the soil conductivity caused by an increase in clay content will be steeper for a high moisture content than for a low moisture content [10].

Third, the pore fluid composition is characterized by the ions dissolved in the soil solution and the viscosity of the fluid. More ions moving in the solution results in a higher current flow, so the conductivity will be higher. The ion composition also plays a role. This factor is mainly important in soils rich in salts, where the conductivity is dominated by the salt content. However, these saline soils were not present in the study areas.

Finally, temperature has an indirect, positive relationship with the conductivity: as temperature increases, the conductivity increases also. This is because the viscosity of the soil solution decreases as temperature increases, which causes the ions to move more easily in the solution. Several empirical relationships have been constructed that are mainly used to standardize seasonal temperature changes [11]. This correction is only relevant if several fields are measured over different seasons and need to be compared. This was never the case in this doctorate.

A large number of functions have been constructed relating conductivity with the above mentioned soil properties [12-14]. The conductivity readings of the FDEM sensors are often converted with empirical relationships to obtain indirectly the soil water content [12] or clay content [13] in non-saline environments. This is important for geoarchaeological prospection, because the natural soil variability is usually well expressed by clay or moisture content differences. For example, regions that were under the influence of tidal flooding often display a large difference in particle sizes (and thus clay content) at short distances, due to the differential stream velocities in and outside the channels. This means that the FDEM sensors can be very suitable to map the natural context of a site.

Knowing the mechanisms that facilitate current flow, the influence of artefacts on the local soil conductivity can also be estimated. It all depends upon the conductivity contrast between the artefact and the soil. The same structure (e.g. a ditch) can produce a low or a high anomaly in a conductive (clayey) or resistive (sandy) soil respectively. The anomaly can also change over longer periods (seasonally) due to changes in moisture content [14].

2.1.2 Magnetic susceptibility

The magnetic susceptibility χ is the capacity of materials to increase the strength of an external magnetic field. If the applied magnetic field has a strength H then the strength of magnetization M (or magnetic dipole moment per unit volume) is linear with H for low values of H according to the susceptibility:

$$\chi = \frac{M}{H}. \tag{2.3}$$

Both M and H have the same unit (A m^{-1}), so the susceptibility is dimensionless. However, its value is different depending on the system of units

used. To avoid confusion, "SI" is often written behind the value, refering to the international system of units. In a strict sense, the susceptibility[1] is actually the volume magnetic susceptibility or the susceptibility per unit volume (to distinguish it from mass and molar susceptibility). The total magnetic induction *B* is given by:

$$B = \mu_0(M + H), \tag{2.4}$$

or after substituting M:

$$B = \mu_0(1 + \chi)H, \tag{2.5}$$

with μ_0 the magnetic permeability of a vacuum. Often the terms magnetic permeability μ, relative permeability μ_r, magnetic susceptibility χ and magnetic permeability of the vacuum μ_0 are used for the same meaning. They are related by:

$$\mu_r = \frac{\mu}{\mu_0} = 1 + \chi. \tag{2.6}$$

Therefore, if a material is not magnetized, μ is equal to μ_0, μ_r is 1 while χ is equal to 0. If the material is magnetized, all three parameters will increase.

Materials are classified into the following groups depending on the way they are magnetized: diamagnetic, paramagnetic, ferromagnetic, ferrimagnetic and a special group called canted antiferromagnetic [15]. Diamagnetic materials have no magnetization or even a slight negative magnetization. Most minerals in the soil that do not contain iron all belong to this group, such as quartz and feldspars, kaolinite clay, calcium carbonate, water and organic matter. Paramagnetic materials have a weak magnetization, which disappears when the external field is removed. Many minerals containing iron are paramagnetic, such as most clay minerals (except kaolinite), iron sulphate and biotite. Ferromagnetic materials such as pure iron have the highest susceptibility and remain magnetic after the external field is removed (permanent or remanent magnetization). However, more important to soil studies are the group of ferrimagnetic materials, which are also strongly magnetisable but a bit less than ferromagnetic materials. Minerals such as magnetite and maghaemite are

[1]Similar to the word "electrical", the word "magnetic" will be sometimes omitted from the term "magnetic susceptibility".

the principle causes of magnetism in soils. Finally, canted antiferromagnetic materials show a weak magnetization, being slightly higher than paramagnetic materials. This group contains the iron oxides haematite and goethite, which are abundantly present in soils. They act as a source for the formation of more magnetic particles under certain soil environmental conditions.

The magnetic particles can be further divided according to the way their magnetic moments are organized in domains (single domain, multidomain). Different types of magnetic particles are distinguished by measuring the susceptibility at different temperatures or by varying the frequency of the magnetic field [16], but this was not applied in this doctoral research. To have an idea of susceptibility values, some reference values are listed in Table 2.2.

Table 2.2 Typical susceptibility of some rocks and minerals, adopted from [8].

Type	χ (10^{-3} SI)
quartz	-0.01
clays	0.2
granite	2.5
hematite	6.5
basalts	70
magnetite	6000

Ignoring soils weathered from highly magnetic substrates such as basalt, increased susceptibility in soils is mainly concentrated in the biologically active layer (topsoil) and is mostly caused by ferrimagnetic minerals. The formation of these minerals can be initiated by different mechanisms, including microbial action, pedogenesis and heating [17]. When the topsoil is disturbed for example by digging a pit, the susceptibility measured at the surface will be different. In addition, paleosols can be detected by measuring the susceptibility of profile samples or measuring the susceptibility directly in a borehole [18, 19]. Water logging lowers the susceptibility, which is important in wet areas. Materials that have been heated will acquire a higher susceptibility, which is the case for fire places [20, 21] or bricks [22]. The degree of magnetization depends on the iron minerals present, the temperature and oxygen level [23].

2.2 Soil sensors

2.2.1 Overview

The first attempts at geophysical surveys for archaeology were conducted in the 1920s but the major developments started only in the 1940s. Most geophysical methods used in geological investigations also have a potential use for archaeology, but after decades of research and applications some sensor types seem to be more suitable than other types. Today, the three most applied methods in commercial prospections are the electrical resistivity method, magnetometry and ground penetrating radar. Their main functionalities will be described in the following sections. Another method, based on electromagnetic induction, is also applied but to a lesser extent. Sporadically, other methods are used such as gravimetry or the measurement of earth gravity anomalies, seismic wave reflection and refraction, self-potential or the measurement of the natural electric potential of the soil, and thermal scanning of the soil surface. These techniques will not be further dealt with in this thesis [24-26].

Methods can be classified as active or passive depending upon whether energy is transmitted from an artificial source or natural energy is used such as earth's magnetic field. A second classification is based on the degree of contact with the soil; some sensor types require penetration into the soil, some require close contact with the soil surface and others do not require any contact. This is important for the practical operation of the sensor in the field. For example, physical penetration is not possible through hard surfaces such as roads in urban areas. Also rough surfaces with large stones impede the application of sensors with close surface contact. A third classification is related to the way the energy is dissipated in the soil; either as a propagating wave in the soil, reflecting on boundaries of different physical properties (e.g. radar or seismic waves), or as a "volumetric" measurement, where a physical property is measured over a bulk soil volume (e.g. electrical conductivity). Finally, the methods can be classified according to the principal physical property of the soil involved in the measurement. The most relevant here are the electrical resistivity (ρ) or its reciprocal the electrical conductivity (σ), the magnetic susceptibility (χ) and the permittivity (ε).

2.2.2 Magnetometry

Magnetometry makes use of the earth magnetic field as an energy source (Figure 2.1). Some materials in the subsoil can locally increase or decrease the strength of this field, causing an anomaly in the general field. Magnetometers are sensors that can measure these very small deviations of the earth magnetic field. A problem with this method is that the earth magnetic field has a natural time variation.

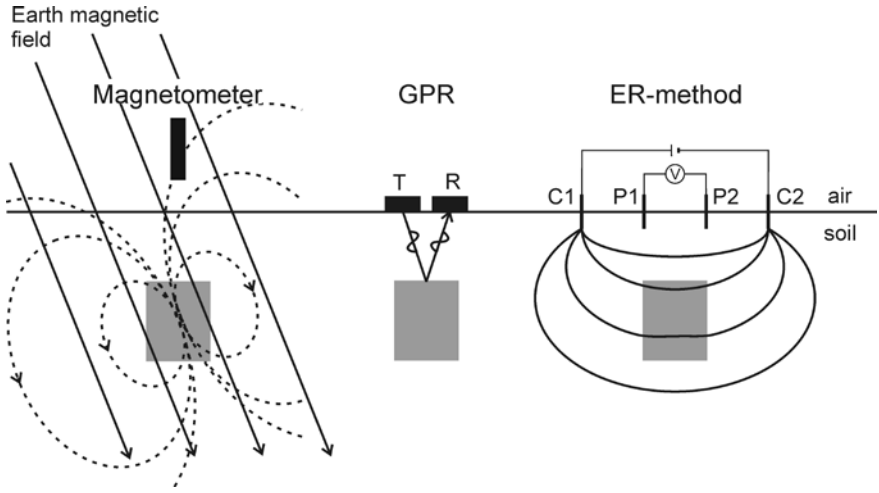

Figure 2.1 Schematic overview of the three most frequently used geophysical methods in archaeological prospection.

To deal with this issue, often two magnetometers are arranged in a gradiometer configuration, where one instrument is placed vertically above the other. The difference between the two measurements is taken (pseudogradient), in this way cancelling the time variations that occur in both sensors. The bottom sensor will be more influenced by small changes in the magnetic field close to the soil surface, which is then highlighted in the pseudogradient. Because the energy source is external, it is a passive method. Magnetometry does not require soil contact and it is a volumetric measurement. The increase or decrease of the earth magnetic field can be caused not only by the magnetic permeability of the materials, but also by remanant magnetism from past magnetisations. Metals with a high magnetic susceptibility have a very large influence on the measurement. Several magnetometer instruments were used to compare with the FDEM sensor (Table 2.3).

2.2.3 Ground penetrating radar

A ground penetrating radar (GPR) transmits pulsed electromagnetic waves with a frequency in the range of 10 MHz-1.5 GHz. These pulsed systems require a close contact between the transmitter antenna and the soil surface, although new stepped-frequency antennas can be operated above the soil surface. The waves propagating in the soil are either transmitted, reflected at discontinuities or are absorbed. The reflected waves are received by an antenna and both the strength and the travel time of the wave are recorded (Figure 2.1). When the velocity of the wave through the soil is known, the depth of the discontinuities can be calculated from the travel time. In this way, detailed depth information of the subsurface is obtained. Thus, GPR is an active method, usually requiring a close contact with the soil surface; and it is a wave propagation method. The main physical property causing reflections at boundaries and determining the wave velocity is the permittivity. The absorption of the wave and consequently its penetration depth is influenced mostly by the conductivity (if significantly high also by the susceptibility) and the wave frequency. Metal causes a very high reflection, so metal objects are easily detected but at the same time they mask deeper structures [27].

2.2.4 Electrical resistivity method

An electrical resistivity instrument (ER sensor, also known as earth resistance, geoelectric, DC current or galvanic current sensor) injects currents directly in the soil through a pair of electrodes (C1 and C2, Figure 2.1). The potential difference between two other locations is measured with another pair of electrodes (P1 and P2, Figure 2.1). The ratio of the potential difference and the current strength is equal to the earth resistance according to Ohm's Law. However, the earth resistance is a bulk measurement of a soil volume, which can be composed of different materials each with a specific resistivity. Moreover, the earth resistance also depends on the geometrical arrangement of the electrodes. To compare measurements of different electrode geometries of different soils, the earth resistance is often converted to "apparent electrical resistivity" (ρ_a) or the resistivity that would be measured as if the soil would be homogeneous medium with a single resistivity value. The word "apparent" will be used in the

same way for electrical conductivity and magnetic susceptibility measurements[1]. The conversion factor depends on the geometric electrode arrangement. The electrodes need to be in a good electrical contact with the soil, which can be a problem in very dry soils or soils with many stones. Therefore, the ER-method is an active method, requires penetration of the electrodes in the soil and is a volumetric method. The physical property involved is electrical resistivity. Several ER-instruments were used in this thesis to evaluate the FDEM sensors (Table 2.3).

Table 2.3 Overview of the instruments used in this research

Method	Sensor type	Name	Producer
Magnetometer	Fluxgate Gradiometer	FM18	Geoscan (UK)
Magnetometer	Fluxgate Gradiometer	FM256	Geoscan (UK)
ER-sensor	rectangular array of electrodes	Geophilus electricus	University of Potsdam (Germany)

2.3 Frequency-domain electromagnetic induction sensors

2.3.1 Introduction

FDEM uses electromagnetic waves such as the GPR method, but with a much lower frequency (kHz instead of MHz range). Although other types of instruments were tested for archaeological prospection, such as passive sensors using very low frequency (VLF) waves from distant broadcasting stations, the most common is the “Slingram” type. From now on, the term FDEM sensor will be used strictly for this type only. The transmitted electromagnetic field induces currents or magnetism in the soil, the strength of which is determined by the conductivity and the susceptibility. Both parameters can be separated and simultaneously measured, which is a big advantage compared to other methods. Consequently, the sensor is

[1]Although in the text, the word “apparent” will be omitted sometimes, as the word “electrical”; so “conductivity” will be used in stead of “apparent electrical conductivity.

sensitive to metals with a low susceptibility but with a high conductivity, such as copper, which are not detectable by magnetometry. This can be advantageous in archaeology, where objects are often made out of bronze (copper-tin alloy). However, the strong response to metal can also disturb the detection of weaker anomalies, especially in urban environments. Another important advantage is that the instrument does not require any contact with the soil surface. To summarize, the characteristics of the FDEM sensors are compared with the three other methods in Table 2.4.

2.3.2 History of applications in archaeology

The first FDEM sensor especially designed for archaeological prospection was the soil conductivity meter, nicknamed “the banjo” [28]. In contradiction to its name, this instrument actually measured only the susceptibility. Later it was found that to measure the conductivity, the quadrature-phase response had to be recorded instead of the in-phase [29] (see section 2.7). Starting in the end of the 1970s, a considerable research effort was undertaken by Prof. Alain Tabbagh. First, he investigated with theoretical computer models what would be the best sensor configuration (transmitter frequency, coil orientation and coil separation) for archaeological targets [4, 30, 31], followed by field trials with a prototype sensor [32, 33]. This theoretical study emphasized the importance of the coil configuration on the sensitivity for both conductive and magnetic targets. Meanwhile, a Canadian company called Geonics Limited developed and commercialized FDEM sensors especially for soil sensing [34]. In 1976, the EM31 ground conductivity meter was launched followed by the EM38 in 1980 (http://geonics.com). Both were oriented towards agricultural or archaeological applications. The EM31, with a coil separation of 3.66 m, measured a bulk volume down to approximately 6 m; while the EM38 response was concentrated in the top 1.5 m, with a coil separation of 1 m. These depth sensitivities are ideal to detect archaeological remains, which explains why they became popular for archaeological research. For example, the EM31 was applied to find relatively large structures such as early Bronze Age burial chambers [35] and prehistoric earthen mounds [36]. Smaller structures such as graves were investigated with the EM38 [37]. All these surveys only used the conductivity response and in most cases a single coil configuration.

Table 2.4 Summary of the characteristics of the three geophysical methods and FDEM.

Method	Energy source	Soil contact required	Energy dissipation	Physical property	Metal sensitivity
Magnetometry	passive	none	volumetric	χ	magnetic only
GPR	active	surface contact	wave propagation	ε	high
ER	active	penetration	volumetric	ρ $(1/\sigma)$	low
FDEM	active	none	volumetric	σ and χ	high

In a study of [38], the magnetic response of the FDEM sensor was compared with magnetometry measurements on a Neolithic site with a filled ring ditch. Although both methods produced similar results, differences in spatial sensitivity and type of magnetization (induced-remanent-viscous) can make them complementary in some cases. When the conductivity is very low, the soil susceptibility can disturb the conductivity response [32], so that its anomalies resemble more magnetometer anomalies than ER-anomalies [5]. However, in general the conductivity response corresponds very well with ER surveys [39, 40].

A disadvantage of the EM38 was that only one physical property (conductivity or susceptibility) at only one coil orientation could be measured at a time. That is why both the EM38B and EM38DD were developed. The former instrument was able to measure both components simultaneously and the latter sensor could measure two orientations simultaneously. Recently, a new sensor has been developed, the EM38-MK2, which is capable of measuring both components simultaneously at two coil separations, 0.5 and 1 m. In addition, similar FDEM sensors have been developed by Dualem Inc. (Canada), which are able to measure coil separations of 1, 2 and 4 m simultaneously.

2.3.3 Large area surveys

Parallel to the applications in archaeology, the EM38 sensor was also applied to agricultural studies such as soil salinity mapping [41], water content measurement [12] and soil texture mapping (clay-sand-silt fractions; [13]. Only the conductivity response was used, but several measurements at different coil orientations or sensor heights were exploited to reconstruct the soil profile in depth [42]. Surveys where the sensor was carried

by hand while walking along predefined lines, such as conducted in archaeology, were too slow to map large agricultural fields of several hectares. Therefore, platforms with sleds and carts were developed, so that the sensor could be pulled behind an all-terrain-vehicle and georeferenced with a GPS [43]. These platforms were only later used for archaeological applications [44, 45].

2.4 Electromagnetic induction

Electromagnetic induction implies the presence of both magnetic and electric fields, with their interactions described by the Maxwell equations [8, 46, 47]. Two of the Maxwell equations are particularly important to understand the principle of electromagnetic induction sensors: the laws of Maxwell-Ampère and Faraday. In general, Maxwell-Ampère's law states that if an electrical field $\mathbf{E}$[1] (caused by moving charges or electrical current) is present in a homogeneous, isotropic medium with conductivity σ and permittivity ε, then a magnetic field $\mathbf{H}$ will be induced according to the following equation (in differential form):

$$\nabla \times \mathbf{H} = \sigma \mathbf{E} + \varepsilon \, \partial \mathbf{E} / t \,, \tag{2.7}$$

with $\nabla \times$ the curl of the field. The first term on the right hand side is the conduction current, according to Ohm's law, while the second term is the displacement current. If the electromagnetic field varies with a low frequency, as in FDEM sensors, then displacement currents can be neglected. GPR operates at relatively high frequencies, where these displacement currents are important. The law of Faraday describes the electric field, which is induced by a changing magnetic field. For a homogeneous, isotropic medium with magnetic susceptibility μ, the electrical field $\mathbf{E}$ is give by:

$$\nabla \times \mathbf{E} = -\mu \, \partial \mathbf{H} / \partial t \,. \tag{2.8}$$

In FDEM sensors, an alternating (time-varying) current is passed through a coil of wounded, insulated wire, generating a time-varying magnetic field according to Ampère's law. This field will be referred to as the primary field $\mathbf{H}_p$ (Figure 2.2).

[1] Vectors will be written in the text as bold capital letters.

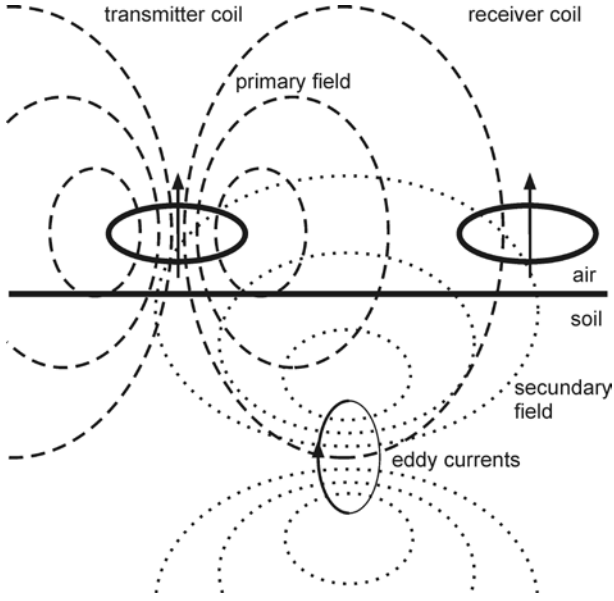

Figure 2.2 Sketch of electromagnetic induction principle of FDEM sensors with two coils of wounded wire (circles) and the induced magnetic dipoles (straight arrows).

If then the transmitter coil is close to an electrically conductive medium (e.g. a clay soil), according to the law of Faraday electrical currents are induced in the medium by the primary field; these are called eddy currents. The time-varying eddy currents generate in their turn another field, which will be referred to as the secondary field $\mathbf{H}_s$. If a second (receiver) coil is placed close to the transmitter coil and the medium, both the primary and secondary fields induce currents in the wire of the coil, the voltage of which can be measured. When the medium has a high susceptibility (e.g. basalt), the primary field also induces magnetization in the medium, according to equation (2.3), which will contribute to the secondary field. Therefore, both the conductivity and the susceptibility of the medium can contribute to the secondary field [48] and thus are measured with electromagnetic induction sensors.

2.5 Sensor output

The primary field is typically a signal oscillating in time with a sinusoidal shape and a fixed frequency (Figure 2.3).

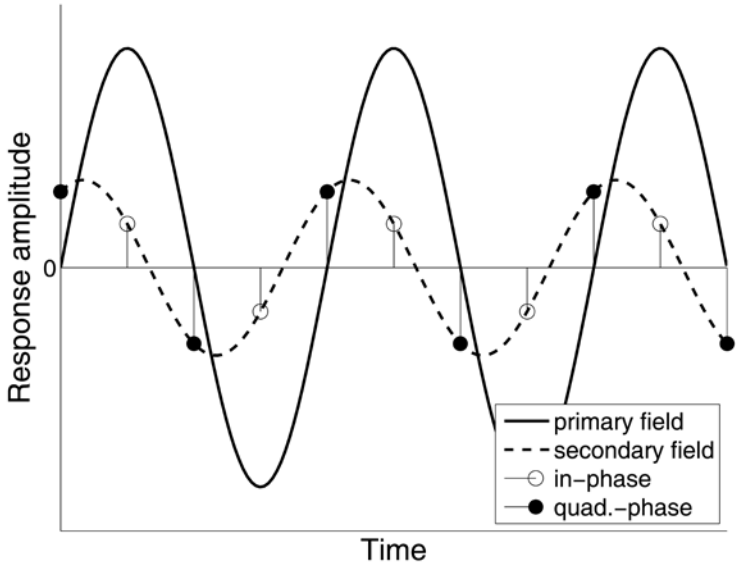

Figure 2.3 Amplitude of the primary and secondary field, oscillating in time.

The secondary field has the same frequency, but has a different amplitude and the phase can be shifted. Commonly, FDEM sensors are designed to measure two components of the secondary field, which are obtained by Fourier transformation during signal processing. The first component is the in-phase response (IP, or the real component in the complex notation). This is the amplitude of the secondary field measured when the primary field is at its maximum. The second component is the out-of-phase or quadrature-phase response (QP, or the imaginary component in the complex notation). This is the amplitude of the secondary field measured when the primary field is 0. Both components are commonly divided by the maximum amplitude (real component) of the primary field in free space, so that the sensor output is given by the ratios $(H_s/H_p)_{in}$ and $(H_s/H_p)_{quad}$ for the in-phase and quadrature-phase respectively. These ratios are dimensionless and very small, so they are usually expressed in parts per thousand (ppt).

2.6 Slingram-type instruments

The term “Slingram” is Swedish and refers to the original development of this method in Sweden in the 1930s. It consists of one transmitter coil and

one or more receiver coils at a certain distance from the transmitter [49]. The transmitter coil generates a continuously oscillating electromagnetic field in one or more frequencies; this makes Slingram sensors a subclass of FDEM sensors. Another type of instrument works in the time domain; these are called time domain electromagnetic induction (TDEM) sensors. This type can be used to distuinguish magnetic viscosity from magnetic susceptibility. The frequency of FDEM sensors is typically around 10 kHz, which is much lower than the frequencies applied in GPR (which are in the order of MHz-GHz). For low frequencies, the measurement distance is much smaller than the free-space wavelength and displacement currents are negligible (which is called the quasi-static approximation). In simple terms this means that the measurement should not be considered as a propagating wave, as is the case with GPR (using higher frequencies), but as a volume measurement similar to electrical resistivity measurements with electrodes.

The configuration of the coils is an important factor in Slingram-instruments; it largely determines their spatial sensitivity. The transmitter and receiver coils can be mutually oriented in several ways. Different nomenclature of the orientation is used in literature, which can be confusing. It is expressed either in respect to the loop orientations of the coils (Figure 2.4, circles), or to the direction of the magnetic dipoles of the coils (Figure 2.4, arrows). Throughout this thesis, the original nomenclature of [50] will be used depending on the loop orientation. The null-orientation does not couple with the soil and consequently does not produce relevant measurements.

2.7 Conversion of sensor output to conductivity and susceptibility

Complex analytical equations have been developed to calculate the in-phase and quadrature-phase outputs resulting from the conductivity, the frequency, the coil orientation and coil separation of the sensor for a homogeneous soil [50, 51]. However, the FDEM sensors that are used for soil surveys are designed to produce a direct measurement of the soil conductivity, applying approximations of the complex equations. This approximation is only true under certain restraints, which are referred to as “low-induction number” (LIN) conditions [48, 52]. To define what

these conditions are, another concept has to be defined, the "skin depth (δ)", or the depth at which the amplitude of a plane wave is reduced to 1/*e* (or 36.8 %) of the amplitude at the surface of a homogeneous half-space (the soil, air being the other half of the space). The skin depth is calculated from:

$$\delta = \sqrt{\frac{2}{\omega\mu\sigma}}, \tag{2.9}$$

with ω the angular wave frequency ($= 2\pi f$, f being the frequency in Hz), μ the magnetic permeability of the halfspace (normally this is assumed to be equal to μ_0 ($= 4\pi \cdot 10^{-7}$ N A^{-2}), the free space permeability, which is true for non-magnetic soils) and the conductivity of the halfspace (in S m^{-1}). Hence, it is a measure of how deep the electromagnetic signal penetrates, depending on its frequency and the conductivity of the soil.

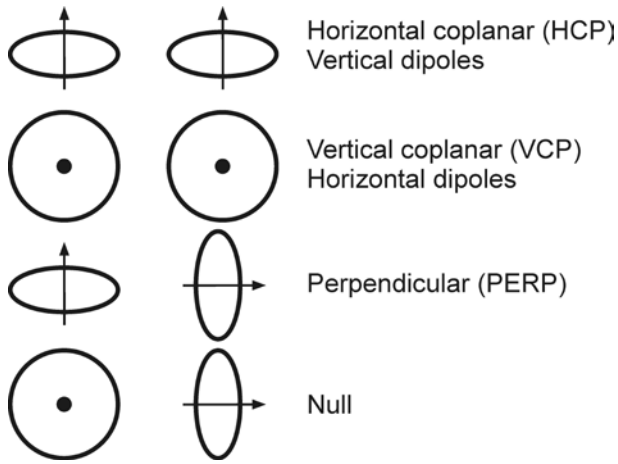

Figure 2.4 Coil configurations with their abbreviations as used in the text. The upper name refers to the loop orientation and was adopted in the thesis, while the name below is found in some texts, such as the operation manual of the EM38.

For example when a wave with a frequency of 9 kHz (of the DUALEM-21S, $\omega = 2\pi \times 9000 = 56548.7$ radians s^{-1}) is passed through a soil with a conductivity of 20 mS m^{-1} (or 0.2 S m^{-1}, typical for a loam soil), then the skin depth is 37.5 m. The induction number is defined as the ratio of the coil separation *s* (in m) over the skin depth. Continuing the example, if *s* is 1 m then the induction number is 1/37.5 or 0.0267. If this number is small enough (how small is not really well defined [53]), then the quadra-

ture-phase response of the sensor is directly proportional to the conductivity using the equation:

$$(H_s / H_p)_{quad} = \frac{\omega \mu_0 \sigma s^2}{4}. \tag{2.10}$$

The conductivity of the halfspace is then calculated from:

$$\sigma = \frac{4}{\omega \mu_0 s^2} (H_s / H_p)_{quad}. \tag{2.11}$$

Under LIN-conditions, the in-phase component is proportional to the magnetic susceptibility of the soil. If the sensor were in a homogenous space, the susceptibility would be equal to the in-phase response. When the sensor is located on the soil surface, only a half-space is measured (which is the soil volume, assuming that air has a negligible susceptibility). The susceptibility is then equal to twice the in-phase response (personal communication A. Tabbagh, [54][1]):

$$\chi = 2(H_s / H_p)_{in}. \tag{2.12}$$

When these equations are used, the following four issues have to be considered. First, the sensor frequency and the conductivity of the soil have to be low for the LIN-approximation to be valid. Second, there is a small influence of the electrical conductivity on the in-phase response, which becomes important if the conductivity is high. Third, a certain type of magnetic particles with 'viscous magnetization' can influence the quadrature-phase response, which becomes significant when the conductivity is low (e.g. sandy soils). This "quadrature-phase susceptibility" is an obstacle to measure very low conductivity values [32, 55]. Fourth, if a FDEM sensor is designed to function under LIN-conditions, then the measurements are independent of the frequency. This is the reason why these sensors only operate at one frequency [56][2].

[1]The EM38 manual of Geonics Limited mentions the factor 58×10^{-6}, which is actually the same factor 2 but with a conversion included from the in-phase response to ppt and then to mS m^{-1}.

[2]Multi-frequency sensors exist, but there is still an ongoing debate about their effectiveness.

2.8 Spatial sensitivity

2.8.1 Depth sensitivity of a layered soil

In the previous sections, the soil was treated as a homogenous volume with a single value of conductivity. In reality, this is of course not true. The soil volume can be very heterogeneous with large differences in conductivity. Therefore, the term "apparent" conductivity (σ_a) is preferred, which is the bulk conductivity of a heterogeneous soil as if a halfspace was measured with a homogeneous conductivity. This is also true for the susceptibility, so the term apparent susceptibility (χ_a) is used as well.

Now imagine the soil consists of thin, horizontal layers, each with a homogeneous conductivity and susceptibility. This is a good approximation of real soils, because soils often have distinct horizontal layering. This is because the soil material is deposited or eroded in horizontal layers and because soil forming processing such as clay migration often act in the vertical direction. Based on the same assumptions of the LIN-conditions, the relative weight of each layer to the sensor measurement can be derived depending on its depth *z* [34, 48, 52, 54]. Important in the assumptions is that the individual layers do not influence each other. This means that the depth-weighting equations are independent from the conductivity or susceptibility of the layers (so they also do not occur in the functions). On the other hand, the equations are dependent on the coil separation *s* and the coil orientation: horizontal coplanar (HCP), vertical coplanar (VCP) or perpendicular (PERP). If now the relative weights of all layers are summed (integrated) from an infinite depth up to the surface, the cumulative weight of all layers below a depth z can be calculated (Table 2.5). These functions can be plotted against the depth z to give an idea of the depth sensitivity of the different coil configurations (Figure 2.5). The relative weight curves for a 1 m coil separation show some interesting features.

The conductivity of both the PERP and VCP orientations is very sensitive to the upper layers while the HCP orientation is more sensitive to deeper layers, with a maximum at a depth of about 0.4 m. The susceptibility curves for the HCP and PERP orientations have a special shape crossing the zero line, showing that some layers contribute a positive response while other layers contribute a negative response.

Table 2.5 Depth sensitivity functions for a layered medium.

		Relative weight[1] R	Cumulative weight C
σ	HCP	$\frac{4(z/s)}{s(4(z/s)^2+1)^{3/2}}$	$\frac{1}{(4(z/s)^2+1)^{1/2}}$
	VCP	$\frac{2}{s}-\frac{4(z/s)}{s(4(z/s)^2+1)^{1/2}}$	$(4(z/s)^2+1)^{1/2}-2(z/s)$
	PERP	$\frac{2}{s(4(z/s)^2+1)^{3/2}}$	$1-\frac{2(z/s)}{(4(z/s)^2+1)^{1/2}}$
χ	HCP	$\frac{12(z/s)(3-8(z/s)^2)}{s(4(z/s)^2+1)^{7/2}}$	$\frac{1-8(z/s)^2}{(4(z/s)^2+1)^{5/2}}$
	VCP	$\frac{12(z/s)}{s(4(z/s)^2+1)^{5/2}}$	$\frac{1}{(4(z/s)^2+1)^{3/2}}$
	PERP	$\frac{96(z/s)^2-6}{s(4(z/s)^2+1)^{7/2}}$	$\frac{6(z/s)}{(4(z/s)^2+1)^{5/2}}$

Close to the surface, the HCP and VCP orientations give no response, while the PERP is strongly negative. An increasing coil separation causes a downwards shift of the depth sensitivity curves, so more weight is given to deeper layers (Figure 2.6). For the susceptibility-measurement in the HCP and PERP orientations, this also means that the zero crossing-point is shifted downwards.

The curves can also be used to model the expected response of a layered soil (which is called 1-D forward modelling). If for each layer i the conductivity σ_i is given, with C_i the cumulative weight at a depth equal to the top of the layer and C_{i-1} from the bottom of the layer (from Table 2.5), then the total conductivity σ_a of the soil is equal to:

$$\sigma_a = \sum_i \sigma_i (C_i - C_{i-1}) . \tag{2.13}$$

[1]These equations are slightly different to the ones given by Geonics Limited (1999). In the denominator the extra variable s was added to ensure that if the functions are integrated to obtain the cumulative functions, the total weight is equal to 1. In the conversion from in-phase output to susceptibility, the sign of the VCP and PERP configurations is also changed, to ensure positive susceptibility values.

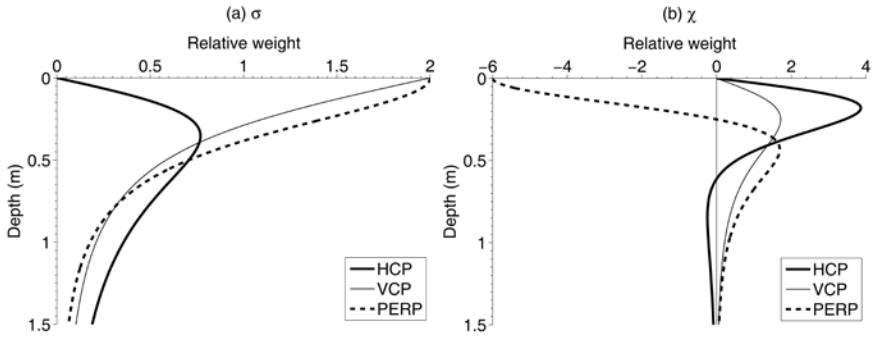

Figure 2.5 Depth sensitivity curves for a 1 m coil separation.

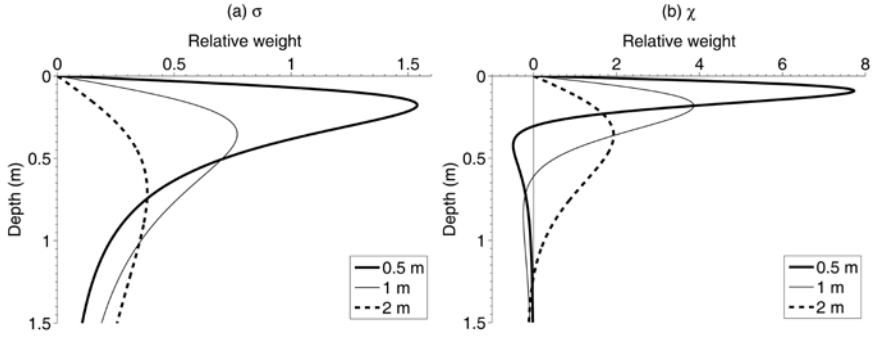

Figure 2.6 Depth sensitivity of the HCP-orientation for increasing coil separations.

The calculation for a layered soil with different susceptibilities is identical. This equation is also valid if the sensor is elevated above the soil surface. In this case, the air layer between the soil surface and the sensor is counted as a layer with conductivity and susceptibility equal to zero. Therefore, the modelled response of raising a sensor at different heights above the soil surface is equivalent to the response of a two-layer soil with the sensor on the surface and a topsoil conductivity and susceptibility of 0. If a soil consists of two layers with a sharp boundary of conductivity, then the depth of the interface and the layer conductivity can be modelled using surface measurements as input for the equations (which is called 1-D inverse modelling) [57, 58].

More complicated soil models are more difficult to reconstruct, due to the fact that equal measurements can originate from different soil models ("principle of equivalence" [10]) and small changes in the measurement values can create large variations (and errors) in the modelled conductivities [59]. Nevertheless, 1-D inversion programs were developed

and are readily available [60], but it is good practice to validate the models with field verification.

2.8.2 Sensitivity to small 3-D structures

In the previous section, it was assumed that the soil consists of horizontal layers with infinite extent and a homogeneous conductivity and susceptibility. In reality, this is often not the case, certainly not in an archaeological context where many small structures are present, such as ditches or walls. When structures are present with dimensions in the range of the coil separation of the sensor, the expected measurement values can only be modelled taking the 3D-shape of the structure into account [61].

To demonstrate the difference between a layered soil model and a small, three-dimensional model, the response of the 1 m HCP configuration was simulated with a 3-D forward modelling program, EMIGMA (more details about this program can be found in Appendix A). Although it is necessary to verify this theoretical model with field measurements, this example still gives a good idea of the influence of the size of the structure relative to the coil separation. A FDEM sensor was assumed to be at 0.1 m height above the soil, which had a homogeneous conductivity of 10 mS m^{-1}. One survey line of 20 m long was simulated, where the sensor was positioned parallel to line. A square structure was placed in the middle of this survey line. It had a conductivity of 50 mS m^{-1}, a thickness of 0.5 m and the top was located at 0.3 m under the soil surface. The width of the structure varied between 0.5 and 8 m. A layer with the same properties as the square structure, but with infinite width was also modelled with EMIGMA. The modelled conductivity of the soil measured without the structure was 9.55 mS m^{-1}, and with the layer, it was 21.33 mS m^{-1}. For comparison, these values were also calculated using the approximate models for layered soils of Table 2.5. The resulting conductivities were 9.81 mS m^{-1} for the homogeneous soil and 21.61 mS m^{-1} for the soil with the layer, almost the same as the EMIGMA values.

Some interesting conclusions can be drawn from this 3-D modelling (Figure 2.7). First, when the width of the structures is 0.5 or 1 m, the measured anomaly is lower than 1 mS m^{-1}, which is close to the noise level of the sensor (see section 3.2.2). The anomaly also displays a negative dip just above the structure. If the structure has a width of twice the coil separation (2 m), it would probably be distuinguished from the back-

ground. Second, even if the width of the structure is eight times the coil separation, the maximum conductivity does not reach the conductivity of the soil with the layer.

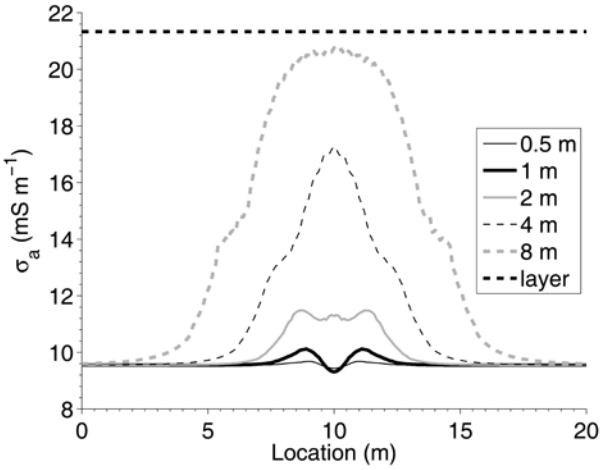

Figure 2.7 Three-dimensional modelling of the 1 m HCP configuration over a square feature of increasing size (its centre is located at 10 m) and for a horizontal layer with the same thickness and conductivity.

2.9 Metal detection

In general, metal has a very high conductivity and ferrous metals have a high susceptibility. Consequently, FDEM sensors react very strongly to metal objects and are often used for unexploded ordnance detection (UXO, e.g. mines and bullets). Magnetometers are also often used, but they have the disadvantage of only measuring ferrous (magnetic) metals. FDEM sensors do measure non-ferrous objects such as bronze because they also react to the high conductivity of the metal. GPR has the disadvantage that the high-frequency (high energy) electromagnetic waves can trigger electronically fused pieces of UXO [62].

However, the working principle of an FDEM sensor designed for soil conductivity measurements is disturbed in the presence of metal [63]. Apart from the strong eddy-currents that occur due to the high conductivity of the metal, also a strong permeability-response can take place due to the polarization of magnetic dipoles. This polarization does not disappear immediately, so it affects both the in-phase and quadrature-phase of the

secondary field. The magnitude of both the eddy current response and the permeability response depends on the orientation of the coils towards the metal object. Therefore, when a Slingram-sensor with separated coils moves over a metal object, both the in-phase and quadrature-phase anomalies are complicated, displaying both strong positive and negative responses. It is then difficult to define accurately the location of the metal object. For these reasons, time-domain electromagnetic induction (TDEM) sensors with coincident coils were developed specifically for UXO detection.

Nevertheless, FDEM sensors do respond strongly to metal, both in the in-phase and in the quadrature-phase and metal pieces often appear as extreme local anomalies. This can be an advantage for archaeological prospection if the metal pieces can provide historical information, but the extreme values can also mask weaker anomalies. For example, metal fences or wires at the border of a field can disturb the signal at several meters distance.

Chapter 3

Adaptations for high-resolution surveys

3.1 Sensor configuration

3.1.1 FDEM sensor types

Three FDEM-instruments were used in the thesis, the EM38DD, the EM38-MK2 (Geonics Limited, Canada) and the DUALEM-21S (Dualem Inc., Canada). All three sensors operated at a single frequency low enough to be in the LIN-range (see section 2.7). Their main characteristics are summarized in Table 3.1 and a sketch of the coil configurations is shown in Figure 3.1**.** The EM38-MK2 can be operated in either the HCP or the VCP orientation. The DUALEM-21S is normally operated with the coil orientations in HCP and PERP. If the instrument is turned 90°, the VCP and NULL orientations can be measured. The NULL-orientation does not produce any response to the soil (no coupling), so it will not give usable results. The coil configurations will be abbreviated in the thesis as for example 1.1PERP (1.1 m coil separation and perpendicular coil orientation).

The location of the measurement is taken as the midpoint between the transmitter and receiver coil-pair. The DUALEM-21S and the EM38-MK2 have slightly shifted midpoints for the different coil separations (i.e. at 0.25 and 0.5 m from the transmitter for the EM38-MK2; 0.5, 0.55, 1 and 1.05 m from the transmitter for the DUALEM-21S). Consequently, if a survey is conducted with the sensor perpendicular to the survey line and if adjacent survey lines are acquired in opposite direction, then it is impossible to obtain regularly spaced measurement lines for all coil separations. The responses of the HCP and VCP orientations are perfectly symmetrical, so it does not matter if a structure is crossed first by the receiver or first by the transmitter coil. However, the response of the PERP

orientation is slightly asymmetric, so if a small structure is crossed the response will be different depending on which (transmitter or receiver) coil arrives first at the structure.

Table 3.1 Characteristics of the three sensors types used.

Sensor	EM38DD	EM38-MK2	DUALEM-21S
Transmitter frequency (Hz)	14600	14500	9000
Recording frequency (Hz)	10	10	8
Measurement resolution	0.125 mS m^{-1}, 7.2×10^{-6} (SI)	0.039 mS m^{-1}, 2.2×10^{-6} (SI)	0.1 mS m^{-1}, 2×10^{-5} (SI)
Coil configuration	1 m HCP and 1 m VCP	1-0.5 m HCP or 1-0.5 m VCP	(1-2 m HCP and 1.1-2.1 m PERP) or 1-2 m VCP
In-phase/ quad.-phase	one at a time	both	both
Calibration	manual	semi-automatic	automatic

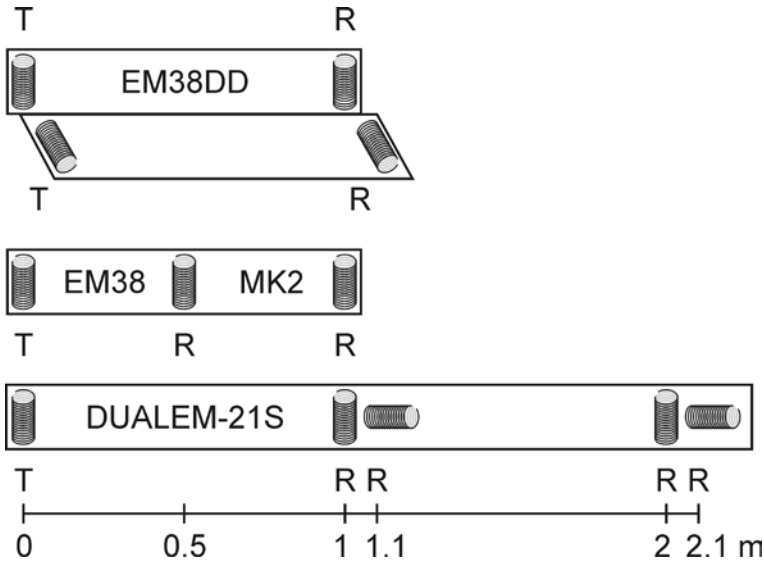

Figure 3.1 Coil configurations of the three sensors. T and R refer to the transmitter and receiver coils. The horizontal distance is on scale.

3.1.2 Motorized sensor platform

Both sensors were operated in a sled, pulled by an all-terrain-vehicle (ATV). The sleds were made of high-density polyethylene, which is very resistant to abrasion and has a low brittleness over a high temperature range (Figure 3.2a). The sled did not contain any metal piece that could disturb the measurements. To maximize the response, they were designed to hold the sensors as close as possible to the soil surface. The sensor position is well secured to keep the coil orientations in the same direction, and it is protected against shocks by foam. The sleds are rainproof, which is convenient in Belgium. The sleds were also covered with white stickers to reflect the direct sunlight, avoiding high temperature changes inside the sleds.

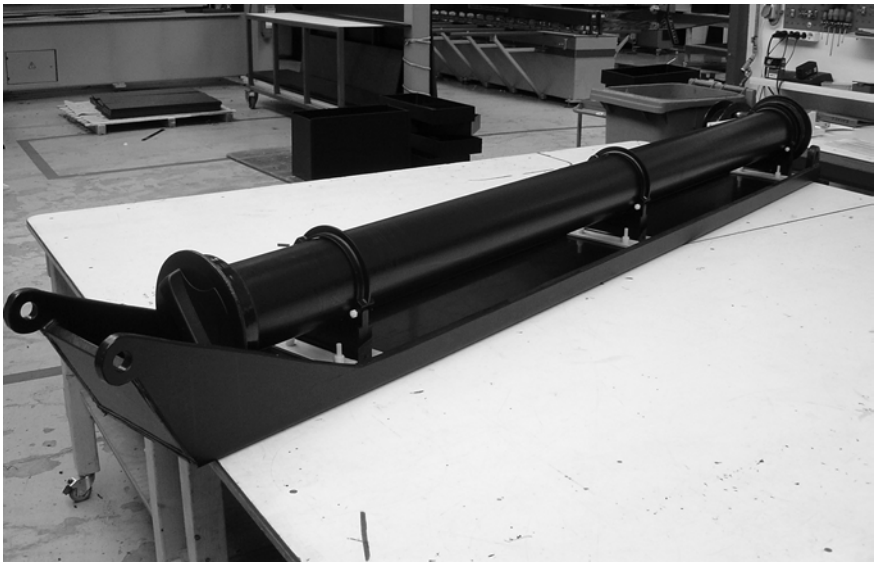

Figure 3.2 Custom-made sled of the DUALEM-21S.

The ATV was equipped with a GPS (Trimble AgGPS332), which has an antenna that can receive L-band frequencies for satellite differential correction (Figure 3.3). A subscription to the Omnistar HP correction signal was activated especially for archaeological surveys, increasing the absolute accuracy to 0.2 m and the pass-to-pass accuracy (between two consecutive measurement lines) to 0.1 m (http://www.omnistar.nl/). The ATV was also equipped with a lightbar guidance system (Trimble EZ-Guide Plus), enabling the operator to drive closely separated, parallel tracks (in driving, 0.4 m was the smallest practical separation).

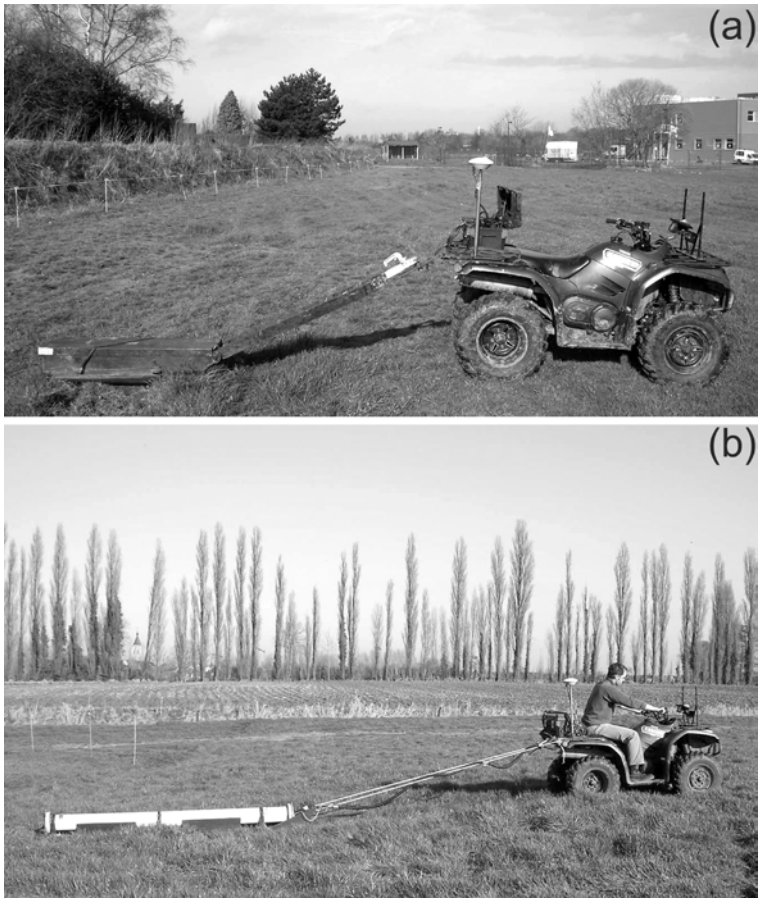

Figure 3.3 Sensor platforms of the EM38-sensors (a) and the DUALEM-21S sensor (b) in action.

The system also allowed the speed of the ATV to be monitored accurately. The influence of the ATV was avoided by keeping a sufficient distance between it and the sensors. For the EM38 sensors this was 1.8 m from the GPS-antenna to the closest coil of the sensor, while the larger spatial sensitivity of the DUALEM-21S required a separation of 3 m. While driving over the terrain, the sensor measurements and the GPS-positions were recorded on a field computer (Allegro, Juniper Systems Inc., USA). Each record line had a time stamp to be able to merge the sensor data with the positions during the processing stage.

3.2 Position and noise control

3.2.1 Sources of measurement errors

A detailed description of the possible errors that can occur in FDEM sensors was given by [49]. In general, three sources of errors can occur: instrumental errors, environmental noise and operational disturbances.

Instrumental errors are caused by three factors: 1) wrong calibration or drift of the absolute values, 2) scale or normalization errors in which the readings are in error by a multiplicative constant and 3) phase or mixing errors in which the in-phase measurement is affected by the quadrature-phase or vice-versa. Instruments from Geonics Limited were designed so that the operator can minimize some of these errors, while the sensors from Dualem Inc. have an internal system check and do not allow the operator to adjust. A very important step in setting up the FDEM sensor before a survey is the calibration procedure. It consists mainly of two procedures: 1) nulling the large primary field in the receiver coil in free space (air), so that only the secondary field is measured and 2) absolute calibration of the in-phase and quadrature-phase so that they measure the right conductivity and susceptibility. Ideally, these procedures should be conducted in a zero conductivity environment, but this is difficult to obtain in the presence of soil. Therefore the EM38-sensors of Geonics are calibrated at 1.5 m height [64]. At this height, the influence of the soil on the primary field is minimal in the VCP coil orientation, so it can be nulled by adjusting the in-phase to read zero. In this way, the in-phase is effectively calibrated to measure the susceptibility because the influence of the soil susceptibility is negligible at this height (Figure 3.4a). The absolute calibration of the quadrature-phase to measure the electrical conductivity is based on the response curves over a layered medium (see section 2.8.1). At a height of 1.5 m, the ratio of HCP to VCP is almost equal to two (Figure 3.4b). There are small errors involved in this assumption, which can be further reduced if the sensor is lifted at 2 m height, but this is less practical [65]. In addition, the presence of small structures or metal pieces close to the sensor coils can disturb the assumption of a layered soil. For all these reasons, the EM38 sensors were always calibrated at 2 m height. During long surveys, the measurements can also suffer from drift of the absolute calibration. This is caused by temperature changes

(related to the ambient temperature and sunlight) that affect some electronic components.

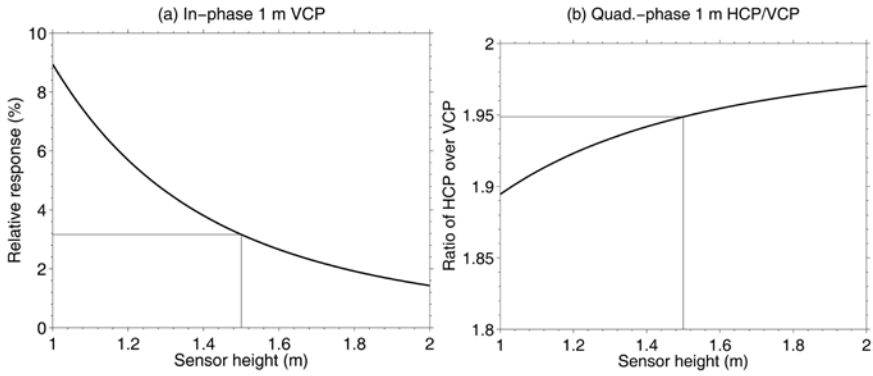

Figure 3.4 Sensitivity of a sensor with 1 m coil separation over a layered soil.

The DUALEM-sensors have a patented automatic calibration procedure, which starts when the sensor is switched on and which takes some seconds. It uses a bucking coil and a calibration coil to null the primary field and calibrate the absolute values [66]. The sensor can be placed on the soil during calibration, but not near disturbing features such as metal objects.

Environmental noise can disturb the measurements and is difficult to manage. First, electromagnetic fields from power lines, radio transmitters or sferics (due to natural lightning discharges) create clutter in the data. In Flanders, the electrical fences around pasture fields can be particularly problematic so it is better to turn the electricity off while measuring. The metal of the wiring and other metal objects can mask the measurement at several meters distance. Some of these factors are difficult to avoid, but should be certainly noted down during the survey so that in the processing stage the cause of some extraordinary anomalies can be explained.

Finally, operational disturbances can have a large impact and have to be minimized. While moving over a rough terrain, the sensor can tilt and turn, changing the coil orientation and thus the spatial sensitivity. In a ploughed field or a field with maize stumps, the coil configurations with shallow depth sensitivities will be more influenced by this. The maps then display a striping pattern parallel to the agricultural management direction.

3.2.2 Noise level

Although noise depends of many factors, it was necessary to have an idea of the noise level in order to evaluate the sensitivity of the sensors. The standard deviation (SD) was used as a measure of the noise level. If the measurements vary according to a random (normally distributed) process, then 68.3 % are within ± one SD unit and 95.5 % are within ± two SD units around the mean. The manufacturer gave the SD values for the EM38DD: 0.5 mS m^{-1} (conductivity) and 4×10^{-5} (SI, susceptibility), but they were not given for the EM38-MK2. The noise levels for the DUALEM-21 were given for each response separately [67]: 0.25 mS m^{-1} and 1×10^{-5} (SI) for the 1-1.1 m coil separations; 0.1 mS m^{-1} and 4×10^{-5} (SI) for the 2-2.1 m coil separations. Of course, these values are only indicative and are influenced by many factors such as the ambient noise at the test site.

A test of the noise level at a fixed position was conducted outdoors in a relatively noise-free environment for the three sensors. The sensors were wrapped in foam to avoid rapid heating from direct sunlight. The output was recorded for each sensor during 25 minutes (Figure 3.5). The conductivity measurements of the EM38-MK2 showed relatively stable fluctuations around a constant mean. However, the mean of the susceptibility was clearly not constant showing a general decreasing trend. For this coil configuration, the trend of the mean had a linear shape. However, other configurations had a trend that was more curved. Therefore, a polynomial regression model of second degree was fitted to all the measurements to remove this trend. Then the SD was calculated of the original measurements subtracted by the trend (Table 3.2).

The noise values given by Geonics for the EM38DD corresponded well with the measured noise and were even slightly lower. There was quite a big difference between the two coil orientations, the 1 m VCP having the lowest noise level. The conductivity noise of the DUALEM-21S was also around the range given by the manufacturer, although the SD of the 2 m HCP and 2.1 m PERP was higher in the test. The SD was also similar for the susceptibility data, the given values were higher than those measured in the test. The 0.5 m coil separation of the EM38-MK2 sensor clearly performed better than the 1 m separation. The 1 m HCP of the EM38-MK2 was noisier than for the same configuration of the EM38DD. Generally, the noise levels of the different sensors were

in the same range. So an overall noise level was assumed to act as a reference, being the maximum values given by both manufacturers: 0.5 mS m^{-1} and 4×10^{-5} (SI).

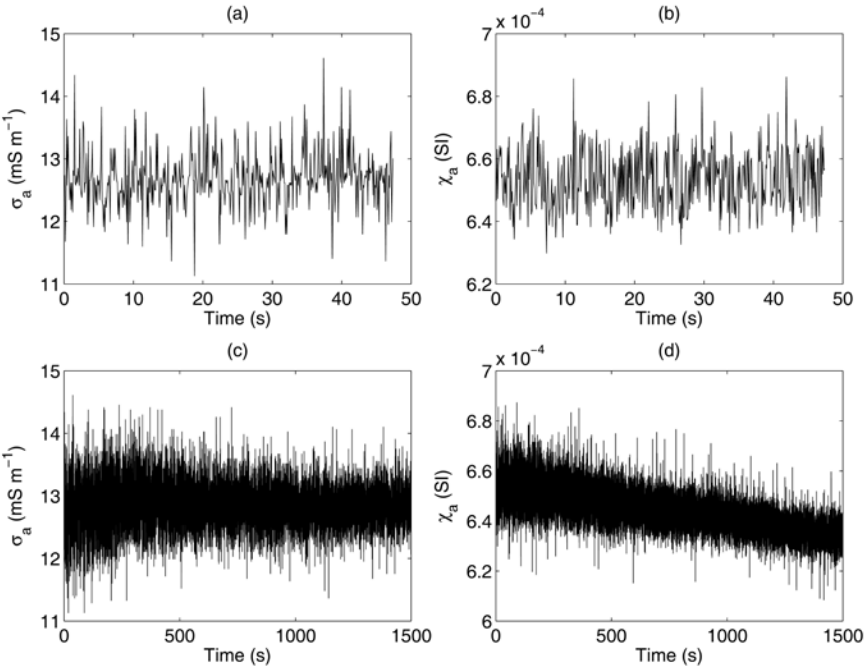

Figure 3.5 Measurements of the EM38-MK2 at a fixed position in the 0.5HCP coil configuration; (a-b) 50 seconds time window and (c-d) 25 minutes time window.

The operation in the motorized platform has a significant effect on the noise of the sensor, due to the movements of the sled. However, it is very difficult to evaluate this because it depends a lot on the terrain conditions (smooth pasture will give fewer disturbances than a ploughed field). During numerous field surveys, it was observed that the susceptibility measurements are very sensitive to noise. Particularly troublesome were the PERP-orientations of the DUALEM-21S.

3.2.3 Position control

In geophysical prospection for archaeology, the structures being searched for are often no larger than a few decimetres. Small positioning errors can obscure the anomalies, especially if they are weak. In some cases, interesting anomalies have amplitudes in the same range as the noise level of the sensor. In this case, they are only visible because of their geometrical

shape in the horizontal space compared to the random patterns of noise (e.g. a circular ditch surrounding a former burial mound). The first source of positioning error comes from the GPS-unit, which cannot be improved except by buying a (expensive) real-time kinematic (RTK) GPS. A second source of error is the offset between the sensor midpoint and the GPS-antenna. A third error is time- and therefore also speed-dependant. The sensor needs a certain time to reach its maximum amplitude (personal communication with M. Bosnar, Geonics Limited[1]). This creates a variable spatial offset proportional to the speed of moving the sensor. A factor of 0.285 s was empirically found for the EM38 by [43], to be multiplied by the speed in m s^{-1} to obtain the spatial offset in m. Both the fixed and variable spatial offsets are doubled when lines are measured in opposite directions.

Table 3.2 Standard deviations of the FDEM-measurements over a period of 25 minutes after trend removal.

EM38DD			
(σ_a, mS m^{-1})		(χ_a, $\times 10^{-5}$ SI)	
1HCP	1VCP	1HCP	1VCP
0.192	0.190	0.109	0.910
EM38-MK2			
(σ_a, mS m^{-1})		(χ_a, $\times 10^{-5}$ SI)	
1HCP	0.5HCP	1HCP	0.5HCP
0.552	0.321	3.395	0.685
DUALEM-21S			
(σ_a, mS m^{-1})		(χ_a, $\times 10^{-5}$ SI)	
1HCP	1.1PERP	1HCP	1.1PERP
0.190	0.109	0.910	0.799
2HCP	2.1PERP	2HCP	2.1PERP
0.210	0.196	3.166	3.109

The effect of driving speed was tested on a site where different numbers of metal bars, at locations 5 m apart, were buried at 0.4 m depth.

[1]The time needed for the sensor to reach its maximum amplitude prior to analogue to digital conversion of the signal (the EM38 takes 0.24 s to reach 63% of its maximum amplitude). The sampling rate of the A/D-conversion in the EM38 is 15 records/s and of the allegro field computer 10 records/s.

The metal caused a sharp peak in the data, which could be used as a marker for a fixed location. The sensor platform was driven over and perpendicular to the metal bar, twice on the same track in opposite direction and for a range of speeds (Figure 3.6).

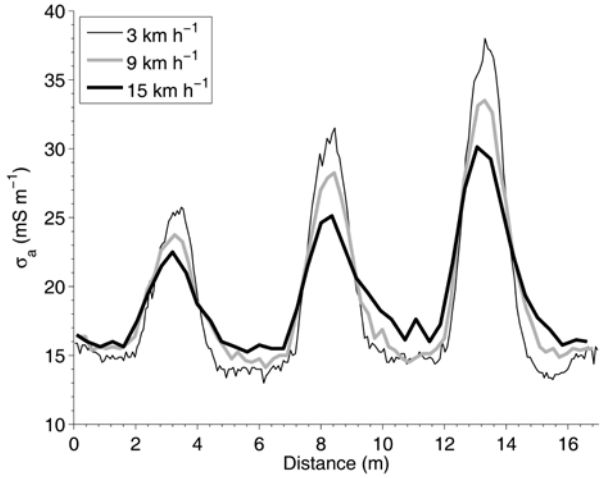

Figure 3.6 Transect over three locations with buried metal bars conducted with the EM38DD for three different speed levels, showing the conductivity in the VCP orientation.

Several important conclusions could be drawn from this test. First, the data of the EM38DD did not show a variable spatial offset due to the speed for speeds up to 18 km h^{-1}. However, the DUALEM-21S data had a large variable offset over a wide speed range. Different correction procedures were applied, using either a fixed spatial correction or a combination of fixed and variable spatial correction. In the end, because the surveys are normally conducted at approximately the same speed, the fixed spatial correction was found to give more stable results. The variable shift sometimes changed abruptly between consequent measurements because it was calculated using the operational speed, which could vary over small distances. The correction program, as well as the other programs of the next sections were written by the author of this thesis in Matlab (version R2008b, The Mathworks Inc., USA). Each measurement was shifted backwards along the driving line, whose direction was determined by a previously recorded measurement. The effect of the correction was quite dramatic, as can be seen in Figure 3.7.

Second, there was a reduction in amplitude if the speed was increased. This was also found by [43], who quantified the reduction to

−0.4 mS m^{-1} per m s^{-1}. Nevertheless, it was clear from Figure 3.6 that this reduction depended on the structure that is measured. The reason for the amplitude reduction was that if the speed is too fast, the sensor response time was too slow to reach its value when standing still. In addition, fewer measurements per line distance were recorded so there was less probability that the peak values were sampled.

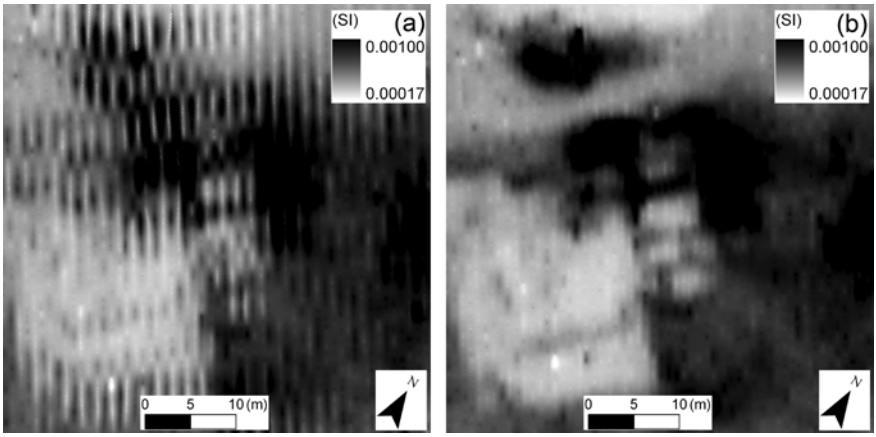

Figure 3.7 Interpolated susceptibility map without shift correction (a) and after shift correction (b).

Third, the slow response time of the sensor created a general smoothing of the data and asymmetric anomalies over the metal bars **(**Figure 3.8**).** At 3 km h^{-1}, the peak over the metal bar was symmetric, but above 5 km h^{-1}, the slope after the peak value was less steep, indicating a time delay in the sensor response. So in order to obtain the highest and narrowest anomalies, it was important to keep the driving speed low. For detailed surveys, the speed was maintained below 5 km h^{-1}.

3.3 Monitoring time drift

FDEM sensors suffer of drift of the absolute value over a relatively short time (in the order of hours). It is mainly caused by changes in resistance or capacitance of the electronic components due to temperature variations [48]. Field tests confirmed the influence of ambient temperature and sunlight, which can be especially large on hot, sunny days with high temperature fluctuations between the morning and the afternoon [43, 68]. To minimize this effect, it is best to isolate the sensor with foam and shield it with a white cover to reflect sunlight. Although the manufacturers claim

to compensate for temperature drift, all three instruments still suffered from it. Moreover, it is often difficult to relate the drift of each coil configuration to the internal temperature of the sensor. In order to monitor or correct the drift, most users return regularly to a fixed location or recalibrate the instrument frequently in the air. However, these methods have some disadvantages. Only a few discrete points in time are sampled to monitor the drift, and if fields of several hectares are surveyed it is often unpractical to go back to a fixed point. For conductivity measurements, this procedure is still applicable because the daily drift varies relatively slowly. However, the drift of the susceptibility can be very large over short time periods [69].

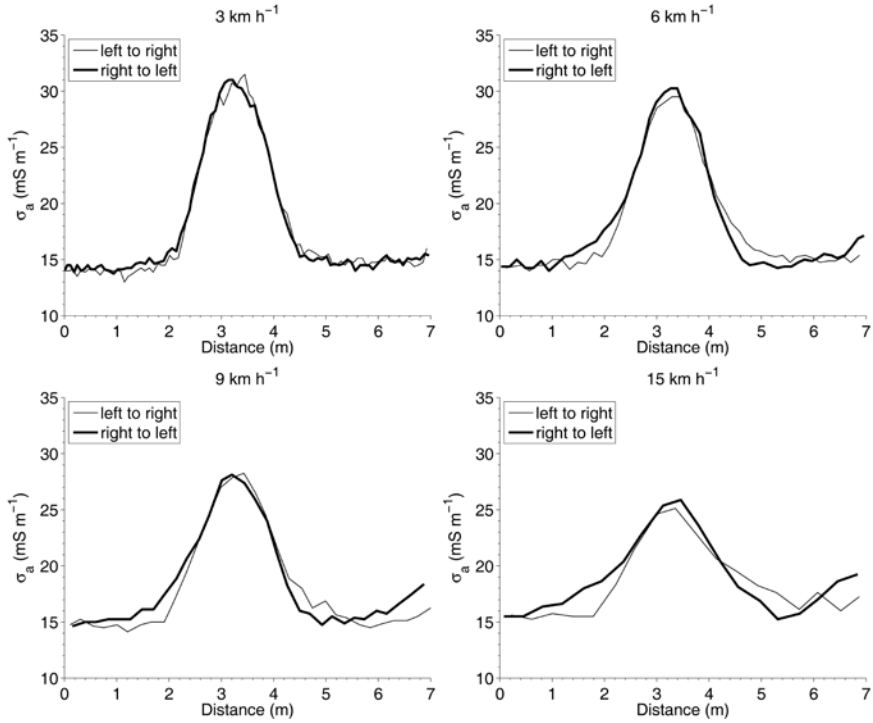

Figure 3.8 Two opposite tracks (left to right or right to left) over metal bars, showing (a) the effect of the driving speed on the decrease of the peak anomaly and (b) the asymmetry of the anomalies between opposite driving directions.

A new approach was successfully developed to monitor, and if necessary, correct the drift without the need to interrupt a survey. Just after calibration, measurements were recorded on a single line (from here onwards called the “calibration line”), which crossed all the survey lines to

be measured afterwards. Because this line was measured just after the calibration procedure, it could be assumed that its absolute values of conductivity and susceptibility were correct. After this, the survey was conducted without interruption. The procedure can be also extended to different fields, as long as the calibration line is the same over all fields and recorded within a relatively short period.

A program was written to process the data; this comprised the following steps. First, the measurements of the calibration line were selected interactively by the user. Then, the measurements of the survey lines were searched for those within a close distance to the reference measurements (e.g. 0.3 m). In this way, pairs of readings were found of the calibration and survey lines at almost the same position. The difference between each pair of survey and calibration values could then be plotted in function of the time when the survey measurement was taken (Figure 3.9).

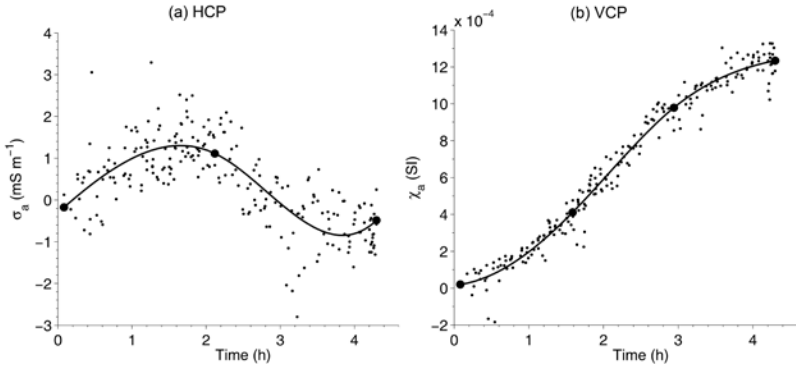

Figure 3.9 Drift of the EM38DD measurements during a 4.5 hours survey of an 8 ha field. The points are the drift data, modelled by a piecewise polynomial curve. The large dots indicate the knots between two polynomial functions.

If all survey lines were crossed by the calibration line, an estimate of the drift was given for each survey line. The calibration line can also cross the survey lines several times, but sometimes this causes the drift to occur in the calibration line itself (especially apparent for large sites).

If the drift was found to be substantial (e.g. more than twice the noise level of the sensor), it could be corrected. Due to the inherent noise on the drift plot, a smooth model was necessary. A piecewise polynomial function of third degree (or cubic spline) was found as the best option to model the drift. This procedure fitted several polynomials using least

squares minimization with the restraint that two adjacent polynomials have to be continuous at the knots (continuous first and second derivatives). The best-suited number of polynomial functions depended on the survey conditions and therefore had to be chosen by the user. The piecewise polynomial function could model relatively abrupt changes, but still preserved the continuity in the data. Other models such as kernel smoothing did not produce good results. The fitted model was then used to correct all the survey data, using the time stamp of each measurement. Finally, the calibration line was removed from the survey data.

In the example given in Figure 3.10, the drift of the conductivity was not very large compared to the noise level of 0.5 mS m^{-1}. Therefore, in this case, the small drift did not really disturb the data (but sometimes the drift can attain several mS m^{-1}, which can mask weak traces). The susceptibility suffered a lot from drift, which was substantially higher than twice the noise level of 4×10^{-5} (SI). Actually, it obscured most of the map (Figure 3.10b). After drift correction, several large features became visible (Figure 3.10c). However, if the model does not fit the data perfectly, striping parallel to the driving direction can occur as can be seen in the northeast corner of the field.

3.4 Filtering of local extreme values

Local extreme values of FDEM sensor measurements are mostly caused by small, metal objects close to the soil surface. It is often surprising how many metal objects can be found on a field. Sometimes they are of archaeological interest, such as coins. In other cases they can be UXO's (especially in Western Flanders), but often they are just recently dumped waste such as drinking cans or pieces of agricultural machinery. Whether the objective is to detect these metal objects or to map other archaeological structures, in both cases it is interesting to identify and extract these extreme values.

Measurements can be extreme at a local scale, but still lie in the middle of the range of values of the total survey. Therefore, to identify an extreme measurement, it has to be evaluated within a local neighbourhood or search window (e.g. a circular search radius, or all measurements within a maximum distance).

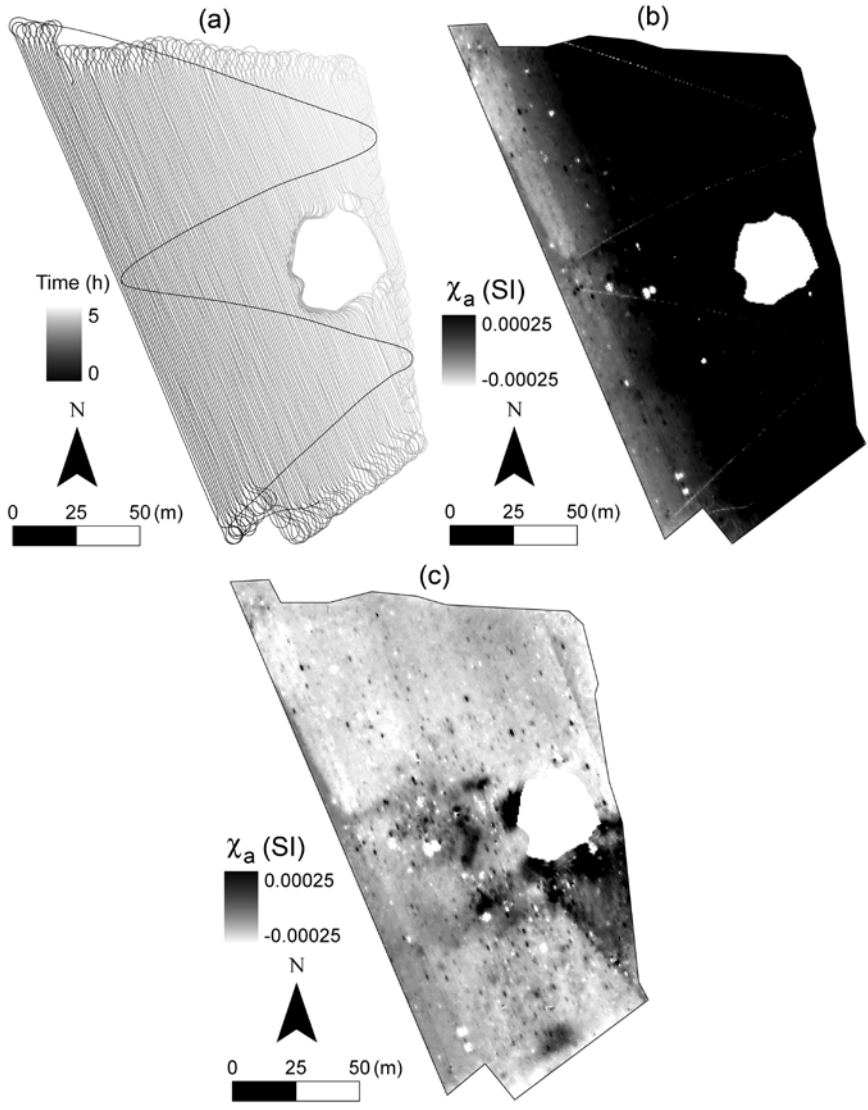

Figure 3.10 Drift correction of data on an 8 ha field: (a) survey lines with the calibration line (the survey time is shown in grey-scale); (b) susceptibility measurements before drift correction and (c) Map after drift correction.

The size of the search window is arbitrarily defined, but has to be large enough to contain enough measurements so that the evaluation is stable enough; but not too large so that the value range will exceed the local extreme value. The criterion to identify whether a value is extreme or not is determined by a parameter similar to a z-score, which is calculated as:

$$z = \frac{|x - m|}{\sigma} \,, \tag{3.1}$$

with x the measurement value, m the mean and σ the standard deviation of all the measurements within the search neighbourhood except x. For extreme measurements, z will be high compared to most other values. Then, an arbitrary threshold for z is chosen, above which the values are considered extreme (as a default, 2 is often a good choice). The measurements with values above the threshold are removed from the original data.

The filter is demonstrated using the same field data as in Figure 3.10 (Figure 3.11a). A search radius of 2.975 m or 3.5 times the line separation of 0.85 m was chosen and a threshold of 1.5. The filter removed most of the local peaks, leaving the larger structures easier to interpret (Figure 3.11b). The extremes can be easily revealed by taking the absolute value of the difference between the original and the filtered maps (Figure 3.11c). Naturally, by adjusting the search neighbourhood or the threshold, more or less values will be filtered.

3.5 Interpolation

The motorized platform records measurements and GPS-locations simultaneously. Although the driving lines are almost parallel using the lightbar guidance system, the coordinates are not on a fixed grid.
Therefore, the measurements need to be interpolated. Usually, a number of measurements are selected within a local neighbourhood around the unknown grid position (such as a circular area within a certain distance from the position). A basic interpolation method is to take the mean of all the measurements within this area. In this case, all the measurements receive equal weight. If the locations of n number of measurements is $\mathbf{x}_i$ with their values $Z(\mathbf{x}_i)$ and $\mathbf{x}_0$ the location of the unknown value $Z^*(\mathbf{x}_0)$, then its value is calculated using the weights w_i as follows:

$$Z^*(\mathbf{x}_0) = \sum_{i=1}^{n} w_i Z(\mathbf{x}_i) \,. \tag{3.2}$$

The sum of the weights has to be equal to 1.

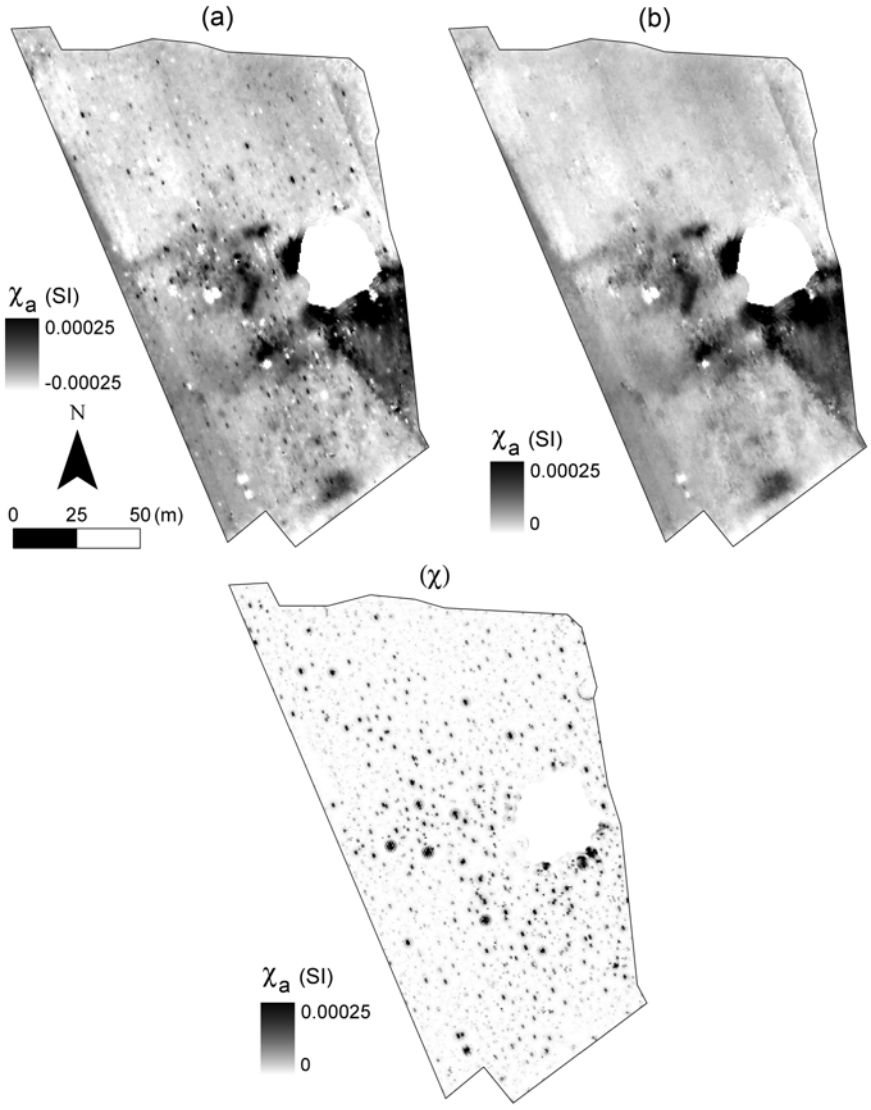

Figure 3.11 (a) Original map, (b) map at the same scale after filtering and (c) the absolute difference between the original and the filtered maps.

Interpolation methods differ in the way the weights are attributed to the measurements. Standard interpolation routines in spatial data programs (e.g. geographical information systems or GIS) are “inverse distance to a power”, “nearest neighbour” or “ordinary kriging”. “Local polynomial regressions”, such as “cubic splines”, are not interpolation methods in the strict sense, but these methods are often used to create smooth grids. The weights of the “inverse distance to a power method” are determined by

the distance d_i between the unknown location and the measurement locations and a user-defined power r:

$$w_i = \frac{d_i^{-r}}{\sum_{i=1}^{n} d_i^{-r}}. \tag{3.3}$$

The logic behind inverse distance weighting is that the closer the measurements are to the location of the unknown, the better it will resemble the value at this location. However, there are some problems associated with methods such as inverse distance weighting. The methods do not account for the spatial distribution of the data, which can be very problematic in clustered data. This is particularly troublesome with sensor measurements obtained with the motorized platform. Many more measurements are recorded along a line than cross-line, creating sometimes a large striping effect after interpolation.

Kriging is a method that accounts for unevenly spaced data, by attributing less weight to clustered measurements than to evenly distributed measurements [70]. Moreover, it accounts for the spatial structure by using a variogram model to attribute the weights. To obtain the variogram model, first the variogram values γ are calculated between n pairs of measurements, which are separated by a distance $\mathbf{h}$ (called the "lag"):

$$\gamma(\mathbf{h}) = \frac{1}{2n(\mathbf{h})} \sum_{i=1}^{n(\mathbf{h})} [Z(\mathbf{x}_i + \mathbf{h}) - Z(\mathbf{x}_i)]^2 . \tag{3.4}$$

The variogram plot of these values for an increasing lag distance provides a model of the spatial structure. As an example, the variogram was calculated of susceptibility measurements that were conducted on a site with a motte and bailey, which was later transformed into a castle. The site was measured with the motorized platform, using a 0.85 m distance between tracks and approximately 0.14 m distance between readings along the tracks (Figure 3.12).

The variogram showed a continuously increasing value, indicating that measurements at increasing separations were less similar than closely spaced data. In this case, the variogram did not reach a maximum value (called the "sill"), because the size of the study field did not allow a large enough lag to attain the distance where the sill is reached (called the "range"). However, the linear model did not pass through zero for lag

distances close to zero, which in theory it should. This variogram value is called the “nugget effect” and is caused by noise in the data.

A mathematical model is then fitted to the variogram plot, which is used to attribute weights to the measurements. The problem with ordinary kriging is that the variogram model is obtained using all the measurements of the survey (global variogram). This is actually an average variogram that does not always correspond to the local spatial structure. Often the variogram is different depending on the location (non-stationary) [71]. In archaeological prospection this can be particularly troublesome, since sometimes a large field is mapped that has local anomalies in a small part of the field. In this case, the variogram characteristics at the local scale can be very different from the global variogram. For this reason, kriging with local variograms was developed [72, 73], where the variogram is calculated in a local neighbourhood around the grid location. This kind of approach is only useful for large datasets, providing a sufficient number of measurements in the local neighbourhood.

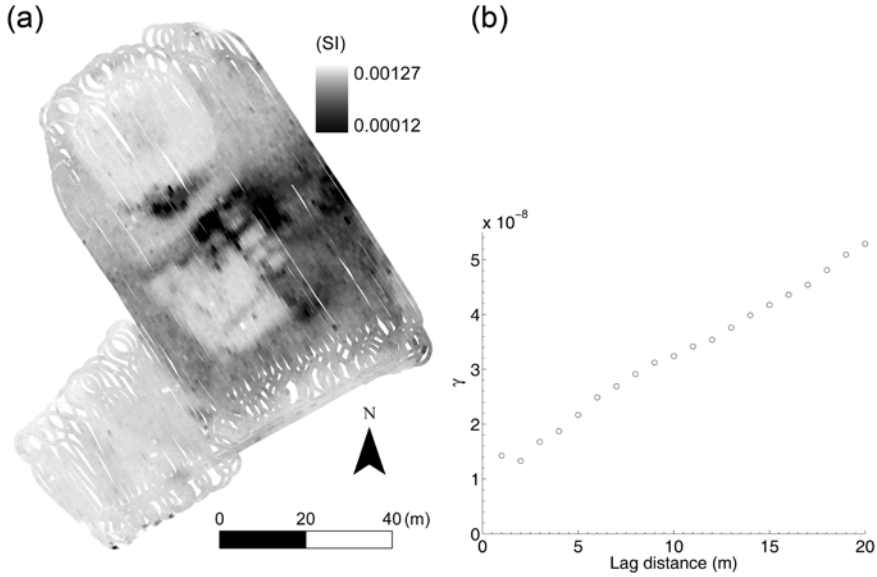

Figure 3.12 Susceptibility measurements plotted as dots, indicating the remains of a castle (a); Variogram of the same data with a 1 m lag distance.

To demonstrate the difference between global and local variograms, the global variogram was compared with local variograms, calculated at three positions with different spatial structures (Figure 3.13). The neighbourhoods were chosen as circular areas with a radius of 4.25 m,

which was five times the cross-line distance (thus including readings from approximately 10 lines). The maximum lag distance was equal to the radius, thus half of the search area diameter. The first neighbourhood was chosen in a relatively homogenous area, the second in an area with some linear structures, while the third had some structures with very high values. The four variograms made clear what the problem is when a global variogram model is used (Figure 3.14). The local variograms were very different from the global variogram, since they represented different spatial structures.

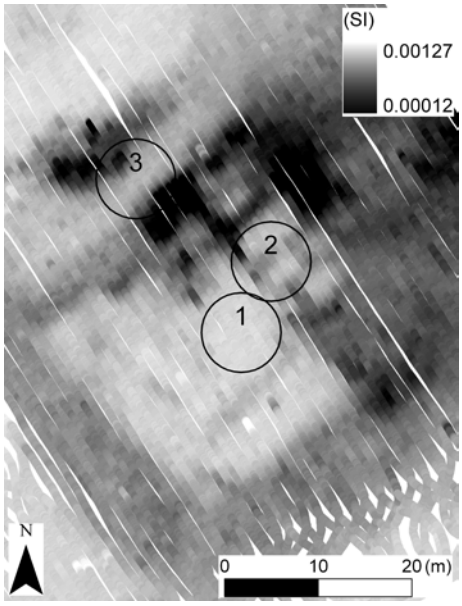

Figure 3.13 Three positions where the local variograms were calculated, within circular neighbourhoods with a 4.25 m radius.

Kriging with local variogram modelling normally starts with choosing one model type, which is then automatically refitted for each search window using, for example, a least squares minimization criterion. The problem with this approach is that one type of model cannot fit all local variograms well, because of their large variation in shape. One solution could be to fit several types of models and select the best fitting model type for each local variogram, but this would cost large amounts of computation time and it is difficult to keep the automatic fitting procedure stable. Another option is to fit a linear model without a sill as in Figure 3.14. Although not all variograms are fitted perfectly, overall the linear model is adequate to capture the local spatial structure. The linear model

without a sill or a nugget has the interesting characteristic that its slope does not influence the calculation of the kriging weights. The reason for this is the condition that the sum of all weights should be equal to one, which scales the variogram values back to the same weights regardless of the slope of the linear model. Therefore, in the case where the nugget and the sill are neglected, there is no need to calculate the variogram model. This seriously reduces the computation time.

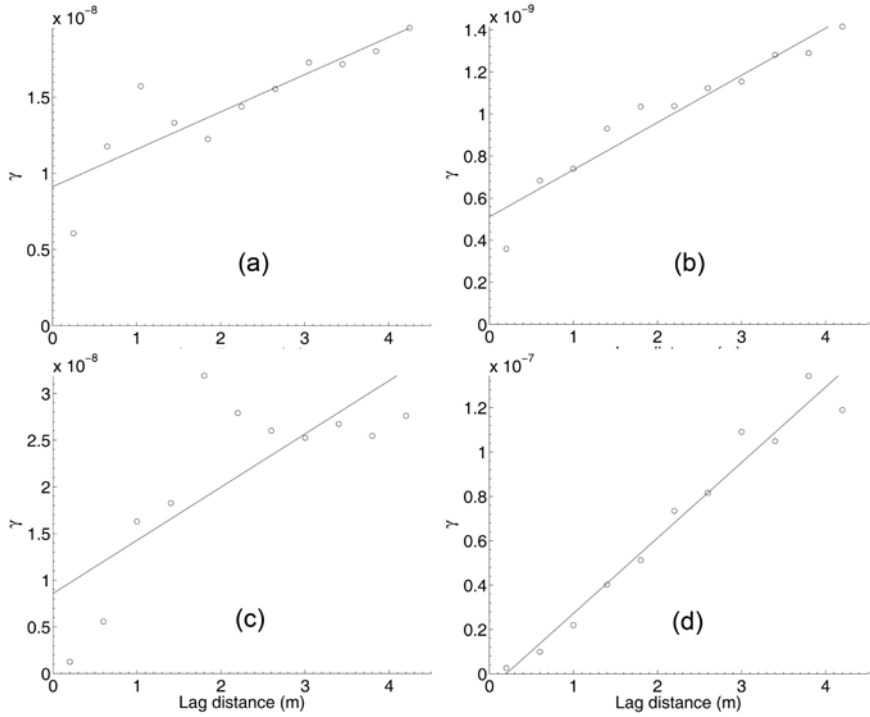

Figure 3.14 (a) Global variogram with linear model; (b) local variogram at position 1, (c) at position 2 and (d) at position 3, fitted by linear models without a sill.

Although the distance is then used as the only input to calculate the weights, there is still an important difference between kriging and inverse distance interpolation. Kriging involves the solving of a set of equations to obtain the weights w_j:

$$\sum_{j=1}^{n} w_j \gamma(\mathbf{x}_i - \mathbf{x}_j) + \psi = \gamma(\mathbf{x}_i - \mathbf{x}_0) \text{ for } i = 1...n \text{ and}$$

$$\sum_{j=1}^{n} w_j = 1. \qquad 3.5$$

The second summation is to ensure that all weights are equal to 1[1]. The variogram value at the right hand side of the first summation is based on the distance between a measurement and the unknown value at position $\mathbf{x}_0$, which is to be interpolated. On the left hand side, the variogram is based on the distance between the measurements. Because of this, measurements that are close to each other (clustered) will receive less weight than measurements that are more spread out. This difference was clear when maps of the different interpolation methods were compared (Figure 3.15). The inverse squared distance map looked similar to the local kriging map, but it suffered from striping parallel to the line direction. The map interpolated with inverse distance to a power of one smoothed the striping away, but the detail of the structures were smoothed as well.

Looking at the global variogram (calculated for the whole field), the linear variogram model could be accepted without a sill; but the nugget effect could not be neglected. This nugget effect was also not constant over all the locations of the field (in other words it was non-stationary). Therefore, the interpolation could be improved by using local variogram calculation and fitting a linear model with a nugget. A higher nugget (caused by more noise) will give a similar weight to all measurements in the search window, and therefore produce a smoother interpolation. If a clear spatial structure is present with a small nugget, more weight is given to closeby measurements, thus the smoothing will be less.

Kriging with a global variogram produced a smoother map at all locations than the map produced with the linear model without a nugget or sill (Figure 3.16). Some local noise was removed, which improved the clarity of the anomalies. However, small-scale structures were blurred by the smoothing; i.e. the edges became less sharp. A good compromise was the map interpolated with a locally varying linear model with a nugget. At locations where there was only noise around a more or less stable mean, the noise was smoothed due to the nugget effect of the linear model. Near locations with clear spatial structures, the smoothing was less and the edges of the structures were sharp.

There was no great difference between the maps interpolated using a linear model with a nugget or a linear model without a nugget.

---

[1]The parameter ψ is a Lagrange multiplier.

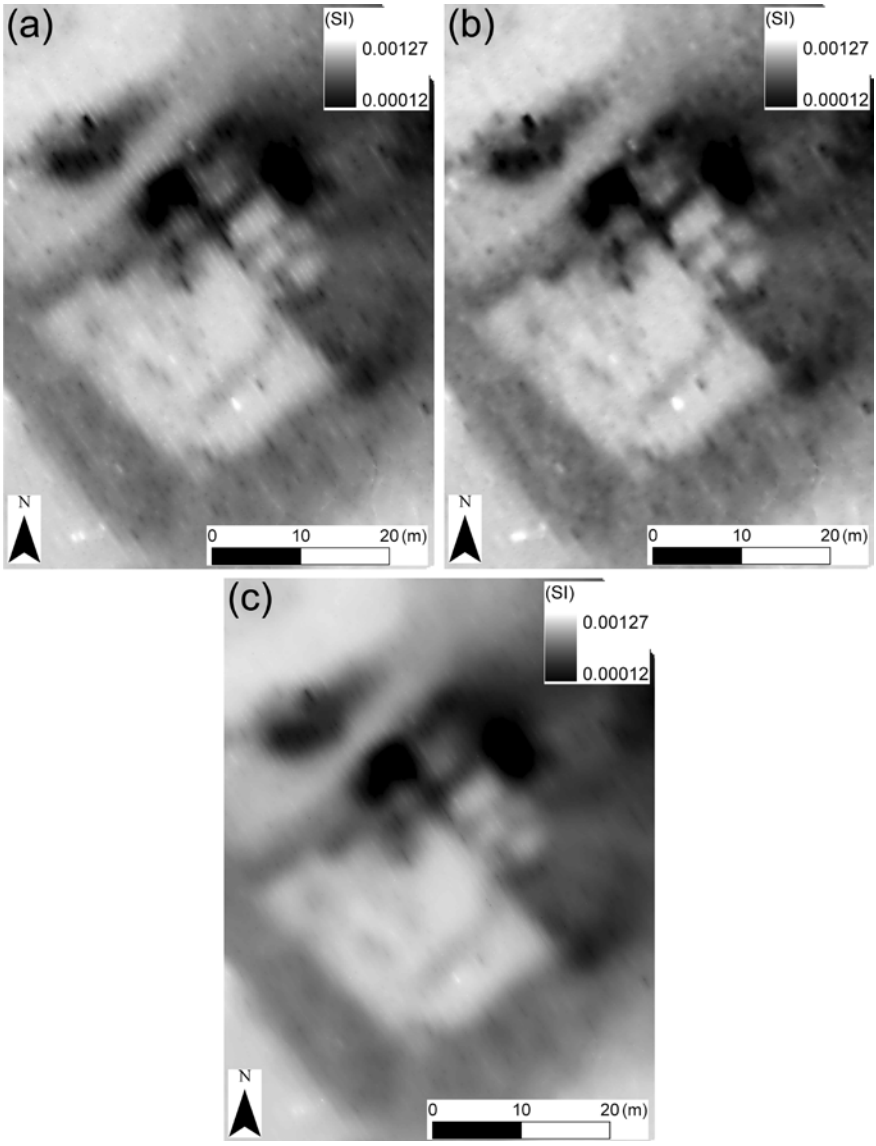

Figure 3.15 (a) Interpolated measurements with inverse squared distance (power 2), (b) local kriging with a linear variogram model without a sill or nugget and (c) inverse distance to a power 1. All maps are at the same scale.

Nevertheless, if one map was subtracted from the other, it became clear where the local variogram calculation made a difference. The linear model without a nugget produced sharp maps and the global model was suitable to produce a smoother map. On occasions where clear spatial structures are present at some locations of the site together with severe

noise, the local linear model would probably be the preffered method. However, the computing time to calculate the local variogram interpolation was 19 times longer than the other two methods (to calculate this example it took 13 hours on a Pentium 4 desktop processor).

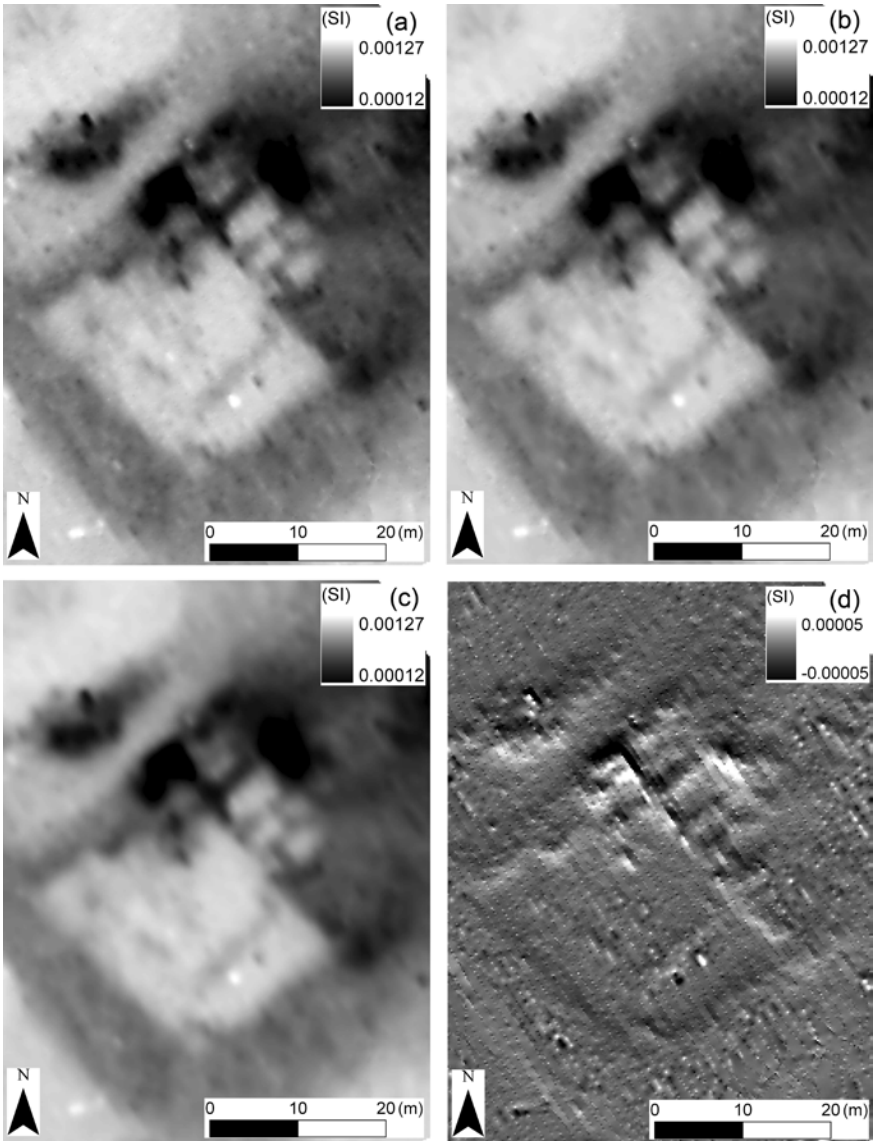

Figure 3.16 Interpolated maps with local kriging: (a) linear model without a nugget, (b) local linear model with a nugget, (c) global linear model with a nugget and (d) the difference between maps (a) and (b).

Chapter 4

Sensitivity of the magnetic susceptibility response[1]

4.1 Abstract

Magnetic susceptibility is an important indicator of anthropogenic disturbance in the natural soil. The change in this property is often mapped with magnetic gradiometers in archaeological prospection studies. It is also detected with FDEM sensors, which have the advantage that they can simultaneously measure the electrical conductivity. The detection level of FDEM sensors to magnetic structures is very dependent on the coil configuration. Apart from theoretical modelling studies, a thorough investigation with field models has not been conducted until now. Therefore, the goal of this study was to test multiple coil configurations on a test field with naturally enhanced magnetic susceptibility in the topsoil and with different types of structures mimicking real archaeological features. Two FDEM sensors were used with coil separations between 0.5 and 2 m and with three coil orientations. First, a vertical sounding was conducted over the undisturbed soil to test the validity of a theoretical layered model, which can be used to infer the depth sensitivity of the coil configurations. The modelled sounding values corresponded well with the measured data, which means that the theoretical models are applicable to layered soils. Second, magnetic structures were buried in the site and measured at a very high resolution. The results showed remarkable differences in amplitude and complexity between the responses of the coil

[1]Modified from: Simpson D, Van Meirvenne M, Lück E, Rühlmann J, Saey T, Bourgeois J. Sensitivity of multi-coil frequency domain electromagnetic induction sensors to map soil magnetic susceptibility. Submitted to the *European Journal of Soil Science*, April 2009.

configurations. The 2 m horizontal coplanar and 1.1 m perpendicular coil configurations produced the clearest anomalies and resembled best a magnetic gradiometer measurement.

4.2 Introduction

Although the measurement of the magnetic susceptibility with FDEM sensors was explored decades ago [47], most archaeological prospections only apply the conductivity response of the FDEM sensor. A possible reason for this is the difficult interpretation of the susceptibility response, which can produce completely different results depending on the coil configuration of the instrument and the depth of the target [5]. Another difficulty is the occurrence of both positive and negative anomalies for some coil configurations, which are related to a change in sign of the susceptibility response at a certain depth [4]. But when the response of the different coil configurations is well understood, it can be used to deduce the magnetic susceptibility variation in the soil profile [74].

FDEM-responses as a function of depth were derived for a homogeneous medium [50, 52] and these equations were further approximated for the conductivity [34] and the susceptibility response [48, 54]. Due to their simple, analytical form, the conductivity models were already frequently applied in soil science to reconstruct the soil profile with good results [57, 75]. However, case-studies using the depth-sensitivity models applied in a layered soil with varying magnetic susceptibility are rare. Therefore, it was not certain if these models are accurate enough to describe field measurements.

Structures with horizontal dimensions in the range of the coil separation cannot be modelled using a layered approach; in this case 3-D models are necessary which take lateral variations into account [61]. The effect of the coil orientation for a coil separation of 1.5 m was evaluated with theoretical 1-D and 3-D models, where the PERP and VCP orientations had a deeper exploration depth for the magnetic response than the HCP orientation [4, 31]. In another study, both theoretical modelling and a field model were used to conclude that the magnetic response of Slingram-type FDEM sensors was less influenced by the soil electrical conductivity and had a better depth response than coincident loop instruments [76]. These studies were largely based on theoretical modelling,

because building prototype sensors and testing them on representative field models is difficult. Recently however, FDEM sensors with multiple coil separations and orientations were developed, making a detailed field study possible. No such comparison between different sensor configurations was performed until now.

This study aimed to test the spatial sensitivity of different coil configurations of FDEM sensors measuring the susceptibility. Both a layered soil model and small structures were investigated, but excluding metal objects. For this purpose, field measurements were conducted on an experimental site with magnetic structures of different sizes and shapes, resembling typical archaeological features. The response of the undisturbed soil was simulated based on the analytical, layered models. With this experiment, the goal was to answer two specific research questions: (1) are the theoretical, layered models well correlated with the field measurements for different coil configurations? (2) What is the sensitivity of each coil configuration for both layered soils and 3-D artefacts?

4.3 Vertical sounding on a layered soil

The test site was located at the Institute of Vegetable and Ornamental crops in Grossbeeren (Germany). The soil consisted of glacial till deposits, dominated by coarse sand. Therefore, the conductivity was in general very low, less than 10 mS m^{-1}. This was important because high conductivities can influence the IP response of the FDEM sensors [76]. A test strip of 200 by 10 m at the site was reserved for geophysical tests. Before the measurements, the soil surface was smoothened with a shallow cultivator to reduce the noise due to instability while moving the sensors.

To test the validity of the theoretical models for layered soils, a vertical sounding was conducted on an undisturbed soil with the DUALEM-21S in the HCP and the PERP orientations and with the EM38-MK2 in VCP orientation. The susceptibility of the soil profile was determined in a freshly dug pit nearby the sounding location with a handheld meter (Kappameter KT-6, SatisGeo, Czech Republic). The profile was measured several times at 0.1 m intervals down to 0.8 m depth, measuring the susceptibility at the contact surface of the sides and the bottom of the pit (Figure 4.1).

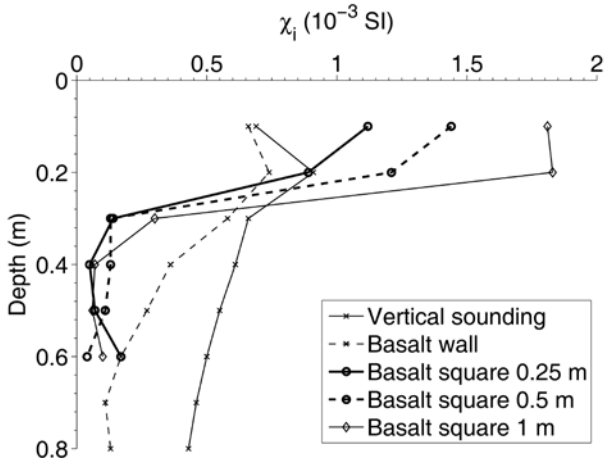

Figure 4.1 Susceptibility of different soil profiles at the test site, measured with a handheld meter. The freshly dug profiles were used where the structures were buried afterwards (the names of the structures are mentioned in the legend).

These values were then used to model the apparent susceptibility of the vertical soundings. The soil profile was divided in layers of 0.1 m according to the depths of the handheld measurements. The bottom of the deepest layer was assumed to be at infinite depth. The contribution of each layer to the total apparent susceptibility of the soil was calculated by multiplying the weight, based on the cumulative depth models, with the susceptibility of the layer.

The IP measurements of a FDEM sensor can suffer from a serious drift. This disturbed the vertical sounding measurements in two ways; the absolute values were different when the sounding was initiated and the measurements were changed during the sounding. To verify if any drift occurred during the sounding, each profile was measured from 2 m height down to 0 m and then repeated from 0 m to 2 m height (Figure 4.2). The drift was large relative to the sounding values, so it required correction. Therefore, two repeated readings at the same height were averaged to remove the drift. Then, to correct the absolute value error, the measurements were all shifted with a constant value, so that the readings at 2 m height corresponded with the modelled values.

The simulated sounding curves based on the profile values of Figure 4.1 were strongly related to the measured values of the two sensors (Figure 4.3). The best fitting coil orientation was the HCP. The PERP orientation was more noise sensitive, which explains why the measured

values were less precisely represented by the modelled curves. The measurements of the 1.1PERP were significantly higher than the curve for shallow layers. The VCP showed a slight decrease of the measured values between 0.5 and 1.5 m for both coil separations, which was not followed by the model curves.

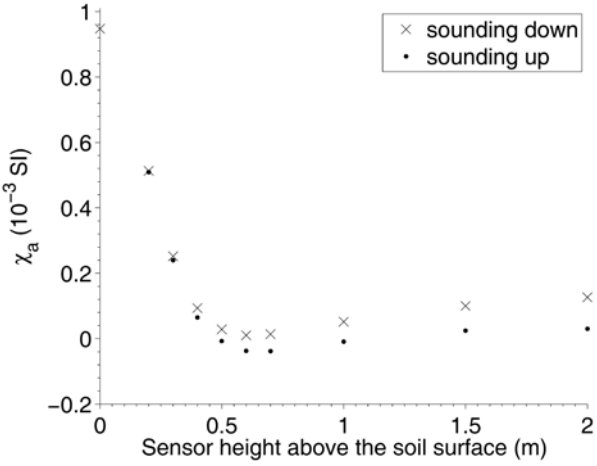

Figure 4.2 Difference between the 1 m HCP sounding measurements, measured from 2 m height downwards to 0 m and back upwards to 2 m height. The longer the time difference between two readings at the same height, the higher the difference was due to the drift.

Apart from these small deviations, the approximative, theoretical models of [48] follow closely the measured soundings in this low-conductive environment. Therefore, these analytical functions could be used to infer the depth sensitivity of the magnetic signals of FDEM sensors with different coil configurations. The change in sign from positive in shallow layers to negative in deeper layers in the HCP orientation was already mentioned by [4] as problematic for the depth response. The PERP-orientation also demonstrated a similar sign change, which was not mentioned by [4]. This sign change occured at a shallower depth than the sign change of the HCP response for the same coil separation. It is often proposed to lift the instrument above the inflection point, so that the sign change is effectively cancelled. However, lifting the sensor can considerably reduce the signal to noise ratio of the configurations with shallow depth sensitivity.

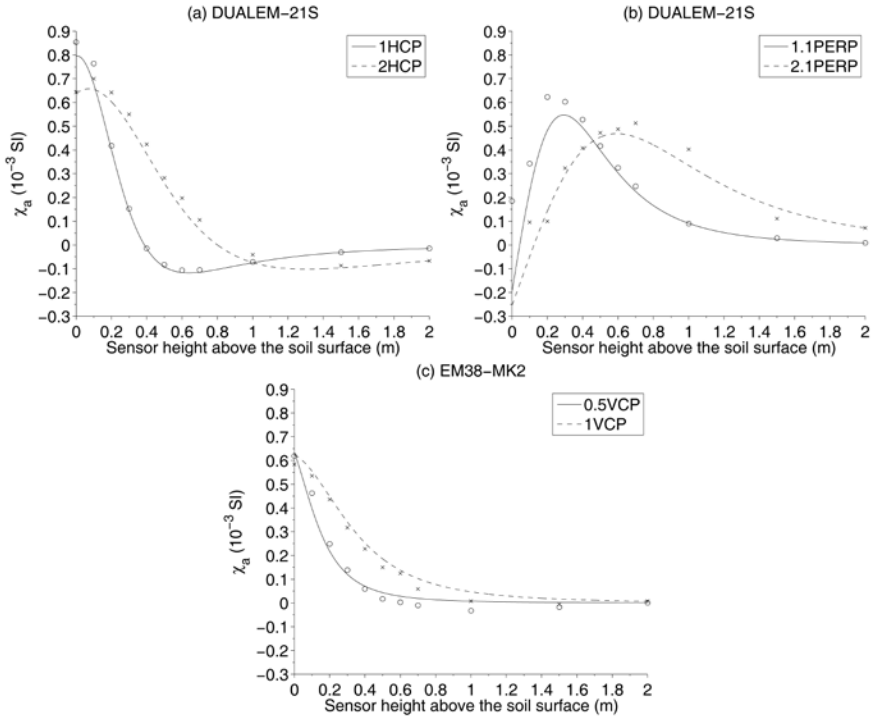

Figure 4.3 Vertical sounding measurements (marks) and theoretical models (lines). (a) HCP-orientation of the DUALEM-21S, (b) PERP orientation of the DUALEM-21S and (c) VCP orientation of the EM38-MK2.

4.4 Sensitivity to small 3-D structures

4.4.1 Field models

Four structures were buried in the test site, to approximate as closely as possible typical magnetic anomalies of archaeological interest, excluding metallic artefacts. The structures consisted of basalt stone powder, with a relatively high susceptibility (0.01 (SI)) compared to that of the average soil (in the order of 0.0005 (SI), Figure 4.1) and a conductivity of 50 mS m^{-1} (the soil conductivity was lower than 10 mS m^{-1}). First, a pit of 0.8 m depth, 5 m in length and 0.5 m width was dug perpendicular to the test strip, filled with the basalt up to 0.3 m depth and then the remaining 0.3 m was covered by the original topsoil. In this way, any change in the topsoil susceptibility was minimized. This structure mimicked linear artefacts often found at archaeological sites such as remains of walls,

ditches and roads. Therefore, this structure is referred to as the "basalt wall". In agricultural fields, the topsoil is commonly disturbed to a depth of 0.3 m by ploughing, so that most artefacts are preserved just under the plough layer. Before the pit was refilled, handheld susceptibility measurements were carried out at the bottom and sides of the pit surface at different depths. After filling the pit with the basalt, and refilling the topsoil, the susceptibility was measured at the surface with the handheld meter. Although the topsoil above the feature was mixed after the filling, the average susceptibility after mixing approximated the susceptibility of the undisturbed profile. The basalt powder was not contained in a box or other protection, so it was in direct contact with the surrounding soil. After some time, the structures will probably not remain intact due to e.g. bioturbation, but the measurements in this study were conducted some days after the structures were built, so they were still intact.

Three other structures were buried using the same procedure as the basalt wall, but with other dimensions. They were chosen to act as models for smaller artefacts such as a fireplace or a garbage pit. All three had a square shape and a thickness of 0.3 m, starting at 0.3 m depth. Their sizes were 1 by 1 m, 0.5 by 0.5 m and 0.25 by 0.25 m. These structures are referred to as "basalt squares". The positions of the basalt wall and squares were determined with the differential GPS.

Measurements were conducted with the DUALEM-21S and the EM38-MK2 on a cart, which was pushed at walking speed and georeferenced with the dGPS. The cross line distance was 0.25 m for the basalt squares and 0.5 m for the basalt wall. The inline measurement distances were on average 0.1 m. Both sensors were positioned at 0.2 m above the soil surface, thus 0.5 m from the top of the structures. One survey was also conducted with the DUALEM-21S at 0.5 m height in HCP-PERP orientation, so that the distance to the top of the structures increased to 0.8 m. All measurements were processed using the same procedures: (1) correction of the offset between the GPS antenna and the midpoint of the sensor coils, (2) noise filtering using a local search window, (3) interpolation with kriging to a grid with a 0.1 by 0.1 m cell size and (4) subtraction of the average background value (based on pixels at least 2 m away from the edges of the structures).

Finally, the site was also prospected with a Fluxgate Gradiometer (type FM18 of Geoscan, UK), measuring the 0.5 m vertical magnetic

gradient (expressed in nT/0.5 m). The instrument was manually operated, holding it at waist height (the lower sensor at approximately 0.4 m above the soil surface). The survey lines were laid out with tapes at a 0.5 m distance and measurements were recorded inline every 0.5 m distance at the basalt wall and every 0.25 m at the basalt squares, in a zig-zag mode. This sensor is often used in archaeological prospection and therefore served to evaluate the detection limits of the FDEM sensors.

4.4.2 Results

The magnetic susceptibility was higher in the organic topsoil for all five soil profiles (Figure 4.1), which is a naturally occurring phenomenon [15]. The profiles varied from smoothly declining values in depth to a sharp decrease between 0.2 and 0.3 m depth.

The different sensor configurations showed diverse responses to the basalt wall (Figure 4.4). The detection quality was based on three criteria: (1) maximum absolute deviation from the background value, (2) width of the anomaly parallel to the sensor and through the middle of the basalt wall, delineated by a detection level of 0.0001 (SI) (more than twice the noise level of the sensors) and (3) complexity of the response, evaluated by the sign (change) and asymmetry of the response.

The maximum absolute deviation was observed on the transects at the middle of the wall and at the middle of the basalt squares (Figure 4.4 and Figure 4.5). These values were then ranked for the different configurations (Figure 4.6). The overall order of the configurations was similar for the basalt squares and the basalt wall. The 2HCP, 1.1PERP and 2.1PERP configurations at 0.2 m height produced the highest deviation. The 1VCP and 2VCP responses had intermediate deviations and the 1HCP, 0.5HCP and 0.5VCP configurations produced weak responses to the basalt wall. An important finding was that the HCP configurations had the strongest response for the 2 m coil separation but the lowest response for the 1 m and 0.5 m coil separations after the 0.5VCP. The sensor responses were also ranked based on the second criterium, which is a measure of the compactness of the anomaly (Table 4.1). A more compact anomaly will results in a sharper delineation of the structures. Except for the DU2HCP, the larger coil separations had a wider anomaly in the direction parallel to the sensor. Overall, the HCP orientation was more compact than the VCP and the VCP was more compact than the PERP.

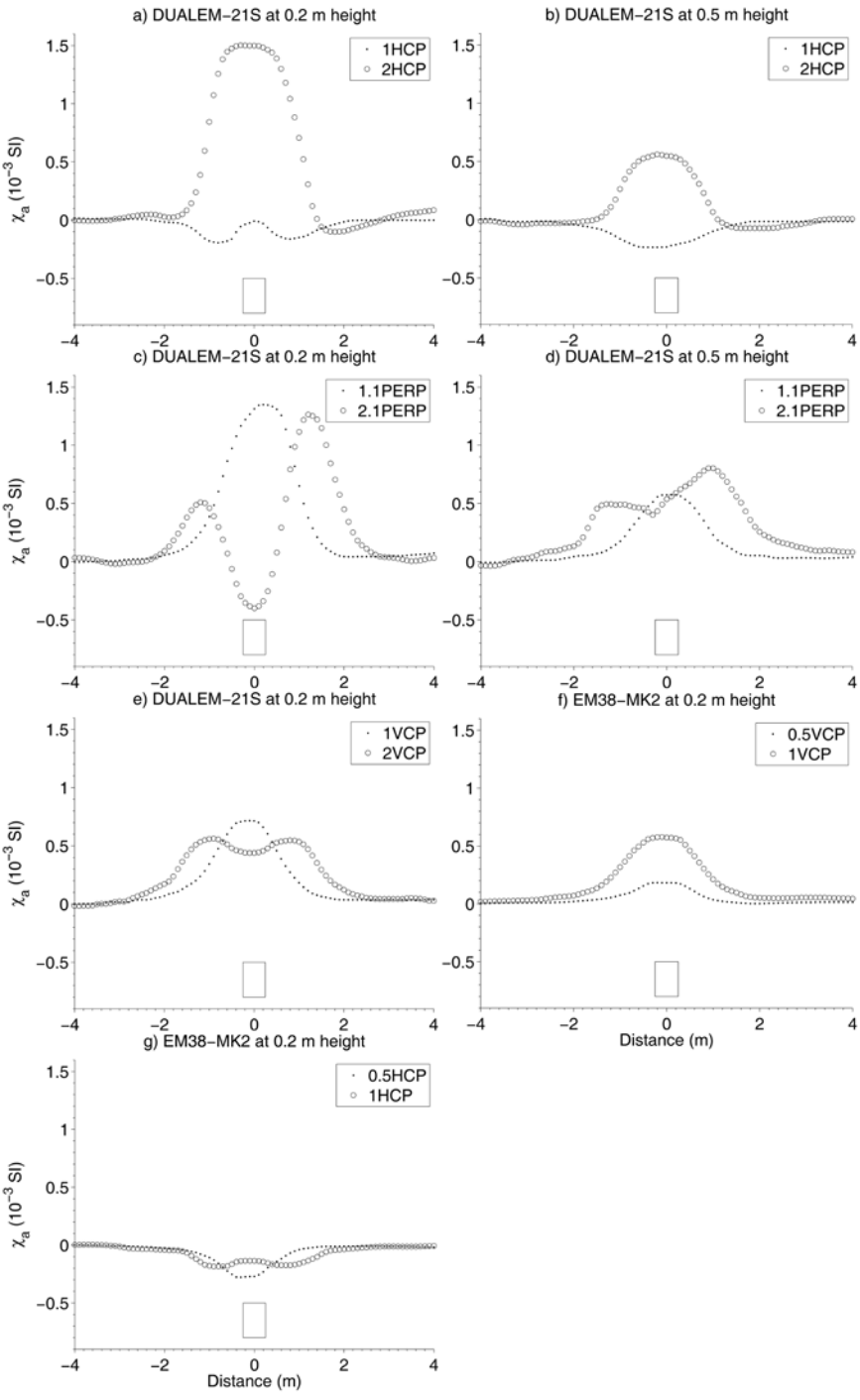

Figure 4.4 Transect through the middle of the basalt wall. The rectangle indicates the horizontal dimension of the wall.

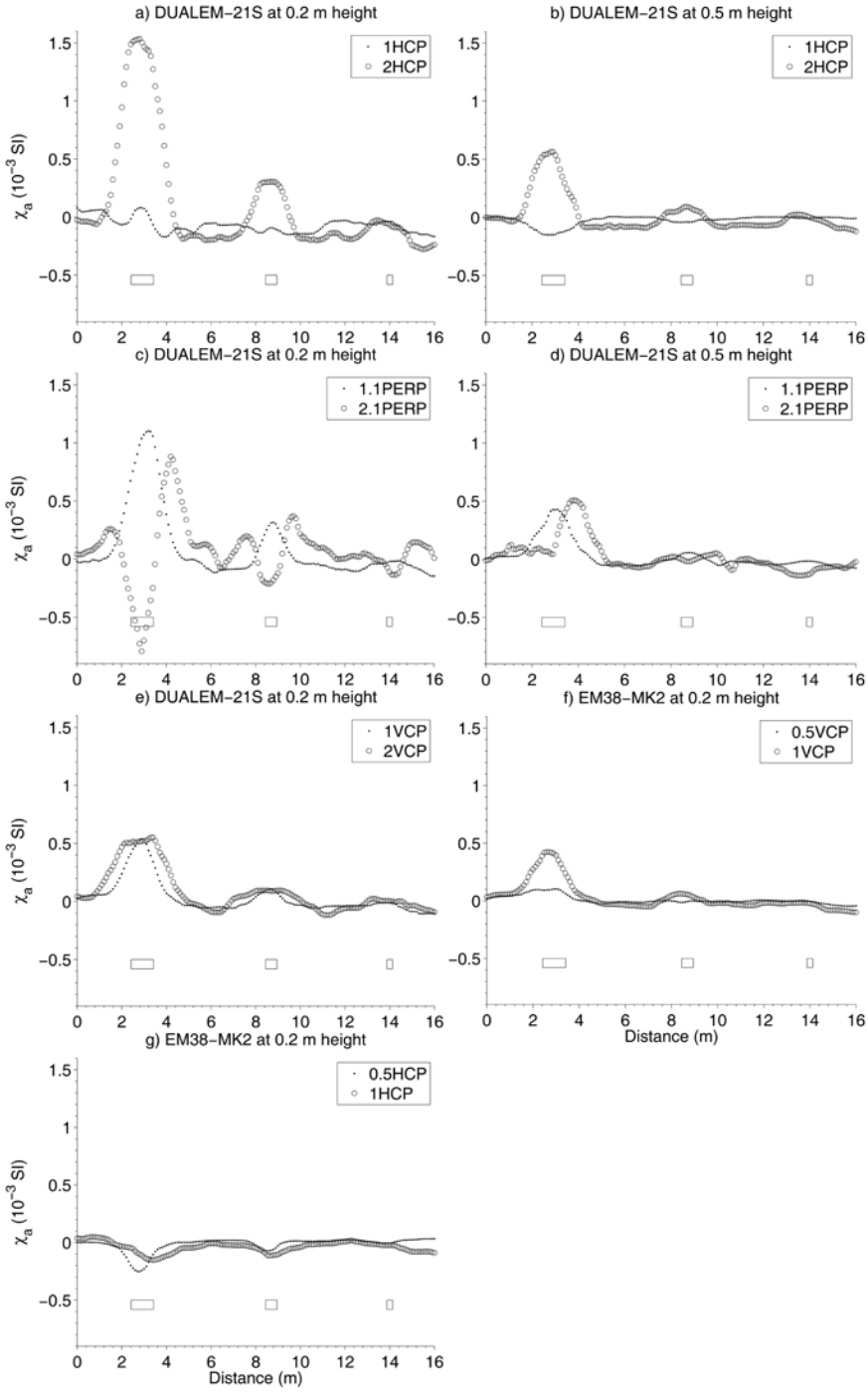

Figure 4.5 Transect through the middle of the basalt squares. The rectangle indicates the horizontal dimension of the wall.

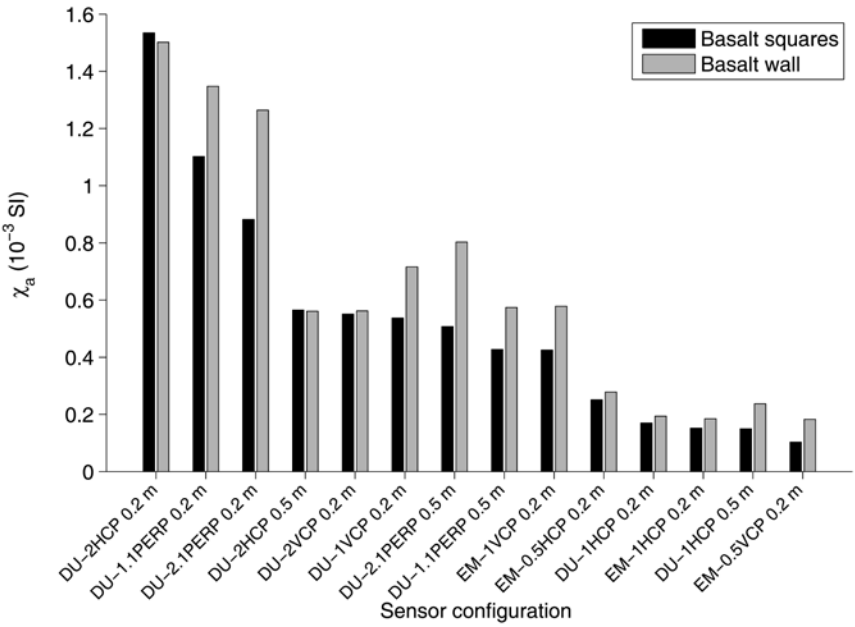

Figure 4.6 Maximum absolute deviation from the background susceptibility for the different sensor configurations. The abbreviations EM and DU refer to the sensors EM38-MK2 and DUALEM-21S sensors.

The third criterion can be evaluated visually from the transects shown on Figure 4.4 and on Figure 4.5. The 2.1PERP anomaly was asymmetric and drastically changed sign over the structures, making it more difficult to interpret. This is in accordance with Tabbagh (1986) who investigated a 1.5 m PERP configuration at 0.15 m height. On the contrary, the 1.1PERP was symmetric and did not show any sign change at either heights. Both the VCP and HCP orientations were symmetric, as expected. The HCP orientation displayed a sign change at 0.2 m height for the small coil separations of 0.5 and 1 m, while the sign change was negligible for the 2 m separation. This probably explains the very weak response of the small coil separations compared with the 2 m separation. For layered media, the response of a shallow structure can be partly positive and partly negative, so that they cancel each other out. Raising the instrument to a certain height can eliminate the positive response (see Figure 4.4b for the sensor height of 0.5 m above the soil surface), but this also reduces the overall signal to noise of the response. The VCP orientation did not suffer from any sign change; only the largest coil separation (2 m) showed two maxima instead of one.

Table 4.1 Horizontal width of the basalt wall anomalies for the different sensor configurations.

Coil configuration	Sensor height (m)	Anomaly width (m)
EM-0.5VCP	0.2	1.4
EM-0.5HCP	0.2	1.7
DU-2HCP	0.5	2.2
DU-1HCP	0.5	2.4
DU-1HCP	0.2	2.6
DU-1.1PERP	0.5	2.7
DU-2HCP	0.2	2.8
EM-1HCP	0.2	2.8
DU-1VCP	0.2	3.0
EM-1VCP	0.2	3.2
DU-1.1PERP	0.2	3.3
DU-2VCP	0.2	4.4
DU-2.1PERP	0.2	4.5
DU-2.1PERP	0.5	5.5

Finally, the maps of all the sensor configurations were plotted in the same value scale (Figure 4.7). This allowed to evaluate the anomalies visually in two dimensions. At 0.2 m height, the 2HCP and 1.1PERP configuration appeared to give the clearest response to the basalt squares. The 2.1PERP response was very strong, and even detected the square structure with a 0.25 m width, but its anomalies were complicated by positive and negative responses. The 1VCP response was weaker but it was very compact and well centred on the location of the structure. The 2VCP anomaly was elongated in the sensor direction. At 0.5 m height, the 1HCP was more successful in detecting the structures, because the positive response was eliminated which strengthened the negative response. The 2HCP and 1.1PERP were able to detect the 1 m and 0.5 m sized basalt squares. The 0.25 m square was only weakly visible. Overall, lifting the instrument, and thus increasing the distance to the structure seriously reduced the detection level.

The gradiometer detected the basalt squares well, but also here the smallest structure was less clear.

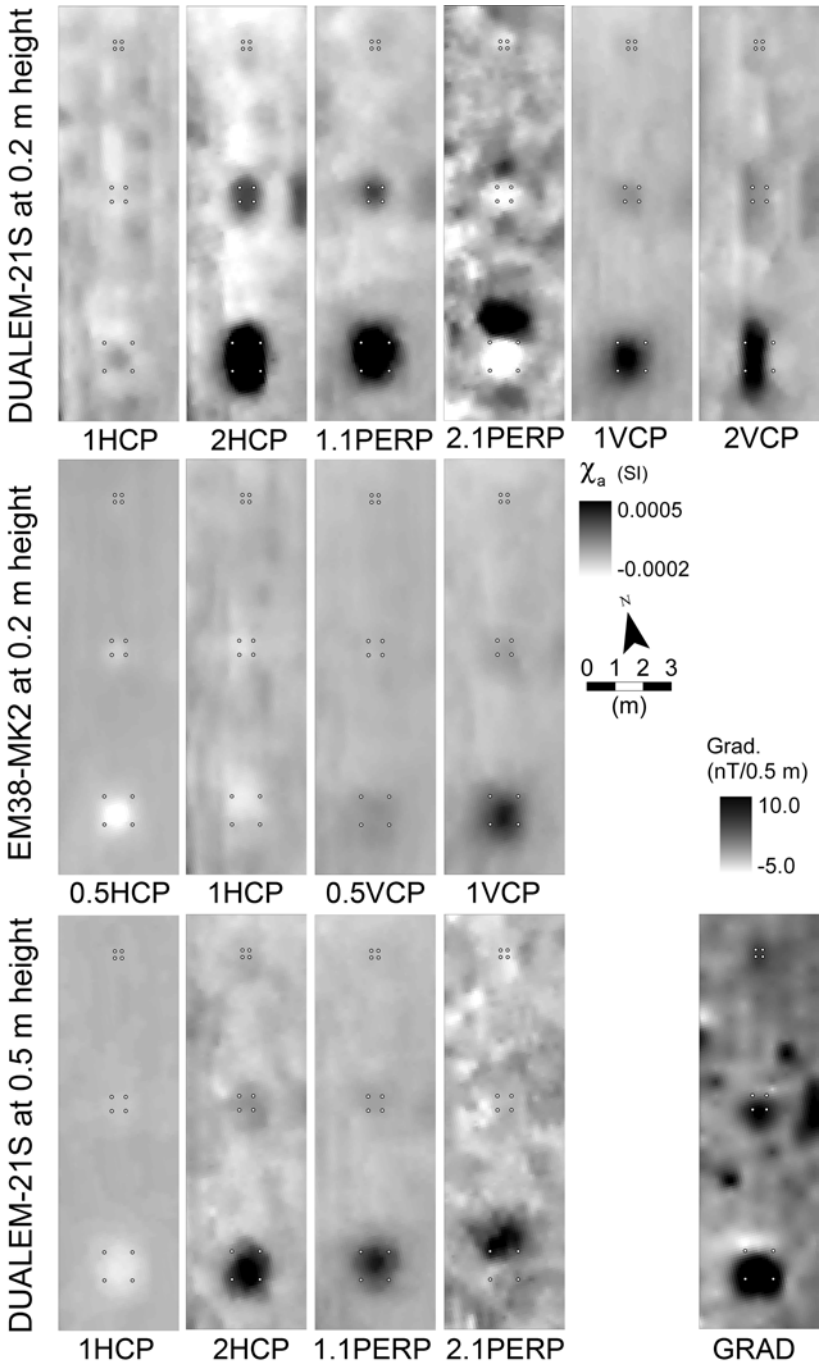

Figure 4.7 Maps of the sensor configurations, in the same value scale, and of the gradiometer. The corners of the three basalt squares are indicated by dots.

As expected from gradiometer surveys at latitude 51° north, the positive anomaly was slightly shifted to the south, accompanied by a small negative anomaly to the north [8]. Apart from the anomalies that were caused by the basalt squares, there were some other anomalies visible on the gradiometer map of unknown origin, for example to the east of the square structure with a 0.5 m width. Considering these anomalies, the 2HCP map resembled best the gradiometer measurements.

4.5 Conclusions

Since the layered models fitted well with the measured vertical soundings of the FDEM sensor configurations, they can be used to describe the depth sensitivity of each configuration. An important aspect of the IP measurement is the sign change that occurs in both the HCP and PERP orientation at a depth depending on the coil separation. For the HCP, this sign change seems to be mostly disturbing for small coil separations, while the 2 m separation is less affected. The VCP response is entirely positive, making the interpretation of the anomaly a lot easier.

The detection of small, archaeological structures with a magnetic susceptibility contrast was highly variable between different coil configurations of the FDEM sensors. Taking into account different criteria for the quality of the anomalies, the 2HCP and 1.1PERP configurations showed the best results. These configurations were the only ones to reach a quality on a par with the gradiometer measurements. The HCP orientation with the smaller coil separations was very poor in detecting the structures. The VCP configurations showed a symmetric and one-directional response, but the anomaly of the 2VCP was relatively wide.

Chapter 5

Magnetic survey of a 17th century castle[1]

5.1 Abstract

This study aimed to evaluate different configurations of a FDEM sensor, the EM38DD (Geonics Limited, Canada) with Fluxgate Gradiometer measurements on an archaeological site. The selected site was a pasture field surrounded by a large square ditch, containing the remains of brick castle built in the beginning of the 17th century. The castle was demolished in 1876 and its materials reused for other buildings in the area. The results of the first survey with a FDEM sensor showed very strong magnetic anomalies in the central field; they were caused by the brick remains of the castle. A smaller area was chosen within this field to compare the different configurations of the FDEM sensor with the gradiometer in the same measurement resolution. The most useful results with the FDEM sensor were obtained from the susceptibility measured in VCP orientation. Its anomalies corresponded well with the gradiometer anomalies. The gradiometer anomalies were sharper defined than the FDEM-anomalies, but were complicated by the bipolar response pattern. The susceptibility map in HCP orientation was very difficult to interpret, because both positive and negative anomalies were present. The wall remains were not visible in the conductivity map measured in the HCP orientation, but other structures such as a ditch were detected.

[1]Modified from: Simpson D, Lehouck A, Verdonck L, Vermeersch H, Van Meirvenne M, Bourgeois J, Thoen E, Docter R 2009. Comparison between electromagnetic induction and Fluxgate Gradiometer measurements on the buried remains of a 17th century castle. *Journal of Applied Geophysics* 68, 294-300.

5.2 Introduction

Although FDEM sensors and magnetic gradiometers are both capable of measuring contrasts in magnetic susceptibility, the latter sensor is usually preferred for archaeological prospection. In fact, it is very difficult to evaluate which sensor works best, because many parameters are involved in both measurements that can influence the quality of the survey, such as measurement resolution, sensor orientation and coil configuration (FDEM). Case-studies applying both sensors at the same location are scarce. Moreover, the maps of both sensors can often not be compared because different survey parameters have been applied. A good example is the case-study of [33], where a Neolithic ring ditch was found by a caesium gradiometer and with the in-phase response of an FDEM instrument. However, the conductivity was not measured and the resolutions of the two surveys were different. Many studies have only used the conductivity response [39, 77-79]. One case-study has mentioned the preferred use of an FDEM sensor for a survey over volcanic soil to measure the susceptibility variations because a magnetometer was too disturbed by the high remanent magnetism (which is not sensed by the FDEM sensor) [80]. Therefore, it is important to compare both methods on a site without major remanent magnetism.

The objective of this study was to compare several configurations of the FDEM sensor with a gradiometer measurement on an archaeological site, containing the buried remains of a 17th century castle. The survey conditions (measurement resolution, time of the survey) were kept as equal as possible to obtain a fair comparison. Several aspects were investigated, such as the driving direction of the motorized platform and the coil orientation of the FDEM sensor. In addition, the complementarity of the susceptibility and conductivity response was verified with auger observations.

5.3 Site description

The study site was located in Vinkem, a small village near the west coast of Belgium (51° 00’ 50.2292’’ N, 2° 39’ 40.8037’’ E) (Figure 5.1). It consisted of three pasture fields of 0.8, 0.8 and 0.5 ha. The central field was surrounded by a large ditch of approximately 5 m wide. The site was

located on a plateau of Tertiary clay, close to the edge of the low coastal area, 8.5 m above the mean sea level (expressed in m TAW, "Tweede Algemene Waterpassing", the reference level of the Belgian ordnance). The regional topography was flat to slightly undulating. The Tertiary clay was covered by a shallow aeolian deposit, consisting of loam (Soil Taxonomy) from the Weichselian Lateglacial. The deeper sediments (from earlier Weichselian periods) were more silty than the upper sediments and they contained free $CaCO_3$ [81]. The average depth of the groundwater was about 1 m, with a moderately wet soil moisture status throughout most of the year.

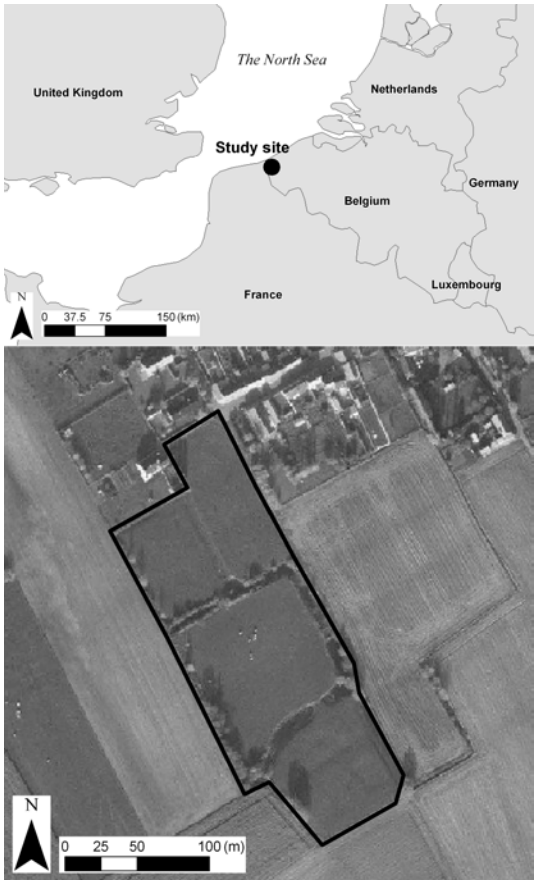

Figure 5.1 Location and aerial photograph of the study site (obtained from AGIV Flanders), with the delineation of the three pasture fields.

5.4 Historical background

The history of the site was investigated by [82]. Vinkem was a prosperous village during the early 16th century until religious wars (known as the Eighty Years War) disturbed the region in the second half of the 16th century. The outcome of this instable period was a large-scale depopulation of the agrarian communities, resulting in abandoned and destroyed holdings and farms. Around 1600, stability had returned to the region, attracting wealthy nobles to purchase the undervalued land (today still considered as very fertile), initiating an increased building activity. The origin of the castle at the study site dated back to this period of the early 17th century. It was erected by the lords "de Moucheron".

A military map made by Count de Ferraris at the end of the 18th century (Figure 5.2a) clearly showed the presence of buildings at the site, surrounded by a large ditch and an entrance in the south. The cadastral map of circa 1820 (Figure 5.2b) showed the same site, with a very accurate delineation of the castle, adjacent buildings, a gate at the southern entrance and an entrance bridge over the ditch in the east.

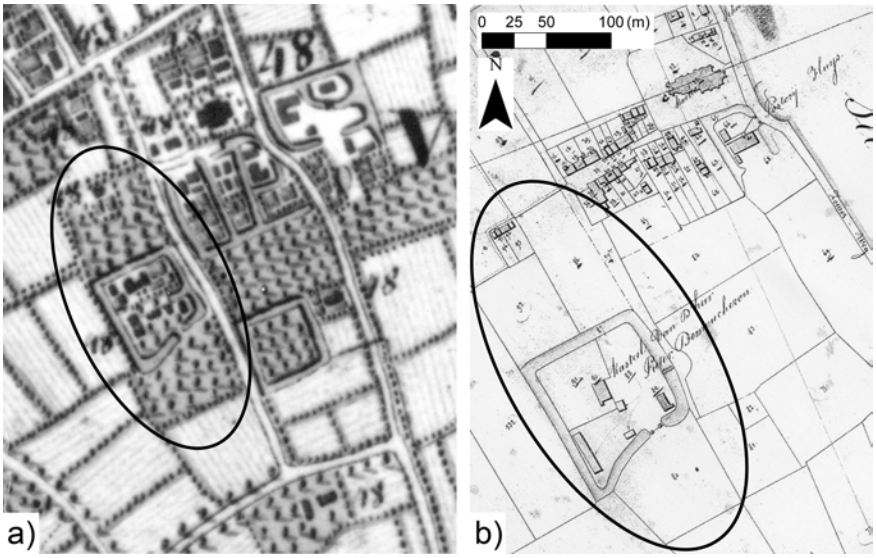

Figure 5.2 a) Map of Count de Ferraris (1771-1778), showing the moated site with contemporary buildings at the village of Vinkem (obtained from the Royal Library, Brussels). b) Dutch cadastral map (1818-1830), showing the castle of "de Moucheron" within the parcel, divided into different cadastral units (obtained from the Cadastral Archives, Bruges).

Although both maps indicated the presence of several buildings, they have been made for different purposes and therefore had a different spatial accuracy. The distribution of the site in various cadastral units suggested that the castle was partially leased out and used as a second residence, which was probably the case during the second half of the 18th century when the lords transposed their residence to the city. Similar examples can be shown in Flanders from the end of the 17th century onwards [83].

By the middle of the 19th century, the castle was left to decay and eventually demolished in 1876. The remains of the castle were largely reused as building material. From this period on the site was exploited as pasture land. No image was available of the castle. The only representative idea of the castle could be derived from contemporary buildings in the region. In view of exhibiting the site to the public, it was important to know what remains were still present and where they were located at the site.

5.5 Geophysical strategy

The field was measured with a FDEM sensor (type EM38DD), operated in the motorized platform. The driving speed was 5-6 km h^{-1}, which is sufficiently slow to avoid errors due to the response time of the system. With a measurement frequency of 10 Hz, approximately every 0.14 m a point was measured in the driving line. For practical purposes, the line distance was kept at 0.85 m, which corresponds with the track distance of the ATV wheels (Figure 5.3).

First, the three pasture fields were measured with the HCP orientation recording the conductivity and the VCP the susceptibility (survey 1). Based on this survey, a square area of 50 by 50 m was selected within the central field. This area was measured with the FDEM sensor, in two perpendicular driving directions to survey 1, with both coil orientations recording the susceptibility (survey 2). Finally, the same square area was also measured in east-west direction with a Fluxgate Gradiometer (FM256 Fluxgate Gradiometer, Geoscan, UK), operated and carried by hand (survey 3). This sensor measures the vertical pseudogradient of the magnetic field strength with 0.5 m separation. Therefore, the measurement units were expressed in nT/0.5 m.

Figure 5.3 Motorized platform operated on the pasture in Vinkem at wheelbase line distances.

The instrument resolution was 0.1 nT/0.5 m. This survey was not guided by GPS; grid lines were laid out within the square area using a tape measure. A line distance of 0.85 m was chosen to correspond with the FDEM surveys, although denser traverse intervals are recommended for detailed archaeological surveys [3]. The measurement distance within the lines was 0.25 m, which was larger than in the FDEM survey. Therefore, the FDEM data were thinned to approach the same measurement distance of the gradiometer data. The gradiometer data were processed with Geoplot 3.0 (Geoscan, UK). The mean of each line was set to zero, except for a few lines where the zero mean traverse treatment caused artefacts. All measurements were interpolated with local kriging, using a linear model without a sill or nugget, to the same grid. To compare easily the susceptibility maps within the square area, they were subtracted with the background value, in order to bring to the same scale.

5.6 Results

5.6.1 FDEM survey of the total site (survey 1)

The elevation of the site was obtained from a LIDAR (light detection and ranging) survey, conducted for the whole Flanders with an average density of one measurement per 20 m^2 (Figure 5.4a). LIDAR measures the distance between an airplane and the ground by recording the travel time of a laser pulse. In general, the elevation increased gently from north to south. The ditch surrounding the central and southern field was clearly visible as a local minimum. The northern and central field had a similar elevation, while the southern field was up to 1 m higher. Both the conductivity and susceptibility maps were very homogeneous in the northern field (Figure 5.4b-c). The area was divided by a north-south oriented ditch of approximately 1 m deep, where no measurements could be taken due to wetness. Only one local extreme anomaly appeared in both configurations, probably caused by a metal object.

The central field showed strong anomalies in both maps, indicating human disturbances. The susceptibility map (Figure 5.4c) clearly displayed the buried remains of a square brick structure. Soil augerings confirmed the presence of large concentrations of brick rubble, ceramics and walls, which were the remains of the 17th century castle situated at the highest point of the central field. The square anomaly was surrounded by other anomalies, associated with the remains of smaller buildings.

The conductivity map (Figure 5.4b) showed completely different anomalies than the susceptibility map. Around the strong magnetic anomaly, a band of higher conductivity occurred. At the east side of the magnetic anomaly, a clear ditch structure with organic layers was augered. At the north and west side of the high conductive area, a shallow organic layer with a clay accumulation was found at around 0.6 m below the plough layer. Therefore, this band of high conductivity probably indicated a former ditch system around the main building area.

The values of the conductivity map were lower in the southern field than in the other fields. This was explained by the depth of a clay rich, Tertiary layer below the loam. The altitude of this field was on average 1 m higher than of the other two fields. The loam cover was thicker and thus the clay layer was found deeper than in the other fields, where it was augered at 1.1 m under the soil surface.

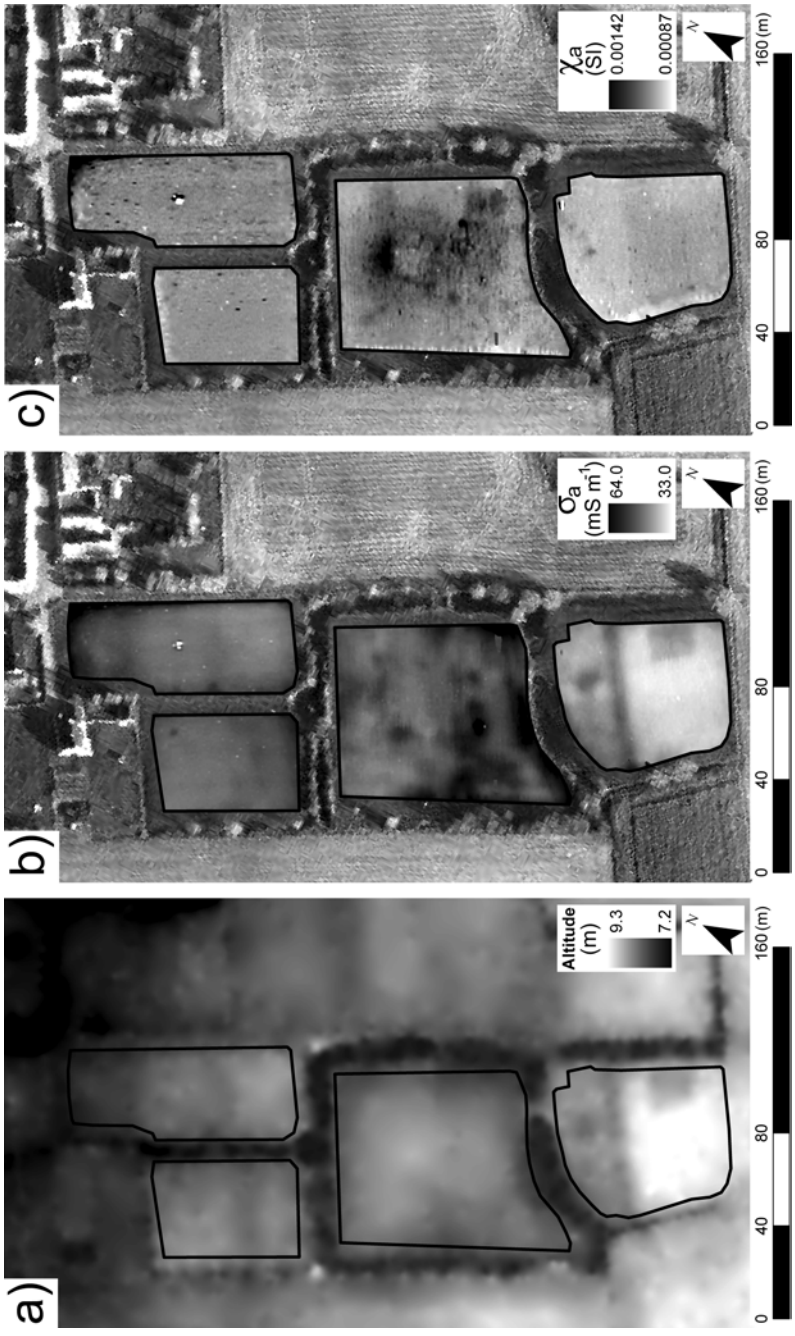

Figure 5.4 a) Altitude above the mean sea level (obtained from the Ministry of the Flanders Community and the Supporting Center OC-GIS Flanders), b) conductivity (HCP) of the three pasture fields, with the aerial photograph as background and c) susceptibility (VCP).

This also explained why local depressions in the southern field corresponded with a higher conductivity, because there the clay layer was closer to the soil surface. These depressions indicated the presence of a former ditch (running in east-west direction) and a rectangular area (to the east). The susceptibility map only showed some small disturbances close to the central field.

5.6.2 Comparison between FDEM and gradiometer maps (surveys 2 and 3)

The results of surveys 2 and 3 were used to evaluate the different FDEM configurations together with the gradiometer measurements. The two perpendicular surveys in the VCP configuration showed the effect of the motorized operation; the anomalies were elongated in the driving direction (Figure 5.5a and b). This was caused by the different sensitivity of objects parallel or perpendicular to the sensor in the horizontal plane and the response time of the system. These patterns can create anomalies that could be mistaken for actual soil anomalies. Apart from this artefact, the general anomalies of both maps were similar.

The susceptibility maps in VCP orientation showed also a remarkable resemblance to the gradiometer map (Figure 5.5c). These anomalies clearly delineated the remains of the castle and related features. Some faint anomalies could probably be attributed to internal divisions.

The gradiometer anomalies had a positive peak, sometimes with a clear negative trough to the north, as can be expected in the northern hemisphere for anomalies created by induced magnetism ([8]). At Vinkem, this corresponded clearly with relatively higher values in the susceptibility map in VCP orientation. The susceptibility anomalies of the HCP orientation were far less straightforward (Figure 5.5e). Both positive and negative anomalies were visible on the map. In general, the susceptibility map in HCP orientation corresponded less with the gradiometer map than the VCP orientation. The conductivity data showed very different anomalies than observed by the susceptibility measurements (Figure 5.5d), which confirmed that both phases often contain different information about the soil physical properties. It was remarkable that the brick wall remains did not produce any anomaly on the conductivity map (in the HCP orientation; other coil configurations were not tested here).

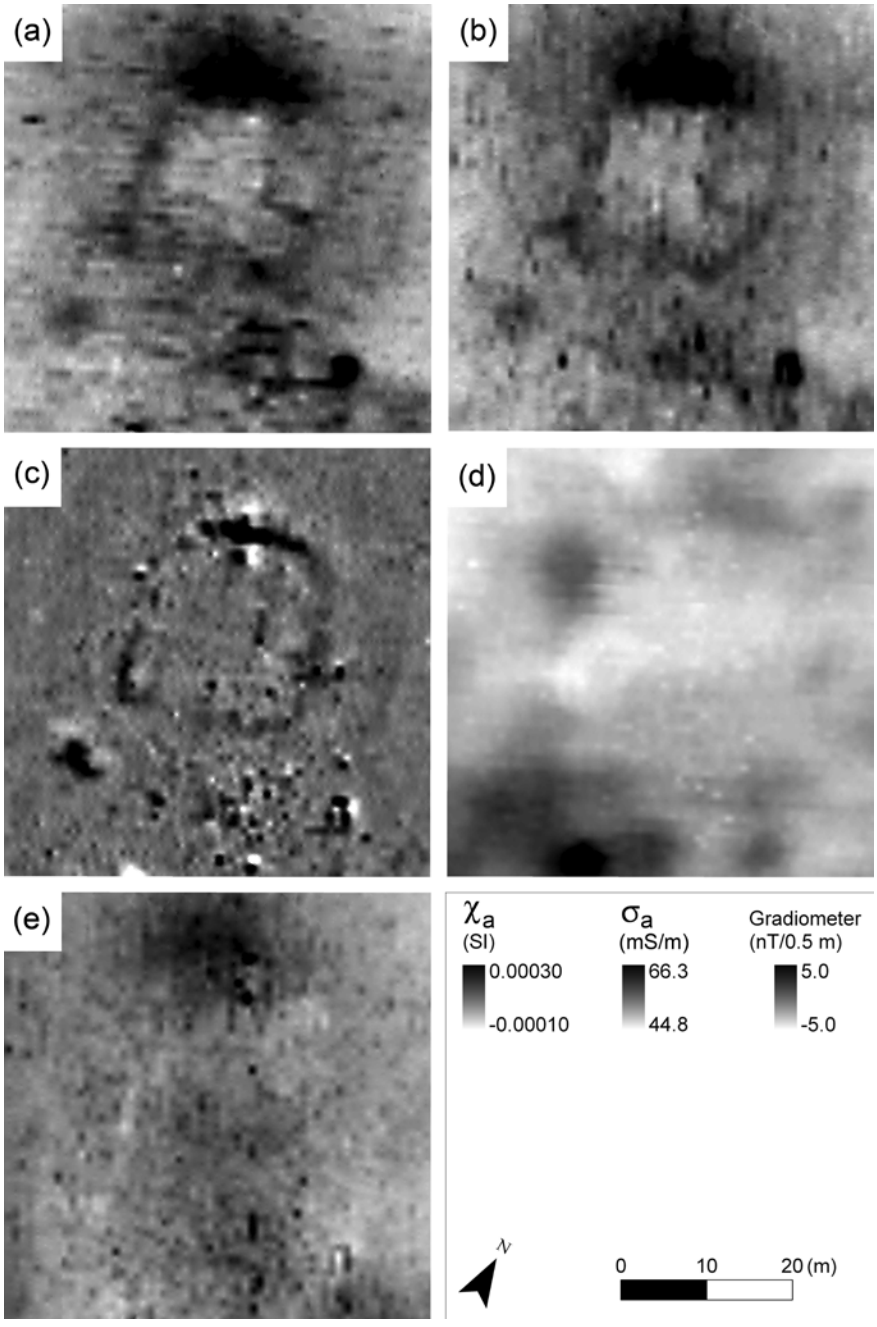

Figure 5.5 FDEM maps of survey 1, cropped to a 50 m square area: a) VCP (susceptibility) and d) HCP (conductivity); survey 2 with a perpendicular driving direction to survey 1: b) VCP (conductivity) and e) HCP (susceptibility); survey 3: c) gradiometer map. The value scales of susceptibility maps (a), (b) and (e) are the same.

Most of the magnetic anomalies were related to the presence of brick, which was verified by the auger observations. Large concentration of ceramics, charcoal, phosphates and both yellow and red bricks were present at the north side of the rectangular magnetic anomaly. A solid yellow brick structure was found at 0.65 m depth, impossible to penetrate with the auger. At the east and west sides of the rectangular anomaly, the augering also revealed solid yellow brick at 0.35 m depth. No solid structure was found at the south side, but large fragments of brick indicated the former presence of a brick structure. The magnetic anomalies were weaker at this location. In the southeast corner of Figure 5.5, a bright red brick wall was augered at the location of the very strong magnetic response. These were the remains of a separate building associated with the main site, which could have been constructed in another period. Brick has a relatively high magnetic susceptibility so it can acquire induced magnetisation [84]. On the other hand, firing may also have caused thermoremanent magnetism, which is sensed by the gradiometer but not by the FDEM sensor. This could have complicated the full comparison of the two sensors. However, the resemblance between the gradiometer data and the susceptibility map of the FDEM sensor was an indication of the relative importance of the induced magnetisation in the bricks. Although the remanent magnetisation of brick can be up to 10 times its induced magnetisation (for 17th century bricks the Königsberger ratio, or the ratio of the remanent over the induced magnetization [85], is normally clearly above 1), a random orientation of the bricks can reduce the remanent magnetisation so that it equals the induced magnetisation [22].

Because all measurements were obtained at the same resolution, the spatial detail of the maps could be compared. The Fluxgate Gradiometer anomaly is asymmetric and has a positive peak that is slightly shifted towards the south of the feature causing the anomaly, due to the inclination of the earth's magnetic field. The magnetic susceptibility anomaly of the FDEM sensor is centred above the structure. The difference between the anomaly location of both sensors could have been corrected by proper processing such as reduction-to-the pole [86] or by transforming the FDEM data [87]. In this case study however, the data were not processed further. Despite the bipolar response, the gradiometer map was clearly sharper than the FDEM-maps; its anomaly borders were more abrupt.

This was partly caused by the motorized operation of the FDEM survey, which smeared out the measurements in the driving direction.

5.7 Conclusions

The FDEM sensor was able to detect the remains of the 17th century castle in the pasture fields of Vinkem. The wall foundations were clearly visible as a strong susceptibility anomaly in the 1 m VCP orientation, which was due to the enhanced susceptibility of the bricks. In the HCP orientation, the anomalies were less clear and showed both positive and negative responses. A remarkable fact was that the conductivity map did not show the walls in HCP orientation. This could be due to either a too low electrical contrast of the brick remains with the soil, the low sensitivity of FDEM sensors to high resistive contrasts or due to the spatial sensitivity of the HCP configuration that could be less optimal for the disturbance at this depth. To test these hypotheses, measurements with other coil configurations and with electrical resistivity arrays should be conducted, but this was beyond the scope of this study.

The magnetic gradiometer measurements were closely related with the susceptibility map in VCP orientation, showing also the magnetic contrast of the bricks. The anomalies were more sharply delineated, but were also more ambiguous due to the typical bipolar response. The FDEM maps were slightly smeared out in the driving direction, but apart from that, the maps in perpendicular driving direction were very similar.

Chapter 6

Sensitivity of multi-receiver electrical conductivity sensors[1]

6.1 Abstract

Two types of electrical conductivity sensors were evaluated to prospect circular ditches surrounding former Bronze Age burial mounds as a complement to aerial photography. The first sensor was based on the ER-method, while the second sensor was based on FDEM. Both sensors were designed with multiple receivers, which measure several depth sensitivities simultaneously. First, the sensitivity of the sensors was tested on an experimental site where a rectangular structure was dug in a sandy soil, with similar dimensions as a ditch. The structure appeared as a more conductive anomaly in contrast to the low conductivity of the sand. Then, both methods were applied on two Bronze Age sites with different soil properties, which were discovered by aerial photography. The first site, in a sandy soil, gave only very weak anomalies. Soil augering revealed that the ditch filling consisted of the same sandy material as the soil; therefore, this filling was not able to cause a high conductivity contrast. Due to its lower sensitivity to noise in the low conductivity range, the ER sensor produced a more pronounced anomaly than the FDEM sensor. The second site was located on top of a ridge with a shallow substrate of Tertiary, coastal sediments. The ditch was very clearly visible on the sensor

[1]Modified from: Simpson D, Van Meirvenne M, Lück E, Bourgeois J, Rühlmann J. Prospection of circular ditches surrounding former Bronze Age burial mounds with multi-receiver electrical conductivity sensors. Submitted to the *Journal of Archaeological Science*, September 2009.

maps as a conductive low. At this location, the soil augering revealed that the ditch was dug through an alternating clay-sand layer and subsequently filled up with silty material from the topsoil. Overall, the shallow receiver separations produced anomalies that were stronger and that corresponded better to the geometry of the ditches. The other receiver separations provided more information on the natural soil layering, and in the case of the ER sensor, they could be used to obtain a cross-section of the actual electrical conductivity with 2-D inversion modelling.

6.2 Introduction

In order to formulate hypotheses on population distributions in the past, mapping the soil environment is as important as mapping the embedded traces of human occupation [88-90]. This is particularly true for the question of burial mound locations in the north of Belgium. Aerial photography during the past three decades indicated more than 1000 circles associated with ditches surrounding former burial mounds of the Bronze Age [91]. A remarkable fact is that most of these circles were detected in an area with dominantly sandy soils, which could be due to the increased visibility of crop marks on these soils or due to a settlement preference of the population in respect of the environment.

In this context, geophysical prospection can be a complementary tool to aerial photography. Considering the importance of the soil environment, sensors measuring electrical conductivity (or its inverse, electrical resistivity) are particularly useful because this physical property is influenced by anthropogenic disturbances [21, 25], but it is also related to natural soil variables such as clay and moisture content [6, 7].

Two geophysical methods are often used to measure the conductivity of the soil: the ER-method and FDEM. Although both methods react to the same physical parameter, the measurements can differ considerably [5]. A first factor is the spatial sensitivity of both methods, which depends on the configuration (separation, arrangement) of the electrodes and the coils [32, 48, 92]. Secondly, ER sensors are more sensitive to low-conductivity structures and FDEM sensors more sensitive to high-conductivity structures [31]. A third factor is the higher sensitivity of FDEM sensors to metal than ER instruments.

Sensor platforms have been specifically developed for agricultural and archaeological applications, to measure several electrodes [93, 94] or coil configurations [95] simultaneously in a continuous mode. The multiple configurations increased the chance of detecting archaeological structures at varying depths and allowed modelling the depth and thickness of the natural soil [58, 96], while the continuous mapping drastically increased the area surveyed per day. Therefore, both sensor platforms could be very useful to complement aerial photography in the search of circular ditches.

The aim was to investigate the sensitivity of both platforms to detect existing circular ditches associated with Bronze Age burial mounds. A field experiment was conducted in Germany over self-made structures with known dimensions and properties. Next, measurements were conducted on two fields in Belgium where circles were seen on aerial photographs, one field inside and one field outside a sandy area. The nature of the ditch and of the surrounding soil was verified with sensor-directed augering.

6.3 Electrical conductivity sensors

6.3.1 ER sensor platform

A new ER sensor platform was used, which was specifically designed for soil sensing [94]. It consists of one pair (dipole) of electrodes, injecting a current in the soil and five pairs (dipoles) of electrodes that measure the potential difference (voltage) between them, arranged as a rectangular array (or equatorial dipole-dipole). The ratio of the measured voltage over the injected current strength is proportional to the soil apparent resistivity, which is equal to the inverse of the conductivity. The dipole width was 1 m and the five potential dipoles were located at increasing separations of 0.5 m, from 0.5 m until 2.5 m. Each electrode is a spiked wheel (also called a “rolling electrode”) to enable continuous mapping behind a tractor or other vehicle. Because of its resemblance to a centipede while moving over the terrain, the instrument was baptized “Geophilus electricus” (Figure 6.1a).

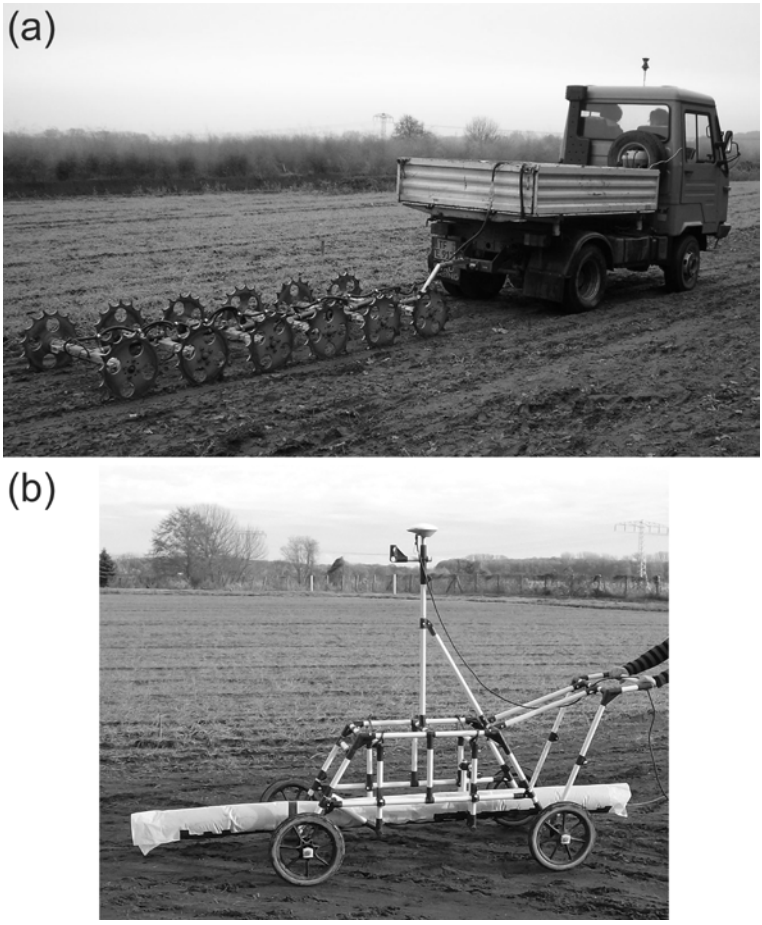

Figure 6.1 Geophilus electricus towed behind a light truck and georeferenced with a total station prism (a). FDEM sensor (type DUALEM-21S) wrapped in a plastic protection on a manually pushed cart with a GPS antenna (b).

The increasing separations between the current and potential dipoles each represent an increasing volume (and thus depth) of exploration. For a soil with a homogeneous conductivity, this depth sensitivity can be calculated according to [97] (Figure 6.2).

When structures are present with dimensions in the range of the electrode separations, these depth curves do not apply; a small feature close to the surface will have a much stronger response than indicated by the curves. With these five surface measurements, the soil conductivity at different depths along a measurement track can be reconstructed using 2-D inversion software. Several transects were inverted with the program RES2DINV (Geotomo Software SDN. BHD., Malaysia), showing a

cross-section through the structures (more details about the inversion are explained in Appendix B). All structures extended far enough in the direction perpendicular to the cross-section, so that the 2-D inversion is appropriate (if the dimension of the structures would change in the perpendicular direction, then only a 3-D inversion can model the structure well). The measurements on the experimental site were conducted with the Geophilus, but it was impossible to bring the Geophilus to Belgium. Therefore, the two surveys in Belgium were conducted with fixed electrodes on a transect simulating one survey track of the Geophilus.

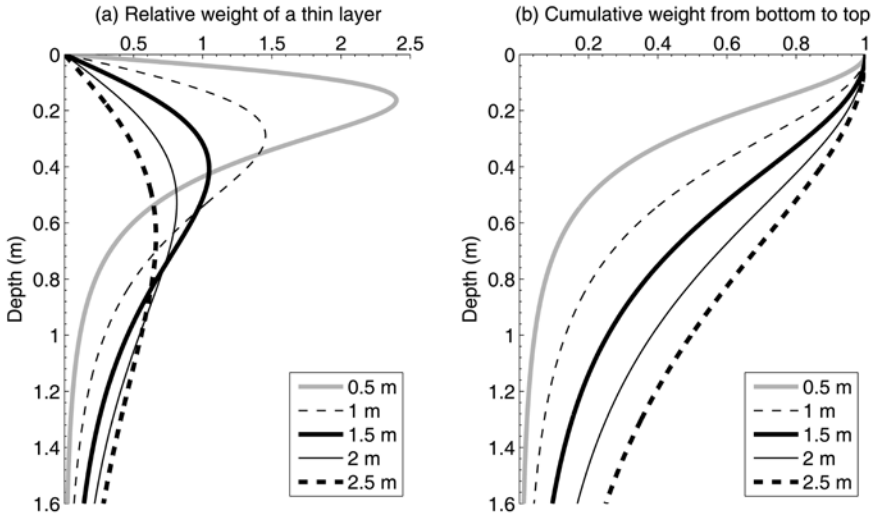

Figure 6.2 Depth weighting in a homogeneous soil for the Geophilus electricus configurations. Relative weight of a thin layer to the total signal (a). Cumulative weight of the layers from bottom to top (b).

6.3.2 FDEM sensor platform

The FDEM sensor used was a DUALEM-21S (Dualem Inc., Canada). For the experiments on the test site in Germany, the sensor was laid on a cart at approximately 0.25 m above the soil surface and pushed by hand (Figure 6.1b), while the surveys in Belgium were carried out using an all terrain-vehicle pulling a sled with the sensors (at 0.16 m above the soil surface). Both platforms were georeferenced by a dGPS with a 0.1 m pass-to-pass accuracy.

6.4 Survey on the test site

6.4.1 Experimental setup

To compare the performance of all configurations of both sensors, several structures were buried in a test site at the Institute of Vegetable and Ornamental crops in Grossbeeren (Germany). One structure will be discussed, hereafter called “basalt wall”. Its dimensions were 5 m in length, 0.5 m in width and 0.5 m thickness. A pit of 0.8 m depth was dug and filled up with basalt stone powder until 0.3 m depth and finally the original topsoil was placed back to fill the remaining 0.3 m. The conductivity of the basalt in situ was 50 mS m^{-1} (measured with a small ER Wenner-array directly in the basalt), which was five times higher than the surrounding soil conductivity (lower than 10 mS m^{-1}), which consisted of glacial till with a high proportion of sand and some coarser fragments. This basalt wall is a good model for a circular ditch of a former burial mound in a sandy soil. Surveys were conducted with the ER array and the FDEM sensor on tracks crossing the structure perpendicular to its length. The measurement distance along the tracks was approximately 0.5 m for the ER array and 0.1 m for the FDEM sensor, because the recording frequencies were 1 and 8 Hz, respectively. In addition, a stationary ER-array, with the same electrode configuration as the Geophilus, was measured on a line trough the middle of the ditch. This measurement was conducted to evaluate the effect of the movement of the Geophilus on the data quality.

6.4.2 Results and discussion

The five dipole separations of the Geophilus produced a different response to the basalt wall (Figure 6.3). The 0.5 m separation, which has the shallowest depth sensitivity, gave a strong positive response directly above the wall. For increasing dipole separations, and thus for increasing depth sensitivities, the anomaly changed to a bipolar pattern with two maxima at an increasing distance and decreasing strength. Hence, the smallest dipole separation produced an anomaly most similar to the geometry of this structure. However, the other dipole separations were useful to invert the surface measurements to reconstruct the conductivity of the soil profile through the middle of the wall (Figure 6.4).

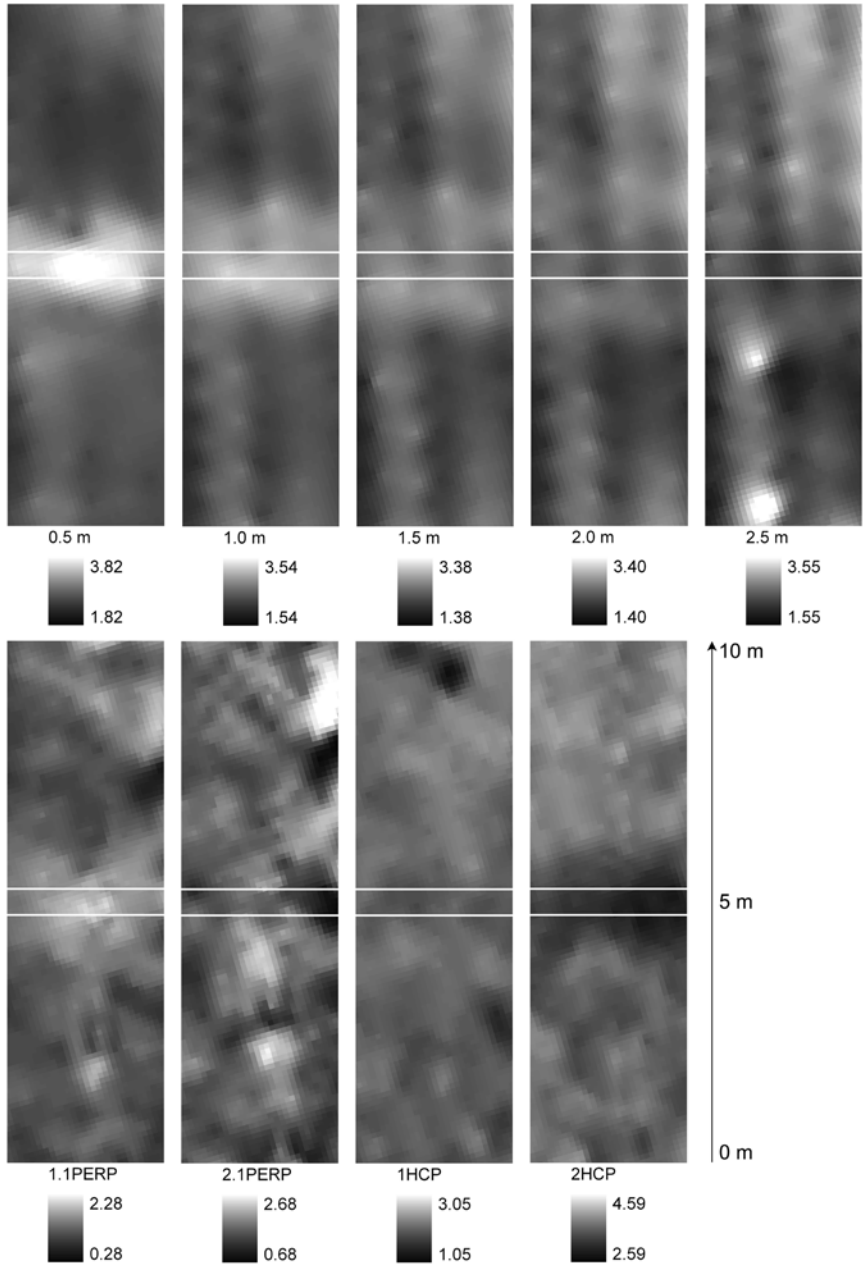

Figure 6.3 Conductivity maps with individual scales but in a common range of 2 mS m^{-1}. Top: ER Geophilus measurements, the dipole separation is indicated below. Bottom: FDEM DUALEM-21S maps with the coil configurations labelled below. The location of the basalt wall is indicated by a white line.

In this cross-section, the location and size of the basalt wall were mapped quite accurately. The cross-sections constructed by the Geophilus and by the stationary array were very similar, which indicated that the movement of the Geophilus had little effect on the data quality. The small overall difference in conductivity could be caused by moisture differences because the measurements were conducted in two periods. The maximum, modelled conductivity value at the basalt wall did not reach 50 mS m^{-1}, the actual conductivity of the basalt. The inversion modelling has its limitations. First, the measurement distance of 0.5 m was quite large to model accurately the wall, which had also a width and thickness of 0.5 m. Second, the resolution of the model is less at larger depths, which can be the cause of the high conductivity zone under the basalt wall in the stationary array profile (Figure 6.4b).

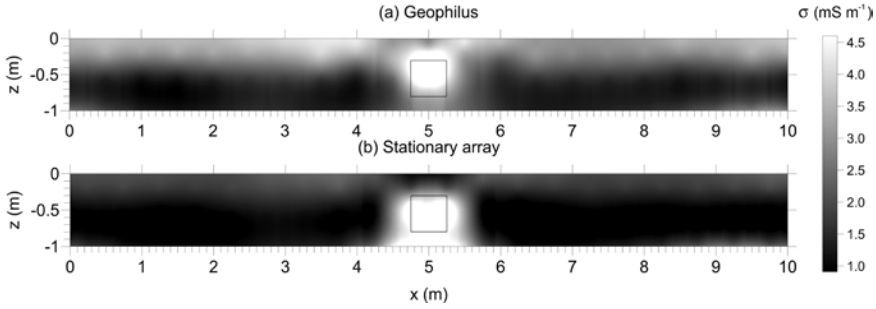

Figure 6.4 Vertical cross-section through the middle of the basalt wall, resulting from a 2-D inversion. The location of the wall is delineated on the map.

The overall conductivity of the FDEM maps was very similar to the Geophilus maps (Figure 6.3), but the anomaly caused by the basalt wall was different. Only the 1.1PERP coil configuration produced a positive response to the basalt wall. The 2.1PERP and 1HCP configurations did not give any response at all. The coil configuration with the deepest theoretical depth of exploration, the 2HCP, gave a clear low anomaly. This contradicted with the higher conductivity of the basalt wall relative to the surrounding soil.

However, this was not surprising because theoretical modelling confirmed that negative responses can occur in the HCP measurements [31, 49]. Hence, it is important to consider that structures with dimensions close to the dipole (for ER) or coil (for FDEM) separation, as often found in archaeological prospection, can produce ambiguous patters. 2-D inver-

sion software, as developed for ER arrays, could eliminate these ambiguous patterns.

The 0.5 m separation of the ER sensor produced a stronger anomaly than the 1.1PERP configuration of the FDEM sensor. This could be due to the height of the FDEM sensor above the soil surface, which reduced the strength of the FDEM anomalies. If the sensor would have been lowered to the ground surface, the anomaly magnitude could have been increased. This was not tested in this study because it was impossible to lower the sensor on the cart.

6.5 Surveys on the Bronze Age sites

6.5.1 Site description

Two sites were selected based on the aerial photograph archive of the Department of Archaeology and Ancient History of Europe of the Ghent University. One site was located in the sandy region of the north-west of Belgium (also called the "Flemish Valley"), where most of the circular ditches have been found by aerial photography (Figure 6.5). The field is in permanent pasture and has a sand content of 90 %, so it dries out very rapidly. The circular ditch was detected on aerial surveys in several periods, with the best example on the 16th of August, 1997 (Figure 6.6a). This was the warmest August of the 20th Century recorded in Belgium, according to The Royal Meteorological Institute of Belgium (www.meteo.be). A very hot month associated with low rainfall provokes a severe drought stress for the crops, which explains why then crop marks are visible (personal communication with Prof. J. Bourgeois).

The second site was located in a transition zone between the sandy region and the loess region, where the soils contain more silt (Figure 6.6b). This field was situated at one end of a ridge, an outcrop of marine sediments from the Tertiary period (Eocene epoch). The presence of shallow Tertiary sediments, covered by a layer of Pleistocene loam with a varying thickness, caused high soil variability over short distances. Burial mounds are often found to be on upstanding landscape spots such as this site [91], where one has a spectacular view over the surrounding, flat landscape of the Flemish Valley. The field was pasture for the last four years, but before it had been used for arable cropping.

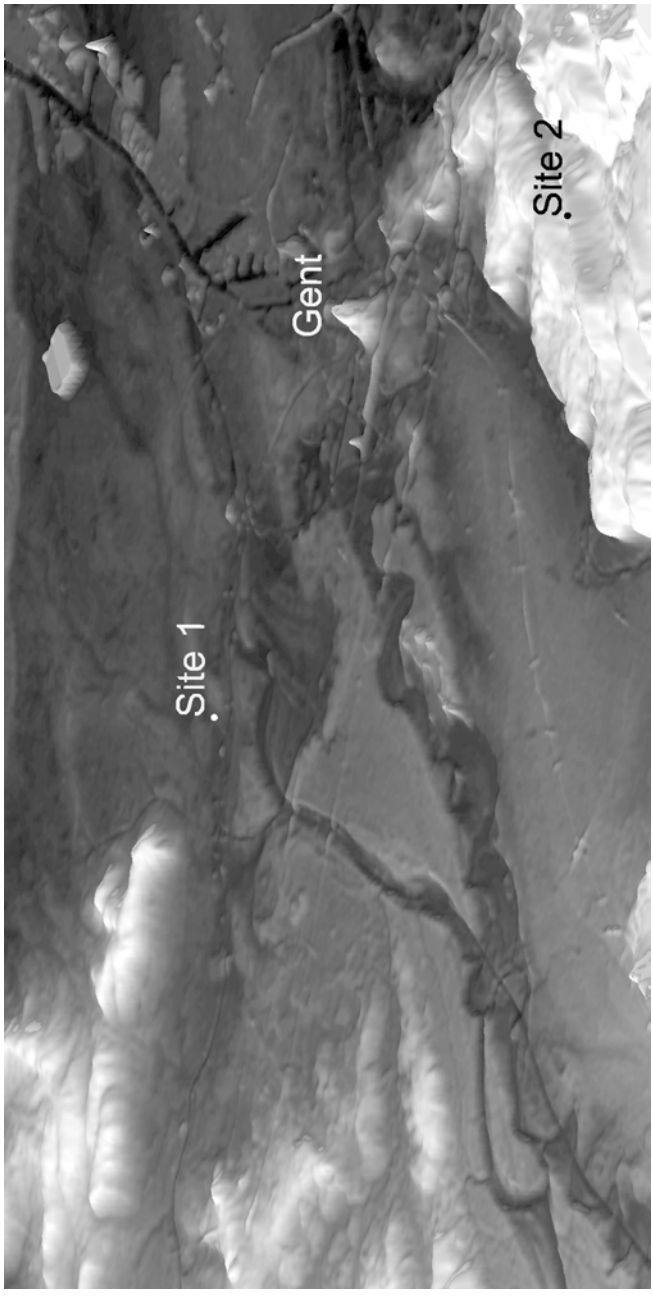

Figure 6.5 Landscape position of the two study sites, close to the city of Gent, where the rivers Schelde and Leie join. Site 1 was located in the Flemish valley, close to the former river Oude Kale, and site 2 on a Tertiary ridge. The image is a 3-D height model, with an exageration factor of 30 and with shaded relief (based on the DHM, obtained from AGIV Flanders).

6.5.2 Survey strategy

Both fields were surveyed following a predefined plan. First, an area surrounding the circle, delineated on the rectified aerial photograph (Figure 6.6), was measured with the FDEM-platform in high resolution (0.4 m cross-track distance and 0.1 m distance along tracks) with the sensor at 0.16 m height. The measurements of each coil configuration were processed and interpolated to raster maps. Based on these maps, the exact location of the circular ditch was determined. A transect of 10 m was laid out crossing the ditch perpendicularly. On this transect, a stationary ER array was laid out with 0.5 m distance between the readings, using the same electrode configuration as the Geophilus. Finally, to verify the sensor measurements, the soil was augered and described at several locations on the transect: in the middle of the ditch and at either end of it (the circles on Figure 6.7**)**. To characterize the natural soil variability of the fields, two locations with a different conductivity were augered.

6.5.3 Results and discussion

The different soil types of the two sites were clearly reflected in the 1.1PERP maps of the FDEM sensor (Figure 6.7). This configuration produced the clearest anomalies caused by the circular ditches. The conductivity of the field in the sandy region was very low and homogenous, with a narrow range of 1.2-2.7 mS m^{-1} (Figure 6.7a), while the other field located on the Tertiary deposits was more heterogeneous with a range of 4.5-17.5 mS m^{-1} (Figure 6.7b).

The first field consisted of homogeneous sand down to at least 2 m depth, found at both auger locations (numbers (1) and (2) on Figure 6.7a). The groundwater table occurred within 1 m depth, which provoked a slightly higher conductivity. The second field had a minor silt fraction in the topsoil that was mixed with the underlying Tertiary sediment. This Tertiary sediment consists of marine sand with glauconite and in some parts of the field, it is covered by thin, alternating clay and sand layers starting around 0.5 m depth (which has been attributed to a lagunary environment [98]). This alternating clay-sand layer was most pronounced at location (1) of Figure 6.7b, where it continued down to 1.25 m depth. Here the conductivity was relatively high. At location (2), only Tertiary sand was found throughout the profile, so the conductivity was lower.

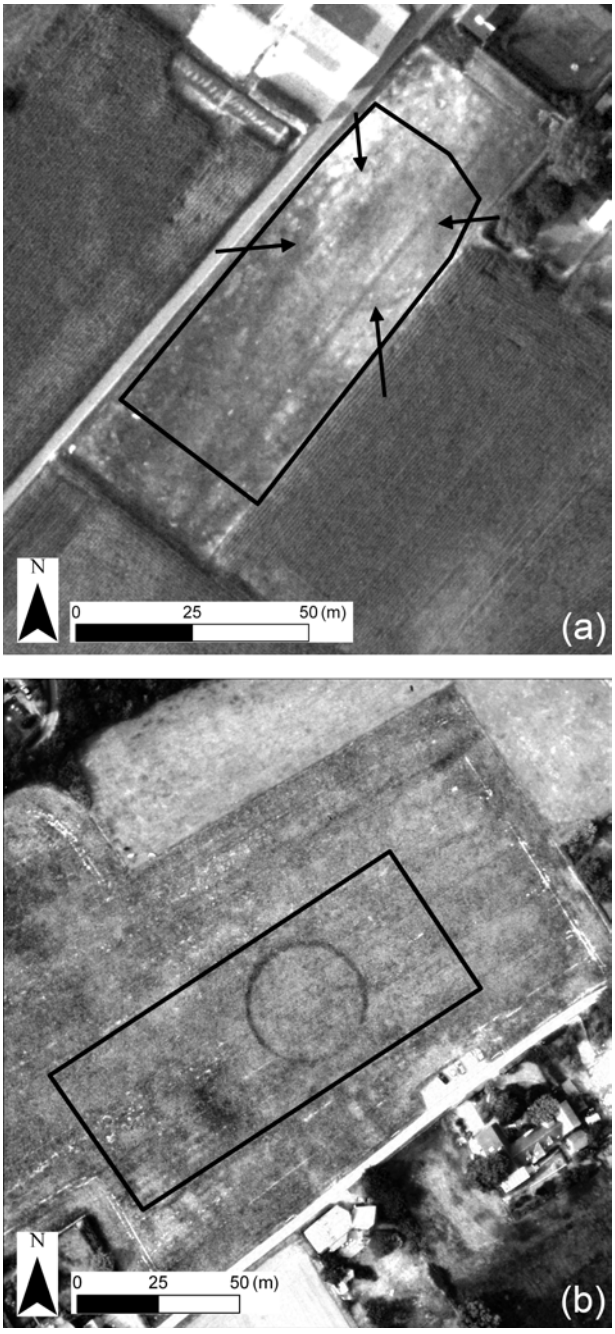

Figure 6.6 Aerial photographs of the two sites; the contrast was adjusted to highlight the circles. The delineated area was surveyed with the FDEM platform. (a) Pasture field in the sandy region, the arrows indicate the location of the circular ditch; (b) site on the Tertiary hill.

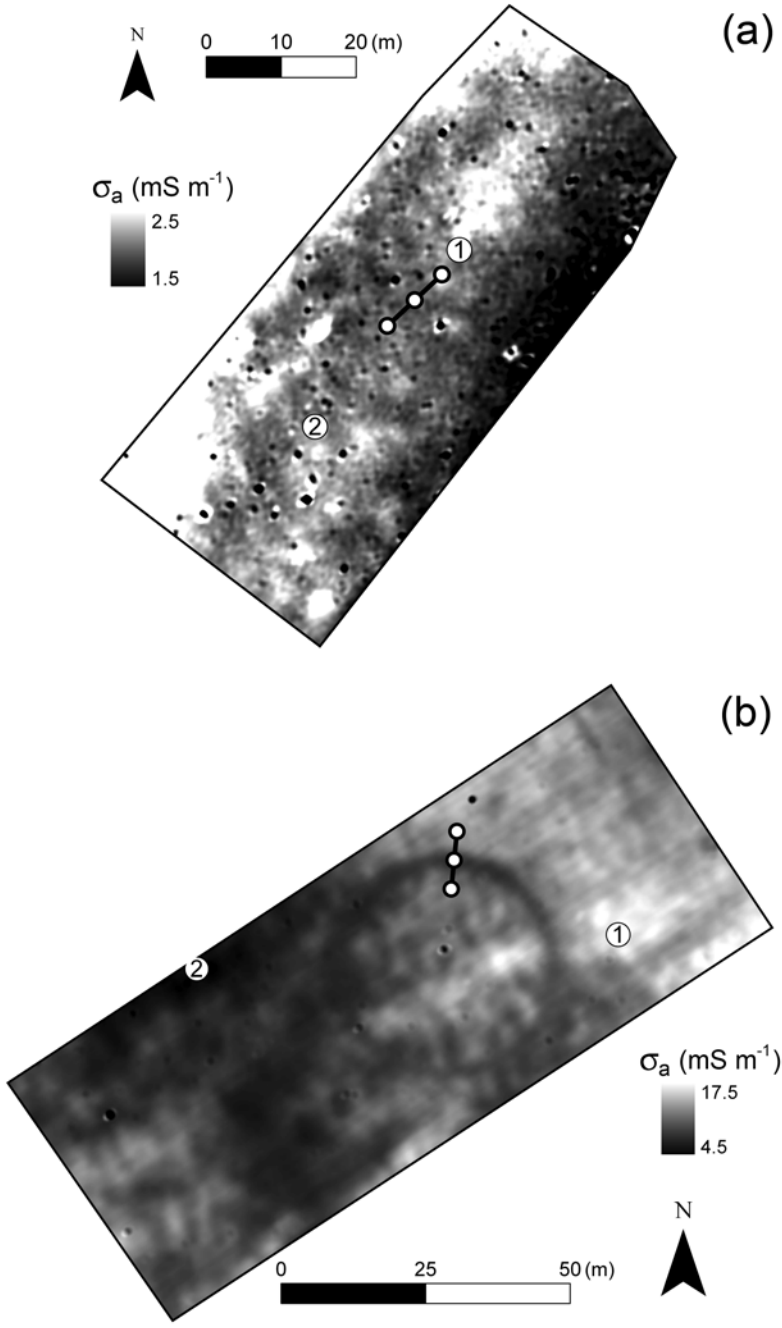

Figure 6.7 FDEM-measurements (1.1PERP) on the two sites, (a) in the sandy region and (b) on the Tertiary ridge. The ER-transects crossing the ditches are indicated by straight lines, auger locations are indicated by white dots with or without numbers.

The ditches were dug during the construction of the burial mound after which they gradually filled up through erosion and agricultural practices. Knowing the soil morphology of the site, it was possible to explain why the ditch in the sandy field (Figure 6.7a) was only faintly detected (and only its southwest part) while the ditch on the Tertiary ridge was clearly visible in the FDEM-measurements (Figure 6.7b). In the first field, the ditch was dug in a homogeneous, sandy soil and consequently the fill did not differ from the surrounding soil, resulting in small conductivity differences. In the second field, the ditch was dug through the alternating clay and sand layer down to 1.5 m depth and filled up with topsoil, which consisted mostly of silt. Since clay is a lot more conductive than silt, this meant that the ditch was clearly visible as a lower conductivity circle.

A more quantitative comparison of the FDEM-configurations was obtained by plotting the values of the transects (Figure 6.8). In the sandy field, only the 1.1PERP and 2.1PERP-configurations showed a very weak anomaly. The low contrast in conductivity was disturbed by noise in the data, inherent to FDEM measurements of such low conductivities. On the Tertiary ridge, the shallowest coil configuration (1.1PERP) produced the most pronounced anomaly. The coil separations with deeper depths of exploration (and thus measuring larger volumes) were more reduced in amplitude and even inverse for the 2HCP configuration. The overall anomaly amplitudes were a lot higher than in the sandy field (6 mS m^{-1} compared to less than 0.5 mS m^{-1} for the 1.1PERP configuration) and thus less disturbed by noise in the data. This was due to the soil type but probably also because of the larger size of the ditch.

The ER array was more successful in detecting the ditch in the sandy field than the FDEM sensor (Figure 6.9a). Although the magnitudes of the anomalies were not very different, the ER data were less prone to noise in the low conductivity range. The most pronounced anomalies were again measured by the smallest dipole separations. The ditch on the Tertiary ridge was more pronounced than the ditch in the sandy region (Figure 6.9b). This was also reflected in the vertical profiles calculated from the 2-D inversion modelling (Figure 6.10).

The ditch in the sandy field was only visible as a small increase of conductivity at shallow depths. On the contrary, the ditch on the Tertiary ridge was very prominant in the vertical profile.

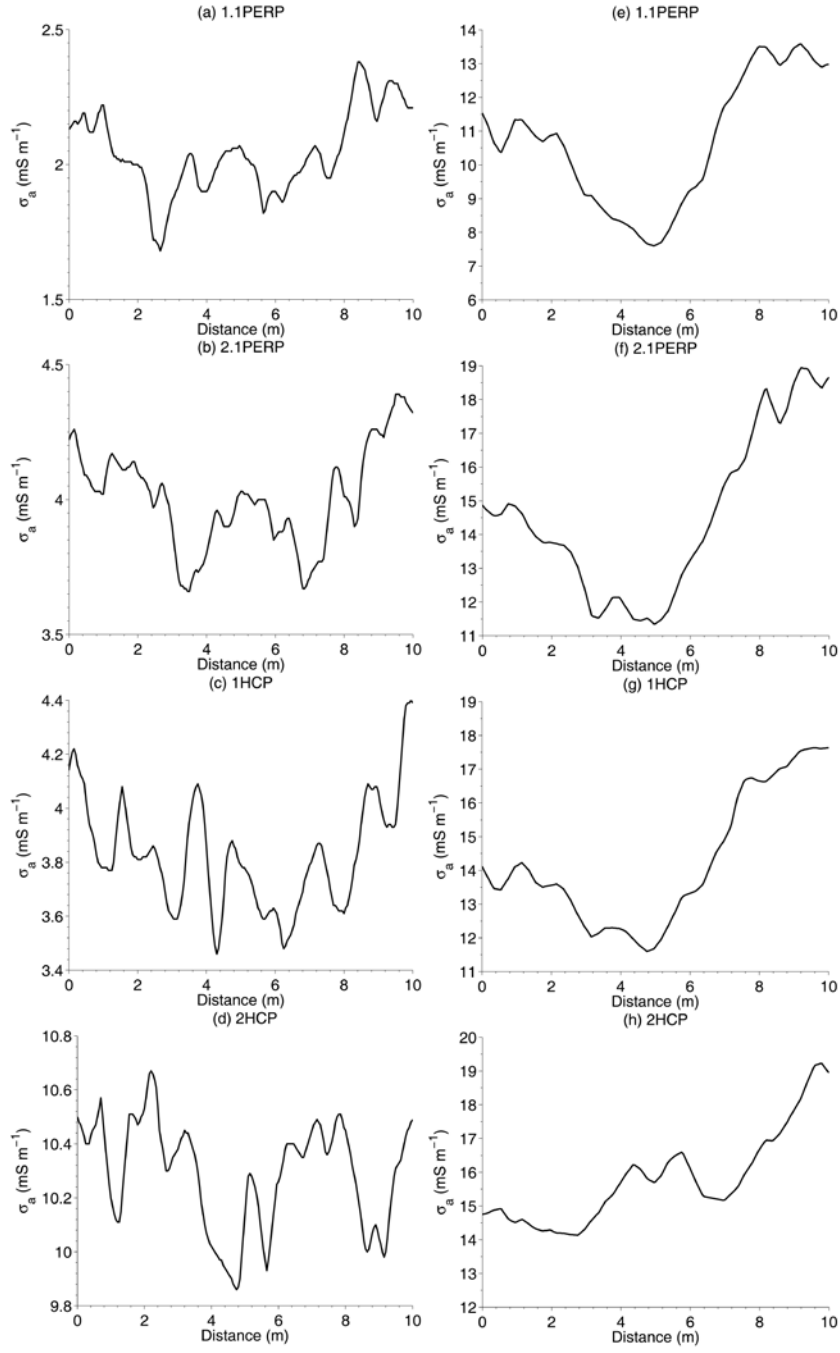

Figure 6.8 Extraction of the FDEM measurements through the ditch, (a) to (d) in the sandy region, (e) to (h) on the Tertiary ridge. The direction of the transect from left to right corresponds with the southwest-northeast direction on the maps.

The horizontal layer of higher conductivity caused by the clay-rich lagunary sediments was interrupted by a wedge of low conductivity, related to the ditch fill with the silty topsoil.

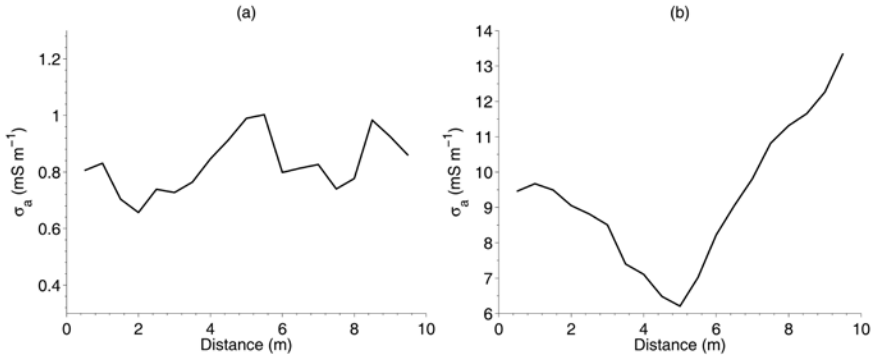

Figure 6.9 ER-measurements with a 1 m transmitter-receiver dipole separation through the ditch; (a) in the sandy region and (b) on the Tertiary ridge.

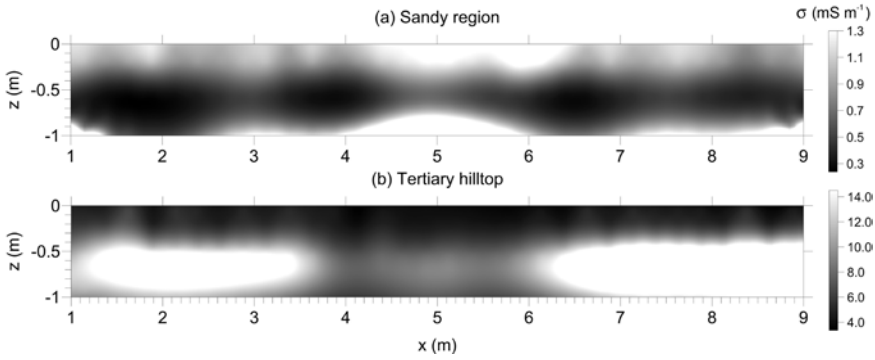

Figure 6.10 Vertical cross-sections based on a stationary Geophilus configuration through the middle of the ditches. The edges of the 10 m transect were removed, because there the spatial sensitivity was lower (see Appendix B).

6.6 Conclusions

The field experiments with the known structure demonstrated the influence of the coil orientation (FDEM sensor) and the electrode separation (ER sensor) on the strength and shape of the measured anomaly. For the chosen structure, the configurations with the shallowest response produced the strongest anomalies with the best resemblance to the geometry of the structure (which confirms the results of [92]). This was also found on the Bronze Age burial sites. However, this finding may not be genera-

lized too much; it is very likely that ditches at a greater depth would be detected better by coil/electrode configuration with a deeper sensitivity. For the ditches prospected here, these deeper sensing configurations produced ambiguous anomalies with positive and negative responses. In the case of the ER array, this ambiguity could be solved by applying an inversion program, which gave a model of the true resistivity of the subsoil. The availability of 2-D inversion programs is a great advantage of ER systems over FDEM sensors, of which 2-D inversion programs are still in development.

The ER methods were more sensitive in a low conductivity environment, such as a sandy soil (as expected from [31]). The FDEM sensor detected very well the ditch that was dug through the high conductivity, lagunary sediment. However, it was poor in detecting the ditch in the less conductive sandy soil, partly because the magnitudes of the anomalies were within the noise level of the instrument. The aerial photographs seemed more successful in detecting the ditches than the electrical conductivity sensors, certainly in the sandy field. However, this observation is biased by three factors. First, to capture a good, clear photograph of the ditch, many years of aerial photography were necessary. Second, the soil water has an important effect on electrical conductivity measurements and thus also on the contrast between the ditch and the soil. Therefore, it is possible that the detection of ditches with conductivity sensors is improved in certain periods with other soil moisture conditions. Third, the Bronze Age sites were selected based on aerial photographs with clear examples of circular ditches. A more objective approach would be to survey a circular ditch with conductivity sensors, which was not detected by aerial photographs, but this was beyond the objectives of this research.

Chapter 7

Evaluation of multi-coil FDEM sensors[1]

7.1 Abstract

The multiple coil configurations of two electromagnetic induction sensors were tested on a field with strong electrical and magnetic contrasts. The goal was to test if measuring with the multiple coils resulted in a better detection of near-surface artefacts and the natural soil variability. The conductivity of all coil configurations was closely related to the depth of a clay substrate beneath the topsoil sandy loam, which was verified by soil augering. Configurations with a shallower theoretical depth of exploration were less influenced by the clay substrate. Combining two coil configurations revealed important conductivity-anomalies, not visible on individual measurements, associated with a brick wall foundation and a former ditch. The susceptibility-maps showed very different anomaly patterns, related to anthropogenic disturbances in the soil, such as the filling-in with brick rubble of a former pond. Depending on the depth and thickness of the disturbance and the relative response of the sensor configurations, the susceptibility anomalies were entirely positive for one configuration while other configurations had also negative anomalies. It was concluded that multiple coil configurations provide a better insight into the buildup of the soil profile and are better able to detect anomalies than single measurements.

[1]Modified from: Simpson D, Van Meirvenne M, Saey T, Vermeersch H, Bourgeois J, Lehouck A, Cockx L, Vitharana UWA 2009. Evaluating the multiple coil configurations of the EM38DD and DUALEM-21S sensors to detect archaeological anomalies. *Archaeological Prospection* 16, 91-102.

7.2 Introduction

In the past, several types of FDEM sensors have been developed with different coil configurations. Each sensor type was more or less successful in detecting archaeological features. [33] measured a Neolithic ring ditch with a prototype FDEM sensor where the susceptibility anomalies were very similar to magnetometer anomalies. One of the most popular commercial sensors is the EM38 (Geonics Limited, Canada), which operates at one frequency (14.6 kHz) and has a fixed coil separation of 1 m. In a study of [5, 99] the conductivity and susceptibility response of the EM38 was compared with gradiometer and resistivity meter measurements. A strong relationship was found between the conductivity and the apparent resistivity values on one hand, and the susceptibility with the gradiometer measurements on the other hand. Although in the former study the anomalies differed with the coil orientation. Another sensor, the EM31 (Geonics Limited, Canada), has a larger coil separation and has therefore been more used to detect bigger features at greater depths than the EM38 (e.g. [100, 101]).

More recently, sensors are being developed that can measure simultaneously several coil configurations. The EM38DD (Geonics Limited, Canada) has two coil orientations, measuring either in conductivity or susceptibility; the EM38B (Geonics Limited, Canada) measures both the conductivity and susceptibility in one coil orientation. [102] combined the two orientations of the EM38DD in the conductivity response to detect frostwedge-pseudomorphs in the soil. [103] measured the conductivity in one orientation and susceptibility in the other, which resulted in the detection of both electrical and magnetic features of an archaeological site. Recently, the DUALEM-21S (Dualem Inc., Canada) was developed, which is able to measure two coil orientations for two coil separations in both the conductivity and susceptibility response. The multiple coil configurations have the potential to detect more artefacts than individual signals, because each configuration has another spatial sensitivity. Moreover, the signals can be integrated easily because they are simultaneously recorded. Nevertheless, until now, the use of FDEM sensors with multiple coil configurations in archaeological prospection has been very limited.

In this study, the EM38DD and the DUALEM-21S were tested on a field where the remains of a priest's house were located. The site contained both strong conductivity and susceptibility contrasts. All possible coil configurations of the sensors were measured on the same day, at the same measurement density. The results of the sensor configurations were evaluated on their complementarity. The anomalies were verified by soil augers to see if measuring with multiple coil configurations had a significant advantage over single measurements.

7.3 Site description

The experimental site was a pasture field of 0.5 ha, located in the north-west of Belgium with central coordinates 51° 0' 26.47" N and 2° 42' 3.75" E (Figure 7.1). It was located next to a small, curved road (Figure 7.2a). The field is situated on the border of a plateau, with a heavy clay substrate (a marine deposit from the early Eocene), covered by Weichselian, aeolian sandy loam. The topography was flat to slightly undulating. The clay substratum occurred on average 2 m below the plough layer. According to the Belgian soil classification [81], the soil series (code: Ldp) indicated a sandy loam texture, with a moderately wet moisture status (gley appearing between 0.3 and 0.5 m depth).

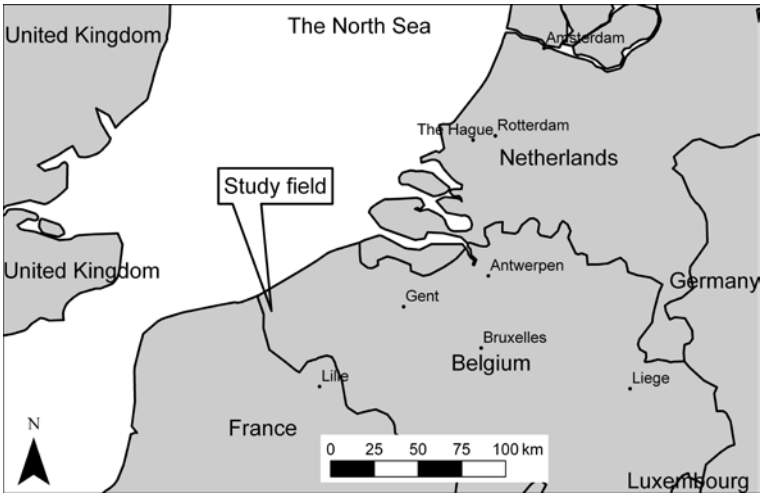

Figure 7.1 Location of the study field in north-west of Belgium.

A historic map of Count de Ferraris (1771-1778) showed in the northern part of the field a square ditch (Figure 2b, indicated by the ar-

row), surrounding a building. This building was probably the house of the priest, associated with the church of the village "Sint-Rijkers" on the other side of the road. The church was demolished in 1812 and the priest's house was demolished before the beginning of the 19th century. An aerial photograph (Figure 7.2a) showed a group of trees in the northwest of the field, where no sensor measurements could be taken. A depression filled with water in the northeast was also not accessible. These areas were delineated on the sensor maps. According to the landowner, this field had been continuous pasture over the last 30 years, mainly because the wet soil conditions do not allow arable cropping. For this reason, the disturbance by land management was expected to be minimal.

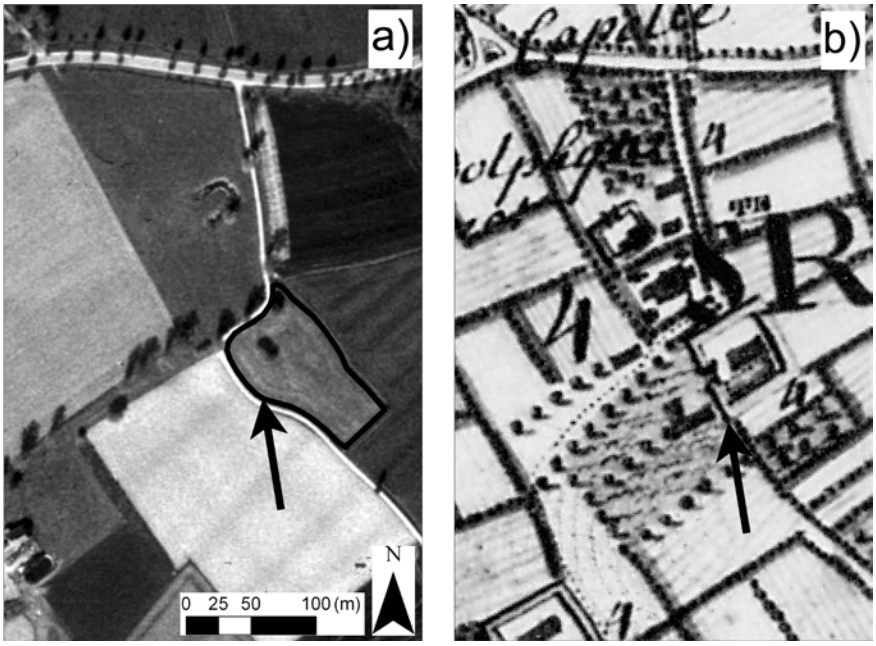

Figure 7.2 (a) Aerial photograph of the site, the arrow indicates the field boundary; (b) historic map of Count De Ferraris (1771-1778), the arrow is at approximately the same location as on the aerial photograph.

7.4 Survey strategy

Both sensors were operated in the sleds of the motorized platform. Because a different sled was used, the EM38DD was situated at a height of 0.05 m and the DUALEM-21S was 0.16 m above the soil surface. The

length of the sensors was oriented in the direction of the driving track. The cross-track distance was 0.85 m. The speed of the ATV was kept at 4-5 km h^{-1}, which resulted in a measurement interval of approximately 0.16 m. Two surveys were carried out with the EM38DD, one with both coil orientations measuring the conductivity and one with both coil orientations measuring the susceptibility. One survey with the DUALEM-21S provided the eight measurement configurations in one run. All measurements were recorded on the same day (February the 12th, 2008) to minimize temporal influences of soil moisture or temperature. The soil temperature was monitored at 0.3 m depth and remained constant at 4.6 °C during the whole survey day. The measurements were interpolated with ordinary point kriging to a grid with a 0.2 m cell size, using a search window of 2 m radius. Finally, the grids were smoothed with a 1 m radius mean filter.

7.5 Soil augering

Auger observations were laid out in two different areas to characterize the conductivity and susceptibility of the soil. The locations were selected based on two criteria: covering the attribute space of one measurement mode and avoiding the areas with strong responses of the other measurement mode. This meant that the samples for the conductivity were chosen in regions with low susceptibility and vice versa. The soil was augered with a gouge auger up to 2.35 m depth. The soil profile was described, with special attention for the depth of the clay substrate in the auger set, directed to the conductivity verification. Samples of topsoil sandy loam and subsoil clay were analyzed for texture (according to the pipette-sieve method, [104]). In the auger observation directed to the susceptibility verification, more attention was given to identify material with a high susceptibility, such as brick.

7.6 Results of the conductivity measurements

The results of all conductivity-measurements showed a dominant anomaly of high conductivity situated in the north of the field (Figure 7.3).

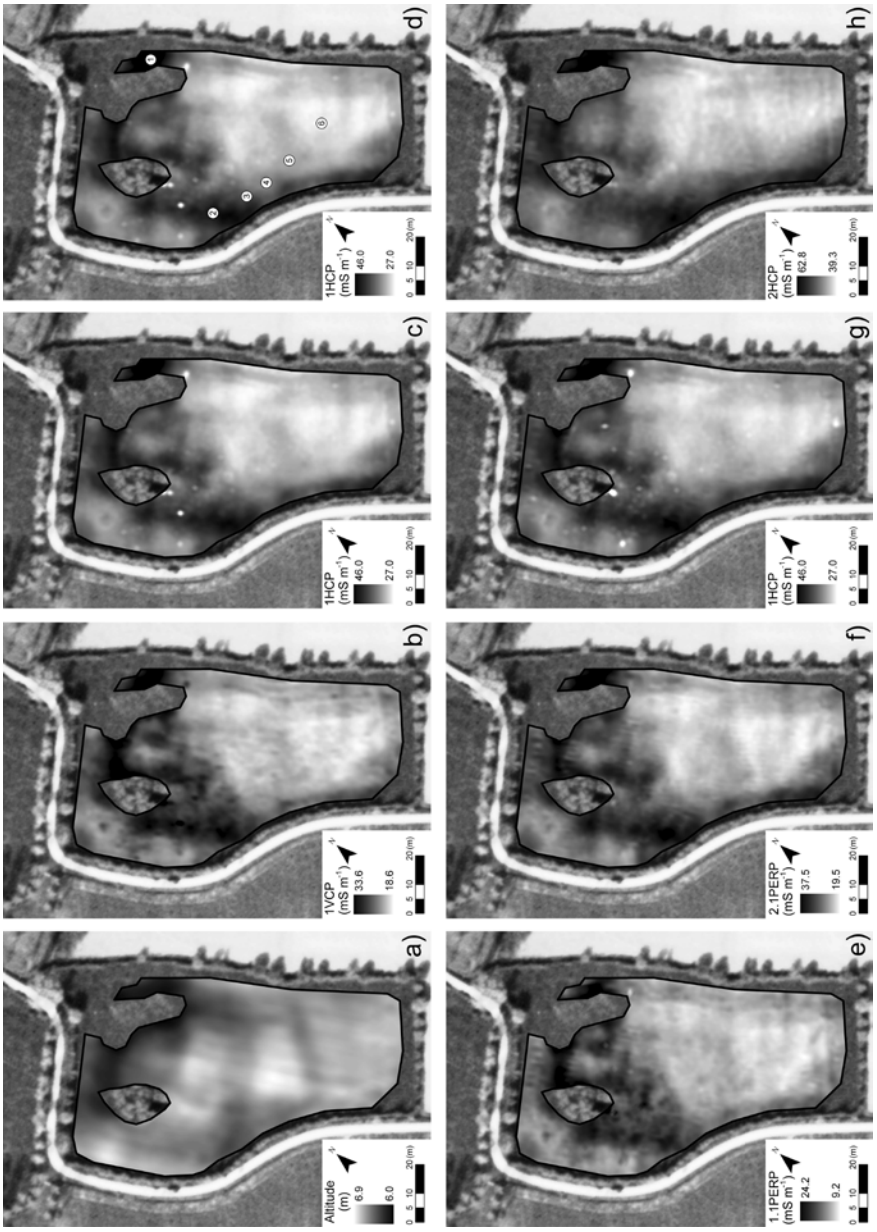

Figure 7.3 (a) Altitude based on the GPS, (b-d) conductivity maps of the EM38DD and (e-g) conductivity maps of the DUALEM-21S. Maps (c) and (d) are the same but in (d) the auger positions are indicated.

the average conductivity of the field increased significantly from the 1.1PERP configuration over the 2.1PERP, 1VCP, 1HCP to 2VCP, respectively. The values of the corresponding coil configurations of both

the EM38DD (Figure 7.3c) and the DUALEM-21S (Figure 7.3g), the 1HCP, were very similar, which meant that both sensors were equally calibrated. The reasons for the conductivity increase of the different coil configurations could be explained by the soil augering, which indicated that the high conductivity was associated with the presence of a shallow clay substrate. The more shallow the substrate, such as at local depressions (Figure 7.3a), the higher the conductivity.

To confirm this observation, the soil was modelled as a two-layered medium. The first layer corresponded with the topsoil sandy loam and the bottom layer with the clay substrate. The conductivity within the two soil layers was assumed homogenous and isotropic, but its value was unknown. The interface depth of the modelled layers was equal to the sum of the sensor height above the soil surface and the depth of the clay layer, observed by the augerings. The bottom of the clay layer was assumed to be at infinite depth, which was an acceptable approximation because according to geological maps, the clay substrate is minimally 10 m thick in this region. With this layer geometry, the unknown conductivities of both layers were modelled (see section 2.8.1) using the 2HCP-configuration of the DUALEM-21S (which has theoretically the largest depth of exploration). The sum of the squared differences between the modelled and the measured conductivities at the auger points (Figure 7.3d) was minimized. The unknown layer conductivities were modelled at 21 mS m^{-1} for the sandy loam topsoil and 79 mS m^{-1} for the clay substrate. Compared with the texture analysis of the topsoil, having 57 % sand and 13 % clay, and the substrate, which has 49.0 % sand and 26 % clay, these conductivity values were very realistic.

The apparent conductivity of the other coil configurations was modelled and plotted against the depth of the clay layer, using the modelled layer conductivities of the 2HCP configuration, (Figure 7.4). The modelled values of the 21PERP configuration underestimated the real conductivity at shallow clay depths and the other models slightly overestimated the real conductivity at deeper clay depths. Overall, the modelled curves fitted the observation points well, for the configurations of both the DUALEM-21S and the EM38DD (Figure 7.4a and b). Consequently, the increase in conductivity for the different coil configurations was most likely caused by the clay layer. Therefore, the multiple coil configura-

tions with a different depth of exploration provided more insight in the structure of the layered soil profile.

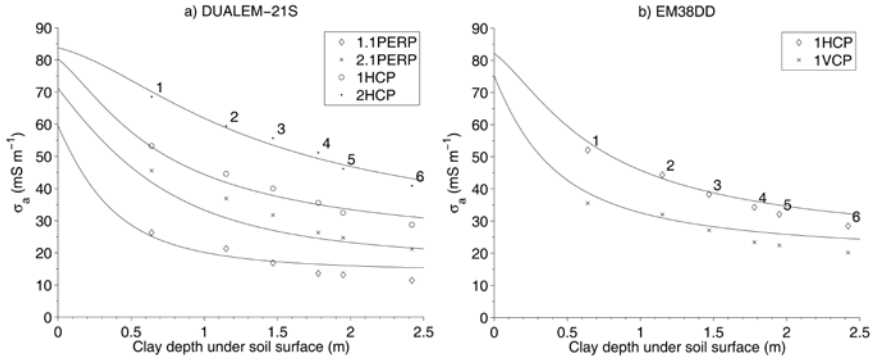

Figure 7.4 Modeling of the conductivity as a function of depth to the clay layer. Markers 1 to 6 are the measurements, while the solid lines are the models.

The conductivities of the 1.1PERP map were subtracted from the 1HCP map of the DUALEM-21S (Figure 7.5a) and the 1HCP map was subtracted from the 2HCP map (Figure 7.5b). This operation highlighted the differences between these sensor configurations, revealing new anomalies. A low, linear anomaly appeared that was situated just south of the ditch indicated by the arrow on Figure 7.5a. At this location, the auger hit a solid brick wall at 0.17 m depth and brick rubble concentrations at both sides. These remains are most likely associated with the priest's house, because no historical evidence was found of other buildings at this site. Another anomaly was highlighted on Figure 7.5b, which coincided with a local, linear depression (Figure 7.3a). This depression was probably a former ditch dividing two land parcels. Other features, such as a linear anomaly close to the southern border, were not verified in the field and were therefore not discussed.

7.7 Results of the susceptibility measurements

In general, the susceptibility results were very different from the conductivity measurements (Figure 7.6), with the exception of the two significant anomalies identified in Figure 7.5. Again, the 1HCP configuration was very similar for both sensors (Figure 7.6c and g). All configurations indicated a very strong magnetic anomaly in the north of the field. The

wall on Figure 7.5a was visible as a high susceptibility anomaly. This was most certainly caused by the high susceptibility of the brick remains close to the surface. The ditch of Figure 7.5b was clearly visible on the PERP configurations of the DUALEM-21S (Figure 7.6e and f). However, other anomalies were detected that did not correspond with the ones visible in the conductivity maps.

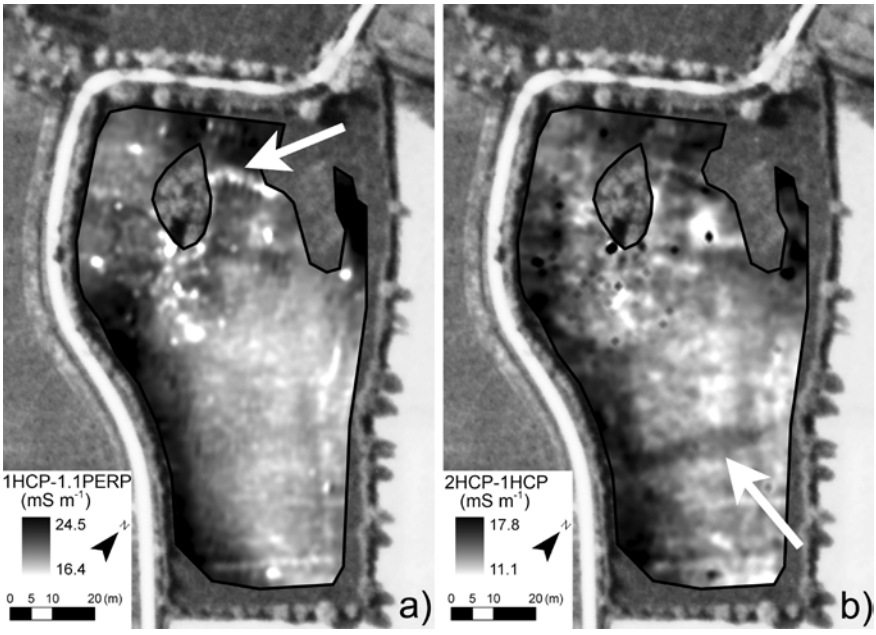

Figure 7.5 Combinations of two conductivity maps of different coil configurations. (a) 11PERP subtracted from the 1HCP, (b) 1HCP subtracted from the 2HCP.

At the location of the auger points of Figure 7.6d, the susceptibility was high in all the coil configurations, except for the 1HCP configuration where it was both low and high. This was explained by the change of sign of this configuration at 0.6 m depth for layered soils (see section 2.8.1). If material with a high susceptibility is present at different depths, the response can be either positive of negative. To verify if this was the case, a vertical profile was constructed based on the auger observations (Figure 7.7). The soil profile representative for the field, with sandy loam at the top covering a clay substrate, was found at positions (1) and (6) (only very small fragments of e.g. brick and charcoal were distributed over the profile).

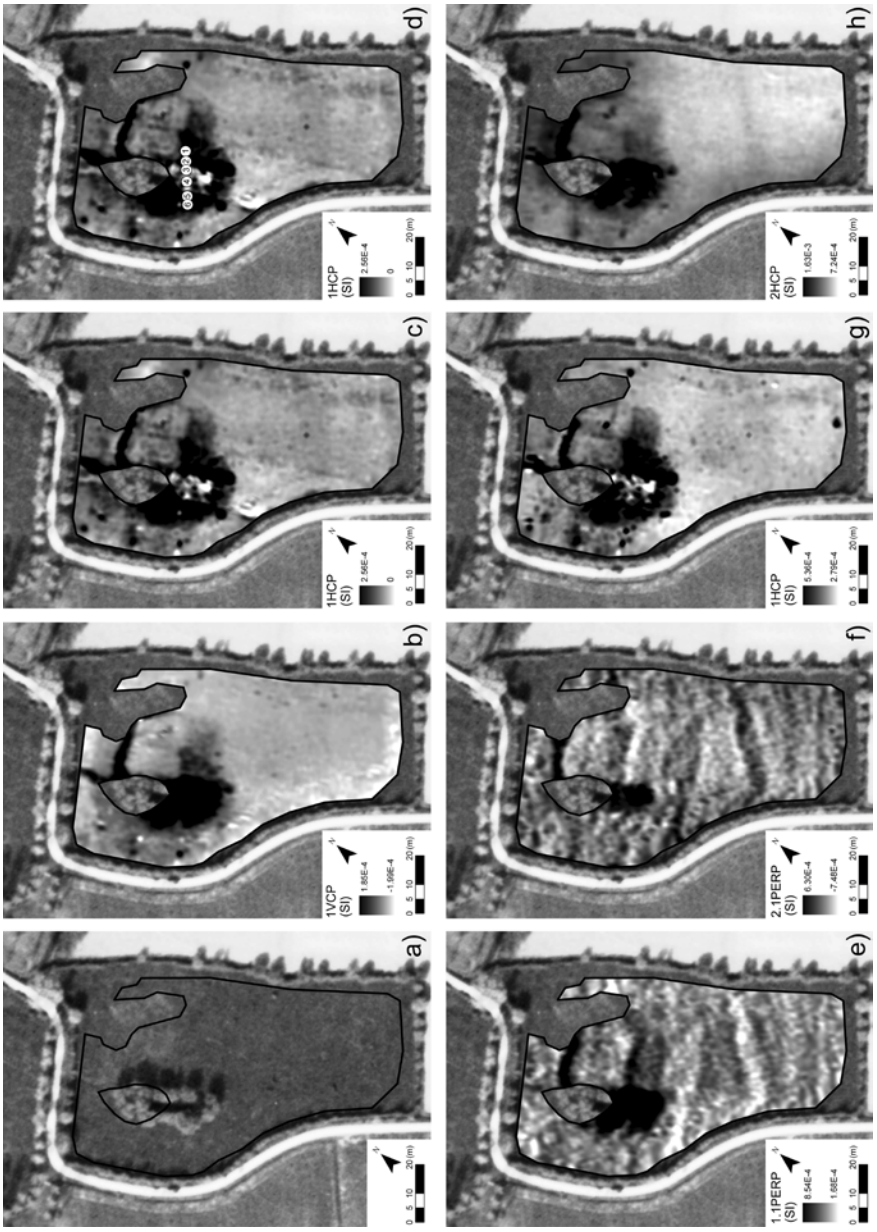

Figure 7.6 Aerial photograph of the Second World War (a), taken the 9th of May, 1944 (copyright: Keele University); susceptibility maps of the EM38DD (b-d) and of the DUALEM-21S (e-h). Maps (c) and (d) are the same but on map (d) the six auger locations are indicated (numbered from right to left).

At the other positions, the profile was partly disturbed by a layer of rubble containing brick fragments. While at positions (2) and (5) this

layer was relatively thin, at positions (3) and (4) the rubble continued down to 1.8 m depth. At these locations, the susceptibility of the 1HCP map was very low.

On an aerial photograph of the US air force taken in May 1944 during the Second World War, a former small pond surrounded by trees corresponded with the low susceptibility anomaly on the 1HCP map. Below the rubble layer, stratified sediments on top of an organic, peaty layer were augered, which confirmed the presence of a former pond. More recently, the pond must have been filled up with rubble, causing the low susceptibility of the 1HCP-map. At the sides of the pond, the filling was less deep, causing a high susceptibility. Thus, it was possible to distinguish areas with a varying depth of magnetically susceptible material, by interpretating the depth sensitivity of the multiple coil configurations. A similar change in sign of the susceptibility response also occurred in the PERP orientations, where the 1.1 m coil separations produced an opposite response to the anomaly of the 2.1 m coil separation (Figure 7.6e and f).

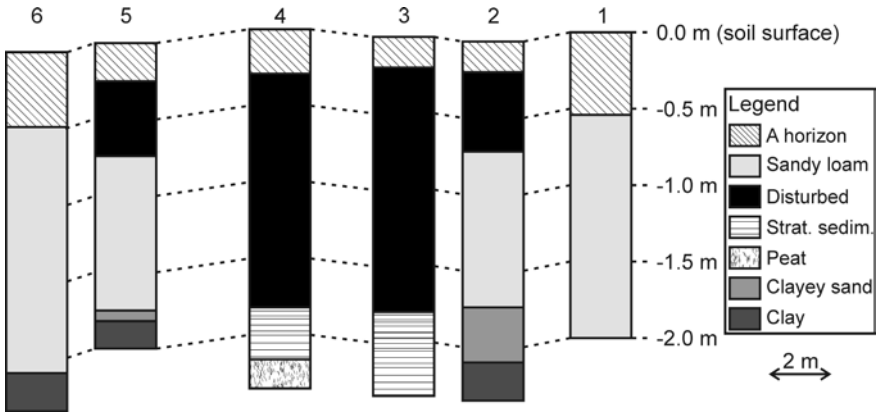

Figure 7.7 Reconstructed vertical cross-section based on the soil auger observations. The layer depths were adjusted to the local altitude.

7.8 Conclusions

The conductivity and susceptibility maps were very complementary, each showing interesting anomalies related to different structrures. The anomalies looked very similar between different coil configurations of the conductivity response; but after subtracting one configuration from another, new anomalies were highlighted. Apart from the detection of extra ano-

malies, the measurements of the multiple coil configurations could also be used to reconstruct the soil profile in depth. In this case-study, prior knowledge of augering was used to fit a model of two layers with a distinct conductivity. Further investigation could explore inversion without prior knowledge using the multiple coil configurations, both for 1-D and 3-D structures.

In the susceptibility response, some anomalies were visible in all coil configurations, while some were limited to particular configurations. Interpretation of this response is complicated by the change in sign at certain depths for the HCP orientation, which has already been mentioned by [4]. The PERP response suffered also from a similar change in sign. Only the VCP responses were all positive and therefore easier to interpret. Although a lot of redundant information was present in the multiple coil configurations, they provided more anomalies and more insight in the soil profile than a single configuration.

Chapter 8

Geoarchaeological prospection of a Medieval manor[1]

8.1 Abstract

In archaeological prospection, geophysical sensors are increasingly being used to locate the buried remains within their natural context. To cover a large area in sufficient detail, a FDEM sensor can be very useful, measuring simultaneously the electrical conductivity and the magnetic susceptibility of the soil. In this study, a field of eight hectares, containing a Medieval manor, was mapped in a submeter resolution using the motorized platform. However, as different soil features can yield similar sensor anomalies, the interpretation of geophysical maps can be ambiguous. Therefore, soil auger observations were conducted along two perpendicular transects of which the location was selected based on the sensor maps. Two soil profiles could be reconstructed to provide a direct verification of the anomalies. Both prospection methods were minimally destructive and proofed highly complementary to delineate both natural and anthropogenic features, which clearly presented a moated site along a former tidal channel.

[1]Modified from: Simpson D, Lehouck A, Van Meirvenne M, Bourgeois J, Thoen E, Vervloet J 2007. Geoarchaeological prospection of a medieval manor in the Dutch polders using an electromagnetic induction sensor in combination with soil augerings. *Geoarchaeology-an International Journal* 23, 305-319.

8.2 Introduction

Archaeological prospection focuses mostly on detecting small-scale features like buried walls or ditches. This requires observations at a very high density, so for practical reasons these observations are often limited to a restricted area of interest. On the other hand, surveying a larger area encompassing the site of interest has significant advantages: 1) to detect other relevant features related to the site, 2) to be able to compare site-specific anomalies with the surrounding measurements and 3) to map the natural context of the site. FDEM sensors on motorized platforms are a very useful tool for all three tasks.

However, too often geophysical maps are interpreted without direct observations of the soil volume. This is particularly dangerous when FDEM sensors are applied, because different objects at different depths can create similar anomalies (called the "principle of equivalence" [10]). This makes it also difficult to reconstruct the real soil profile conductivities with inversion modelling. Therefore, the sensor anomalies need to be verified with direct soil observations down to a reasonable depth. The proposed method to complement the FDEM prospection is to conduct soil auger observations along transects. According to [2], soil augering is one of the most useful methods in geoarchaeology and is very suitable to combine with geophysics. Compared with other prospection methods such as field walking, shovel test pits or excavation trenches [105], soil augering offers a direct observation of the subsoil with minimal soil disturbance, and can cover large areas relatively fast.

The objective of the study was to investigate if conductivity and susceptibility anomalies could be interpreted by soil auger observations to understand the site formation. Therefore, a study area of eight hectares, close to the Dutch coast near the Dutch-Belgian border, was surveyed. Historical records, archaeological relict mapping and historical maps indicated there the presence of a Medieval manor buried by flood sediments. The overlapping of natural soil variability, due to recent geomorphological processes and anthropogenic soil changes, required a geoarchaeological approach to interpret the site. To cope with the large area of the site, a strategy was adopted zooming in on three scales to focus on interesting parts of the field in a higher resolution.

8.3 Site description and historical background

8.3.1 Geographical setting, geomorphology and soil characteristics

The study area is situated in the polder area extending from the north of Belgium into the south-eastern part of The Netherlands with central coordinates 51° 20’ 33.39’’ N and 3° 33’ 4.18’’ E (Figure 8.1). These polders represent a late Holocene landscape that consists mainly of alternations of marine and perimarine sediments (sand and silt) and peat beds [106, 107].

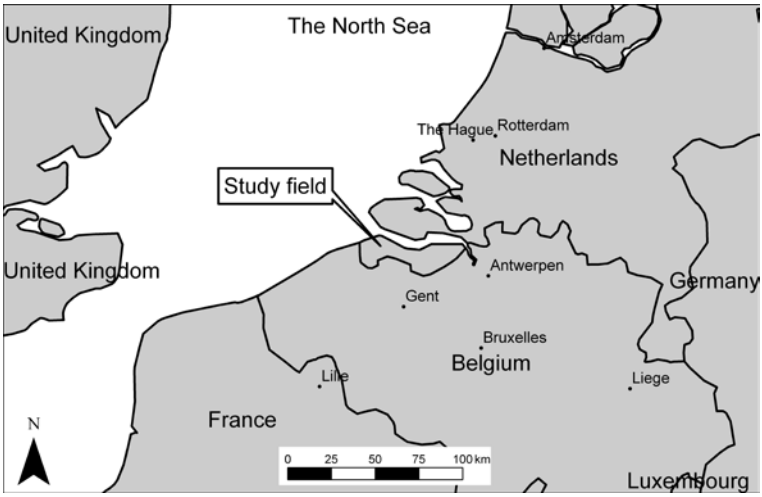

Figure 8.1 Location of the research site, near the Dutch-Belgian border.

Pleistocene loamy cover sands (Boxtel Formation) underlie the Holocene depositional sequence in most parts of the area. In the south of the coastal lowlands, cover sand ridges are present at the surface. In general, the top of the Pleistocene substratum slants down to the north, towards the North Sea shore and the basin of the river Schelde. The study site is situated in the central part of this area, where the top of the Pleistocene substratum is located at approximately 2.5-3 m below the soil surface. Soil maps on scale 1:16 667 [108] and 1:50 000 [109] indicated a sandy clay soil at the study site. Closer inspection revealed that this is a recent, marine sediment deposited between the end of the 16th century and the middle of the 17th century. None of the maps indicated any anthropogenic disturbance of the natural sediments. The geomorphological map on scale 1:50 000 [110] was based on the soil and geological maps, which

were of little use in understanding the geomorphological processes in this submerged area.

8.3.2 Historical and archaeological setting

The Medieval site under study was a lost dependency of the Benedictine abbey of St. Peter in Gent (Belgium). The site, in Medieval texts called "Ruschevliet", has been an important centre for agrarian exploitation, and functioned as storage for tithes. The complex was probably built in the 12th century. The manor has even temporary been an independent priory of the abbey, but from the second half of the 14th century on it was a farm that was leased out by the abbey of St. Peter [111]. The Medieval site was lost during the Eighty Years War (1566-1648) of the Seven Provinces of The Netherlands against the Spanish authority. The area was inundated for military reasons probably shortly after 1583. For a period of seventy years, the old landscape was reshaped into a flooded environment. After the war, the Medieval landscape was completely reorganized. In the 17th century, a new landscape was established in a strict geometrical organization, which is still dominant today.

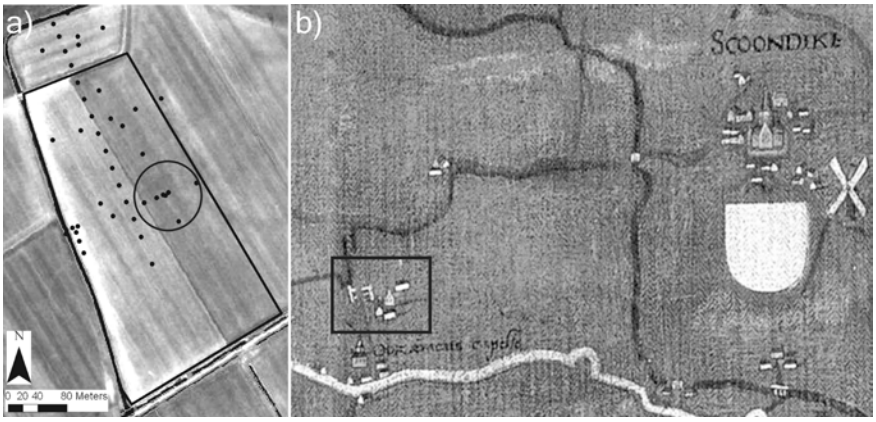

Figure 8.2 a) The study field delineated on an aerial photo, with the coarse auger locations depicted as black dots and the location of the moated site within the circle. b) Detail of the map of Pourbus (1571), the small rectangle indicates the possible location of the Medieval manor "Ruschevliet", on the east side of the "Ruschevliet road".

Historical geographical research during the 1950s did not identify the exact location of the Ruschevliet settlement [112]. Due to recent archaeological and historical research involving new methods, the centre of

the Medieval manor "Ruschevliet" was identified with high certainty somewhere within an agricultural field close to the village Schoondijke in the autumn of 2004 [111]. Relict mapping, field walking and a coarse auger campaign were then conducted on the field, which resulted in the localization of a moated site (Figure 8.2a). Aerial photographs and a Digital Elevation Model (DEM) were used as well. The DEM (het "Actueel Hoogtebestand Nederland", from 1996-2003), was obtained from the "Meetkundige Dienst Rijkswaterstaat". Height measurements with a minimum density of one point per 16 m^2 were interpolated to a 5 by 5 m^2 raster file with a maximum horizontal standard deviation of 16 cm.

The map of Pourbus (1571, Figure 8.2b) revealed the presence of a large building, which could now almost certainly be identified as the demesne centre "Ruschevliet".

8.4 Survey methodology

8.4.1 Sensor strategy

The total field was measured in two days in a 2 by 2 m resolution. The first day, the sensor measured conductivity in both coil orientations and the second day; the susceptibility was measured in both coil orientations (Survey 1, Figure 8.3). Unfortunately, the susceptibility survey suffered from GPS satellite reception losses, so a number of lines had to be removed. Based on Survey 1, a smaller rectangular area of 120 by 230 m (2.76 ha) was measured at a 1 by 1 m resolution with both coils measuring the conductivity (Survey 2, Figure 8.3). Finally, in a small area magnetic measurements were collected at 0.5 by 0.5 m (Survey 3, Figure 8.3). This resolution is adequate to detect small archaeological structures like walls.

8.4.2 Soil augering

The localization of the two auger transects was based on the results of the sensor maps. The focus of this paper was on the occupation zone; cultural relicts near the site were not considered.

During the auger campaign, a Dutch hand auger ("Edelman" auger, 7 cm in diameter) was used for the first meter beneath the soil surface. For deeper horizons, a 1 m gouge auger (2 cm in diameter) was used. Ho-

rizons and layers were described according to the classification system of the Dutch Soil Survey Institute [113], revised by [114]. During the soil survey, visible soil characteristics, as well as the presence of archaeological artifacts (brick, pottery sherds, etc.) and ecofacts were observed. Soil texture and organic material were estimated according to reference soil sample analyses, attached to the commentary of different soil maps available for the area. The presence of carbonates was tested with HCl (10 %), with distinction of three classes (1: without carbonates; 2: some carbonates and 3: rich in carbonates). Marine sediments were originally rich in $CaCO_3$, so this test is important to identify dissolution and/or precipitation processes.

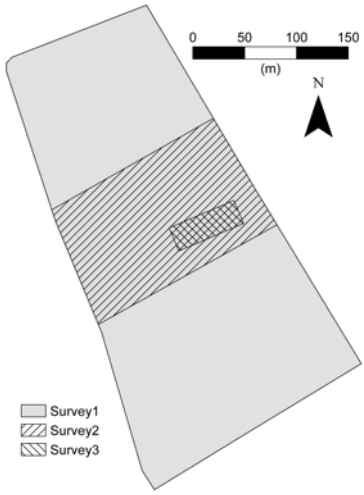

Figure 8.3 Consecutive surveys in a 2 by 2 m (Survey 1), a 1 by 1 m (Survey 2) and a 0.5 by 0.5 m resolution (Survey 3).

Soil cores were taken at intervals of 2 to 4 m along a transect to enable the detection of cultural relicts such as building remains and large ditches. This sampling interval was too coarse to find small features such as walls and small ditches or to have an understanding of the formation processes, since soil observations between consecutive augers differed due to local natural and anthropogenic processes. Therefore, a more detailed sampling procedure (augering intervals of 0.5 to 2 m) was applied at some locations.

Auger descriptions along the same transect were related to each other and graphically presented as a continuous vertical cross-section.

The altitude was expressed in m NAP ("Normaal Amsterdams Peil"), the reference level of the Dutch ordnance.

8.5 Results and discussion

8.5.1 Survey 1

The initial coarse auger observations campaign had indicated the presence of a moated site somewhere within the field of eight hectares. A rough estimation of the ditch system surrounding the manor could be delineated, situated in the centre-east of the field. However, the moated site was undistinguishable on the DEM (Figure 8.4a). A large marine channel running in the east of the field was visible as a local depression. The presence of this channel was confirmed by the auger observations. Apparently, the moated site was located at the west side of this channel. Consequently, the channel was probably developed into a waterway at the time of settlement. Although at this stage the position of the site was known, a very high number of auger observations would have been required to delineate the exact boundaries of the remains with auger prospection. Moreover, since the coarse auger observations did not cover the whole field, there was a risk of missing important structures associated with the site.

The maps of Survey 1 provided the answers to these research gaps (Figure 8.4b-c). In this case study, the conductivity in HCP orientation suffered less from noise than the VCP orientation, because it is less sensitive to disturbance due to surface roughness, and thus produced clearer anomalies. For this reason, the results were shown of the conductivity measured in HCP orientation and the susceptibility in VCP orientation. The conductivity map was strongly related to both natural and artificial soil anomalies. The channel in the east was visible as a high conductive zone, indicating finer sediments and/or higher wetness. Close to the field borders, similar high conductivities were found. The map also confirmed the location of the moated site. The ditch system surrounding the site was sharply delineated, having a rectangular shape. In the southwest corner of the moated site, a smaller square delineation attracted the attention. To the west of the rectangular moated site, the anomalies indicated the entrance path, probably connected to the "Ruschevliet road".

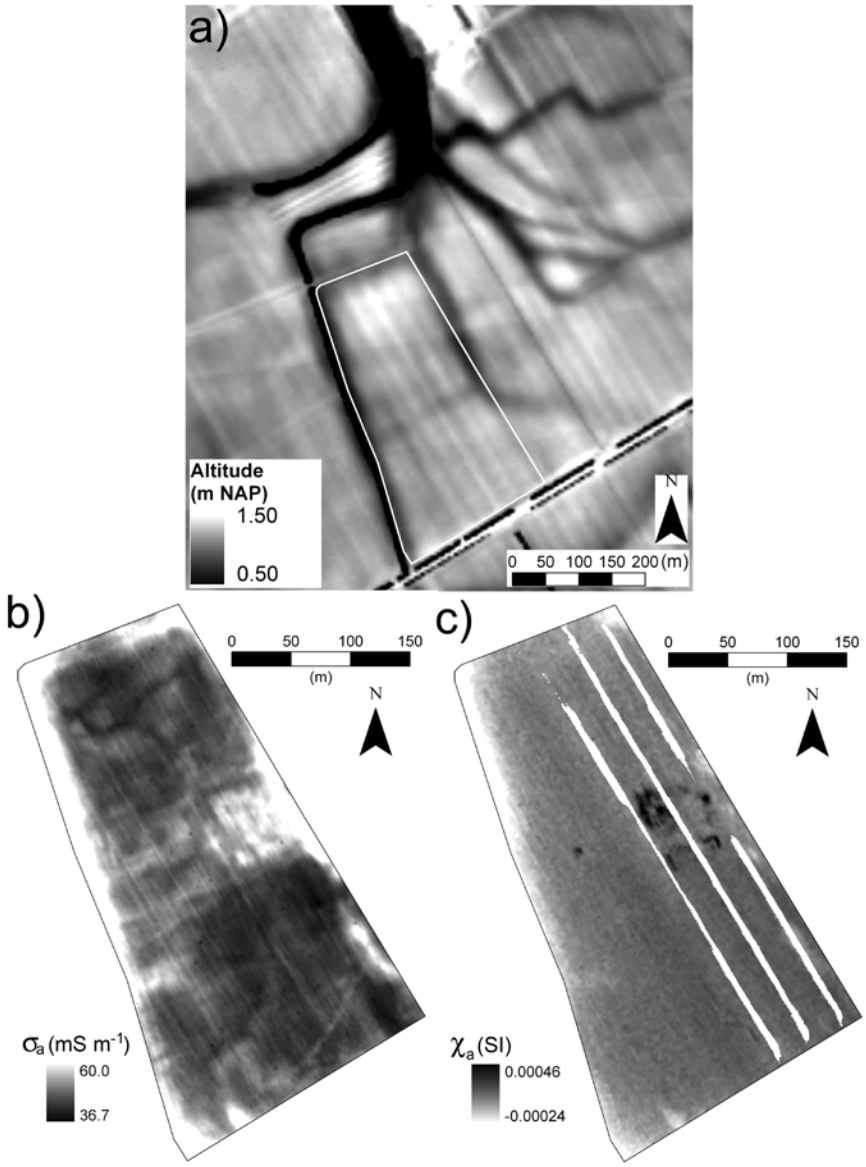

Figure 8.4 a) DEM with delineation of the field boundary; b) Survey 1: conductivity measured in HCP orientation and c) susceptibility measured in VCP orientation.

Parallel to the entrance path, the whole site was flanked by small ditches in the northern and southern areas that indicated the late Medieval field system [111]. The ditch parcel in the southern area was transformed and reoriented probably in the middle of the 17th century. This ditch system could be seen clearly on the DEM and on the conductivity map. In

the rest of the field, anthropogenic anomalies were also visible with no immediate interpretation. The susceptibility map was very homogeneous over most of the field, apart from the moated site itself where the archaeological traces were very clear. Both maps produced complementary anomalies, which together provide more information than just one map. The next research step was focused on the moated site, although the geophysical survey revealed also potentially interesting features in the rest of the field.

8.5.2 Surveys 2 and 3

In the next stage, the moated site and its possible entrance way were investigated in detail with the FDEM sensor at a 1 by 1 m resolution (Survey 2 on Figure 8.3). The conductivity was measured in both coil orientations because this seemed to give the most information on the soil variability around the site. A more detailed map was obtained than the one from Survey 1 (Figure 8.5).

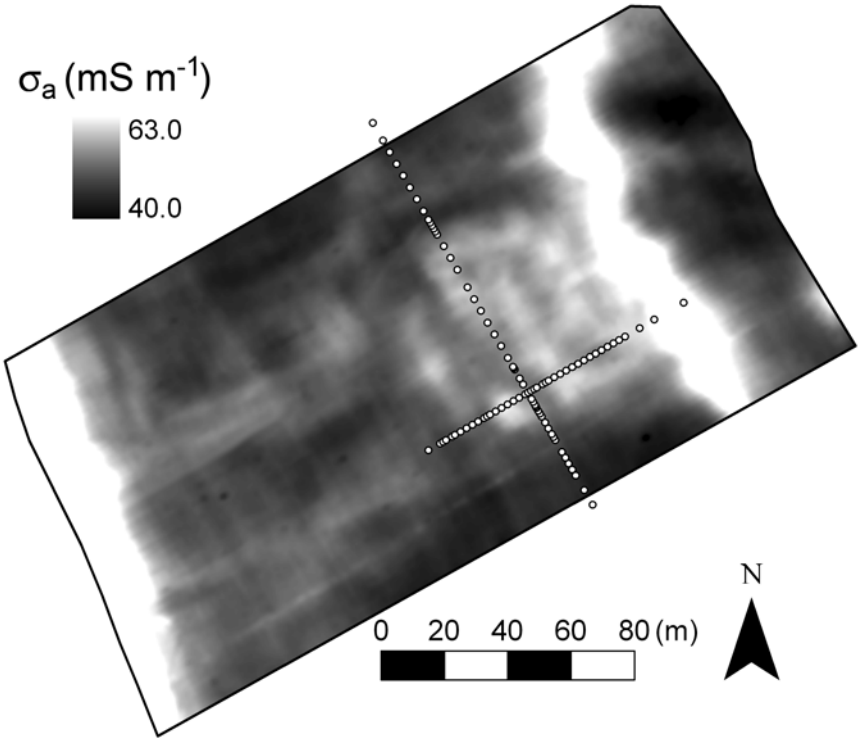

Figure 8.5 Survey 2: conductivity map of the HCP-orientation in a 1 by 1 m resolution. The auger positions are indicated by dots.

The auger observations along the two transects were laid out, a first one running westsouthwest to eastnortheast (W-E) and a second one running northnorthwest to southsoutheast (N-S).

Based on the auger observations, two vertical profiles along the transects were drawn, showing the subsoil heterogeneity down to a depth of 3.5 m (Figure 8.6). At the surface, the thickness of the actual plough layer varied between 15 and 45 cm. Under the plough layer, marine sediments were found, originating from the inundation period of 1583-1651. These sediments displayed a strongly varying thickness between 0 and 1.5 m. The sediment had a texture between sandy clay and clay, a light brown-grey color with iron oxide mottles and it was rich in calcium carbonate. Banks of shells of e.g. *Mytilus* sp. and *Cerastoderma* sp. were found as well. This inundation layer covered the late Medieval cultural level, which contained several interesting structures such as ditches and walls. The cultural layer itself overlied another marine deposit, which had been developed during the late Roman and early Medieval period. This deposit originated from a channel system that had eroded the underlying peat layer. This peat layer was dark brown, maximum 1 m thick with fragments of reed and wood, and was deposited during the middle Holocene until the 3^{rd}-4^{th} century AD. The deepest deposit that was augered was Pleistocene sand at approximately 3 m depth.

Survey 3 was obtained with both coil orientations measuring susceptibility, which gave the most information about the remains of the moated site. The W-E transect locations were projected on the sensor maps to compare the anomalies with the reconstructed soil profile (Figure 8.7). When the sensor maps are compared with the cross-section, the depth sensitivity of the FDEM configuration has to be taken into account. Features below approximately 1.5 m depth did not have any influence. The most striking structures seen on the cross-section were a large ditch in the west and some locations with a lot of brick rubble. The ditch must have been approximately 10-14 m wide and 2.5-3 m deep. The dark grey layer at the west side of the ditch (profile numbers 662-666) was filled up with rubble of brick and charcoal. This zone had a lower conductivity than the ditch itself on the map of Figure 8.6a. Both sensor maps showed a clear anomaly on the east flank of the ditch of low conductivity and high susceptibility. The susceptibility map indicated a large rectangular structure of 42 by 13 m, most likely the remains of a building.

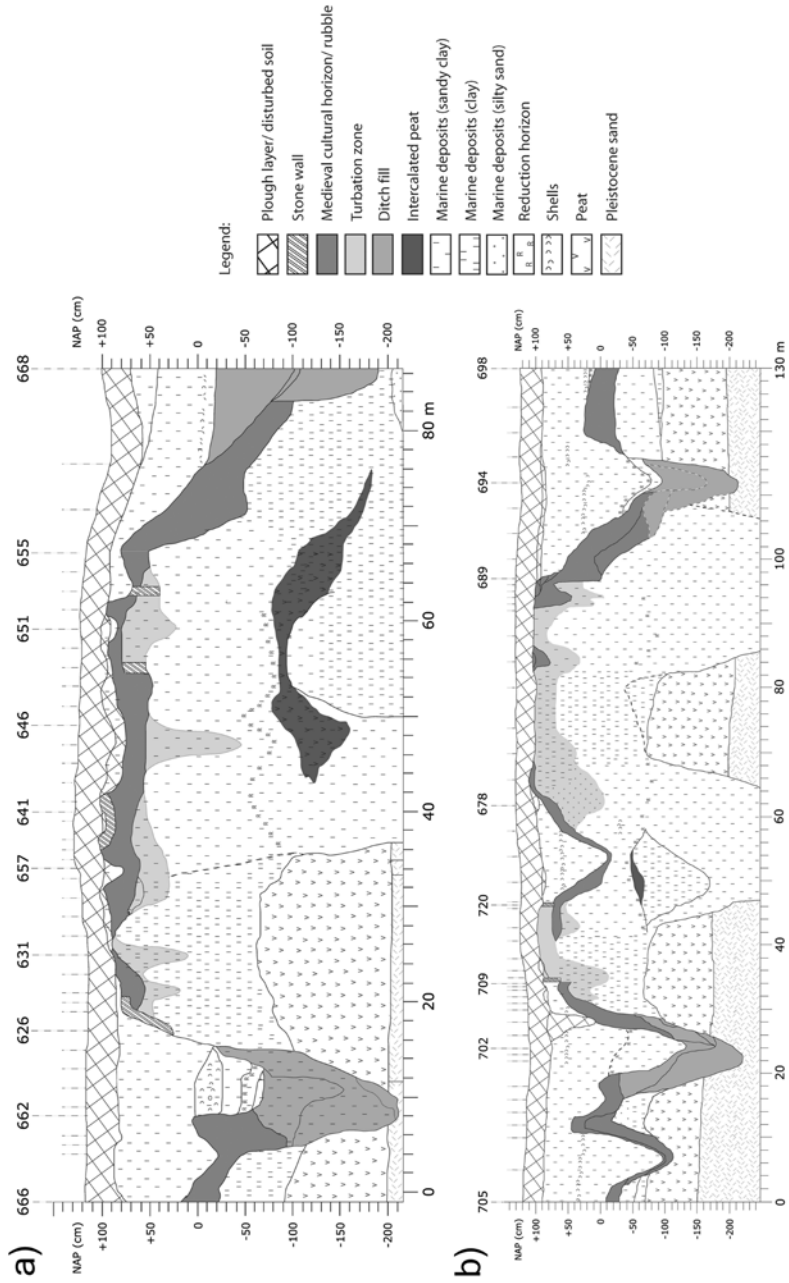

Figure 8.6 a) E-W vertical cross-section based on 42 auger observations. The vertical axis is the altitude, the horizontal axis the relative distance in m; all auger positions and key auger numbers are displayed on top of the section. b) N-S vertical cross-section based on 50 auger observations.

This was confirmed at auger position 626, where a high concentration of large brick fragments and mortar were found, which were difficult to penetrate with the auger.

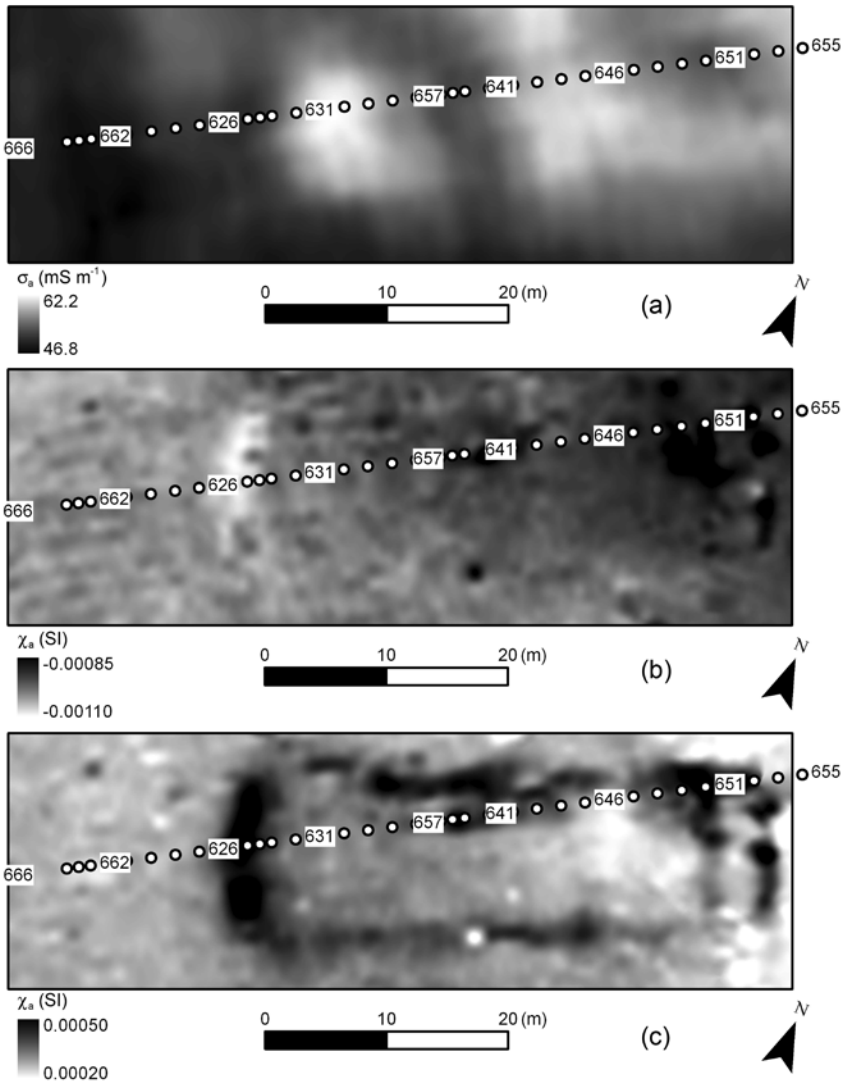

Figure 8.7 (a) Conductivity map in HCP orientation of Survey 2; (b) susceptibility maps of Survey 3 in HCP and (c) in VCP orientation.

It is important to mention that these wall remains were found with the auger survey after the FDEM survey and that the horizontal spatial extend could be identified easily based on the FDEM anomalies. The dimensions of the building were more accurately defined on the sensor

maps. However, the auger observations gave valuable information on the nature of the sensor anomalies and their variation in depth.

Just to the east of the ditch, the conductivity increased with a value of 10 mS m^{-1} from position 626 to position 631 and it decreased back to its original value at position 657. Here, the vertical profile showed a clay deposit occurring almost at the surface. The shallowest position was just under the plough layer at 25 cm depth. Close to position 641, the auger again collided on the remains of a brick wall. Here, the section crossed the north side of the building remains. A less clear structure was found at position 646, having a higher conductivity. Near position 646, the marine deposits under the cultural level must have been mixed with sandy material down to 1.7 m depth, probably caused by deep digging. This structure could not be distinguished on the sensor maps, because it did not contain enough conductivity or susceptibility contrast with the surrounding soil.

Further to the east of the profile, two other brick walls were found together with some brick rubble at the surface. At this location, the conductivity was low and the susceptibility map showed two parallel, linear anomalies, 5 m apart. More to the east, there was a large channel that carved its way even in the Pleistocene sand, which corresponded to the channel that was visible on the DEM. The bedding of this channel had developed into a waterway before late Medieval times. It was used as a ditch to border the east side of the moated site. This filling could be distinguished by slightly higher conductivity values from the larger channel.

All information of the sensor maps and the soil auger transects was integrated in a simplified sketch of the ditch and the main rubble sites (Figure 8.8a). The locations of the two transects are shown on Figure 8.8b. The location of the ditch of the moated site corresponded well at both sides compared with Figure 8.6b of the N-S transect section, as well as the building walls in the south of the site. The circled areas were places where the soil was highly disturbed with rubble. It was possible that another building or structure was located here, but it was probably leveled by the recent plowing of the field. The N-S transect showed that this zone is naturally elevated and that the cultural layer is mixed with the current plow layer. In Figure 8.8a, other interesting features were visible, but because of the lack of auger observations the interpretation of these anomalies would be too hypothetical. The anomalies could be caused by several features, with different form and contrast at different depths. The cross-

sections based on the auger observations showed also other small features, but these could not be extended horizontally since they were not distinguishable on the geophysical maps.

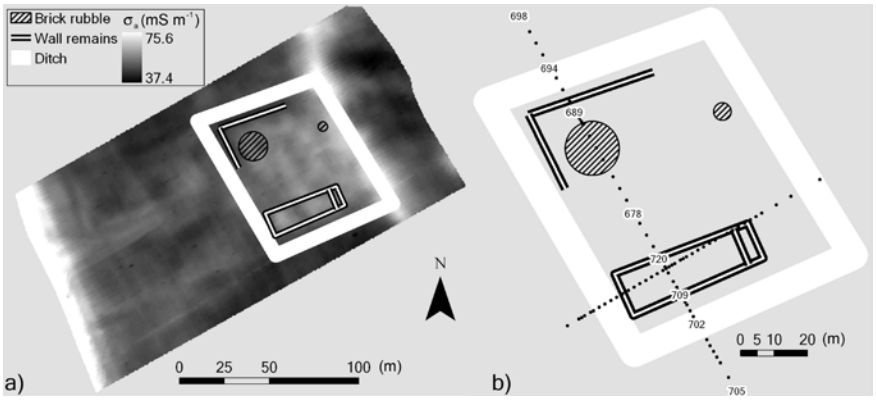

Figure 8.8 a) Conductivity map (HCP) of Survey 2, overlaid by the interpretation of the buried structures. b) Buried structures overlaid by both transects. Relevant numbers of the N-S transect were labeled to use as a reference in the text.

8.6 Conclusions

In this case-study, the combined geoarchaeological approach was successful on two scale levels: 1) delineating the farm site within the total field and 2) mapping of the detailed features within a small area of interest. There was a large correspondence between the structures seen on the geophysical maps and the depth information of the soil observations. The conductivity maps revealed the ditch of the moated site, a large channel that is part of a marine tidal system and large volumes of brick rubble and other features dispersed over the whole field that were not interpreted. The susceptibility strongly reacted to the presence of brick wall remains and it was more suitable to delineate these structures than the conductivity.

Obviously, the limitations of the methodology have to be taken into account. First, to explain the sensor anomalies, it was important that the auger positions were directed by the FDEM anomalies. Second, the number of auger observations had to be sufficient to be able to relate individual transect points and to reconstruct a continuous soil profile. Third, the geophysical survey with the FDEM sensor was limited to a certain depth

and horizontal resolution. Structures deeper than approximately 1.5 m could not be detected. Moreover, the measured signal was an integration of the soil below the sensor, making it difficult to know the depth of the measured anomalies. Small features located in deeper layers could not provide enough contrast. Fourth, not all anomalies found with the sensor could be explained by the auger transect and some structures encountered with the auger did not have sufficient contrast to be distinguished by the FDEM sensor.

Chapter 9

General conclusions and future research

9.1 General conclusions

The general conclusions of the thesis are formulated with reference to the objectives stated in section 1.2. Based on these conclusions, some suggestions will be proposed for future research.

First, a motorized sensor platform carrying the FDEM sensors was adapted and tested to measure several hectares per day in high resolution, which is required for archaeological prospection. These adaptations included the following. A GPS-based lightbar guidance system was installed to be able to drive on closely spaced, parallel tracks. The minimum distance that was still possible to drive was 0.4 m. It was found that the driving speed cannot be too high (< 5 km h^{-1}), in order to maximize the sensor anomaly of small structures and to avoid smearing out the data along the track. The accuracy of the measurement positions was decreased by the offset between the GPS-antenna and the centre location of the coils, which disturbed the anomalies of small structures and therefore needed correction. The spatial offset was shifted back along the track during the data processing, which greatly improved the interpretation of small anomalies. A troublesome issue in FDEM-surveys is the drift in time of the sensor measurements. This drift is especially large for the susceptibility measurement and is often not linearly related with time for long surveys. The drift gives a false image of the background values and can seriously obscure local anomalies. A new procedure was developed to monitor, and if necessary, correct the drift during one survey day, using a calibration line at the start of the survey. Where the calibration and survey lines crossed, the calibration readings were subtracted from the survey data. The drift could then be monitored by plotting this difference

in function of the survey time. In case the drift was substantial, it was corrected by modelling the plotted differences with a piecewise polynomial function. Finally, it was necessary to interpolate the irregularly distributed measurements to a fixed grid. For this purpose, a local kriging program was written using a local linear variogram model. The advantage of the kriging algorithm compared to e.g. inverse distance to a power interpolation was that it accounted for the clustering of the data locations. This reduced the striping pattern in the interpolated maps caused by the high measurement density in the line direction. The local, linear variogram model calculation had the advantage that the degree of smoothing depended on the local noise and spatial structure.

Second, once the sensor platform and the data processing were optimized, the sensitivity of both the susceptibility and the conductivity measurement in different coil configurations was evaluated for a layered soil and for small, three-dimensional structures. The theoretical models for a layered soil based on the LIN-approximation corresponded well with measurements in the field. The conductivity models of the different coil configurations could be used to determine the interface between two soil layers, which is valuable information about the environmental context of a site. The susceptibility response to the small structures revealed a large difference in strength, compactness and complexity depending on the coil configuration and the sensor height. It was concluded that the 1.1 m PERP, 2 m HCP and 1 m VCP were the most suitable configurations for susceptibility mapping. Regarding the conductivity response, the coil configurations with the shallowest response according to a layered model produced the largest anomalies to shallow, three-dimensional structures.

Third, the FDEM sensors were compared with a magnetic gradiometer and an ER sensor. The magnetic anomalies of the FDEM sensors were similar to magnetic gradiometer anomalies when using specific coil configurations such as the 1 m VCP. Other coil configurations, such as the 1 m HCP, showed maps that were more ambiguous. In general, the gradiometer produced sharper anomalies, but they were more complicated due to the bipolar response. The conductivity measurements with the FDEM sensor were more suitable to detect high conductivity contrasts, but they were less sensitive to resistive features such as brick walls. This is partly due to the noise level of 0.5 mS m^{-1}, partly because

of the low sensitivity to high resistive structures. ER sensors were more sensitive to resistive structures and had a lower noise level in this range. Another big advantage of the multi-pole ER sensors was the availability of 2-D or 3-D inversion programs, which could be applied to reconstruct the true conductivity values of the soil.

Fourth, two types of archaeological sites were prospected to evaluate the practical use of the FDEM sensor measurements. The first type originated from Medieval periods, with the presence of clearly identifiable remains such as brick foundations. The second type contained circular ditches surrounding former Bronze Age burial mounds. At the Medieval sites, the structures were relatively easy to detect because of the large magnetic susceptibility of bricks or the high conductivity of large ditches. At the Bronze Age sites, the ditches were more difficult to detect. The natural soil and the size of the ditch played an important role in the strength of the conductivity responses. The susceptibility of the studied ditches was very weak and in most cases undistinguishable from the background value.

Finally, this study proved that multi-coil FDEM sensors can be very useful for geoarchaeological prospection, if both the survey strategy (e.g. high resolution, low speed) and data processing (shift, drift correction and interpolation) are carefully conducted. FDEM sensors offer a good solution to map large areas or to map the soil environment. If only one sensor can be applied, the dual measurement of conductivity and susceptibility of the FDEM sensor can provide more insight on the physical nature of the structures. For detailed surveys on small areas, other sensors, such as a magnetometer or a GPR, can be more suitable. In the optimal (budget-independent) situation, multiple sensors should be applied on the same site.

9.2 Future research

Future research should focus on the sensitivity of the conductivity response to a variety of three-dimensional structures in the field. The combination of field experiments and forward modelling should be examined more to understand fully the expected response from different coil configurations. Hopefully, in the near future, 2-D or even 3-D inversion pro-

grams will become available that are able to process the large amount of data obtained from the motorized sensor platform.

In this research, the focus was on Medieval and Bronze Age sites, situated around the north-west of Belgium. It would be interesting to investigate the success rate on other periods and in other locations. However, a thorough evaluation requires not only measuring the field with the motorized platform. Field verification with auger observations as conducted in Schoondijke or other methods such as borehole sensors or trenches remain necessary.

Nowadays, multi-sensor platforms are used in order to combine the strengths of different geophysical sensors. However, the combination of FDEM sensors and GPR on one platform has not yet been thorougly explored. Nonetheless, this platform could provide measurements of the three principal physical parameters in archaeological prospection: conductivity, susceptibility and permittivity. Moreover, the GPR could provide important information, such as depth of soil layers, which improves the ability to model the conductivity response of the FDEM sensor. On the other hand, the conductivity measured with the FDEM sensor can indicate the penetration depth of GPR waves, which is seriously diminished in clay soils with a high conductivity. Finally, both methods do not require penetration of the soil surface, and they are easily mounted on a platform for continuous measurements. For these reasons, this multi-sensor combination looks promising for future prospections.

Appendix A

Forward modelling of 3-D structures

Forward modelling aims to determine what a sensor would measure if the conductivities of the soil are known at all locations. A computer program was acquired that was able to model three-dimensional structures with varying shapes in a layered earth, both for conductivity and susceptibility and in all possible coil configurations of FDEM sensors (EMIGMA V8.1, 2008, PetRos EiKon Inc., Canada). Technical details about the methodology behind the modelling can be read in [115]. The forward modelling could be very useful to evaluate the sensitivity of the different coil configurations. The advantage of theoretical modelling is that any type of structure (if allowed by the program) can be tested. The disadvantage is that the results are further away from a real survey than when field models are used. Therefore, it is always best to verify the model results with some field model data.

The program was tested for the structures described in Chapter 4. It had a problem with the VCP orientation close to the soil surface (personal communication Ross Groom of PetRos EiKon). Therefore, the results were completely different from the measured data and thus not shown here. Nevertheless, an empty plot was inserted in Figure A.1 to make comparison with Figure 4.4 easier. The conditions of the survey over the field structures were simulated and all processing steps were identical. The modelled anomalies of the HCP orientation all corresponded very well to the measured anomalies (Figure A.1). However, for the PERP orientation, the model did not correspond well, especially not for the 1.1 m coil separation that displayed much lower amplitudes. It was not known if this was due to a problem in the modelling program. To conclude, only the results of the HCP modelling looked reliable enough to test the sensitivity to other structures.

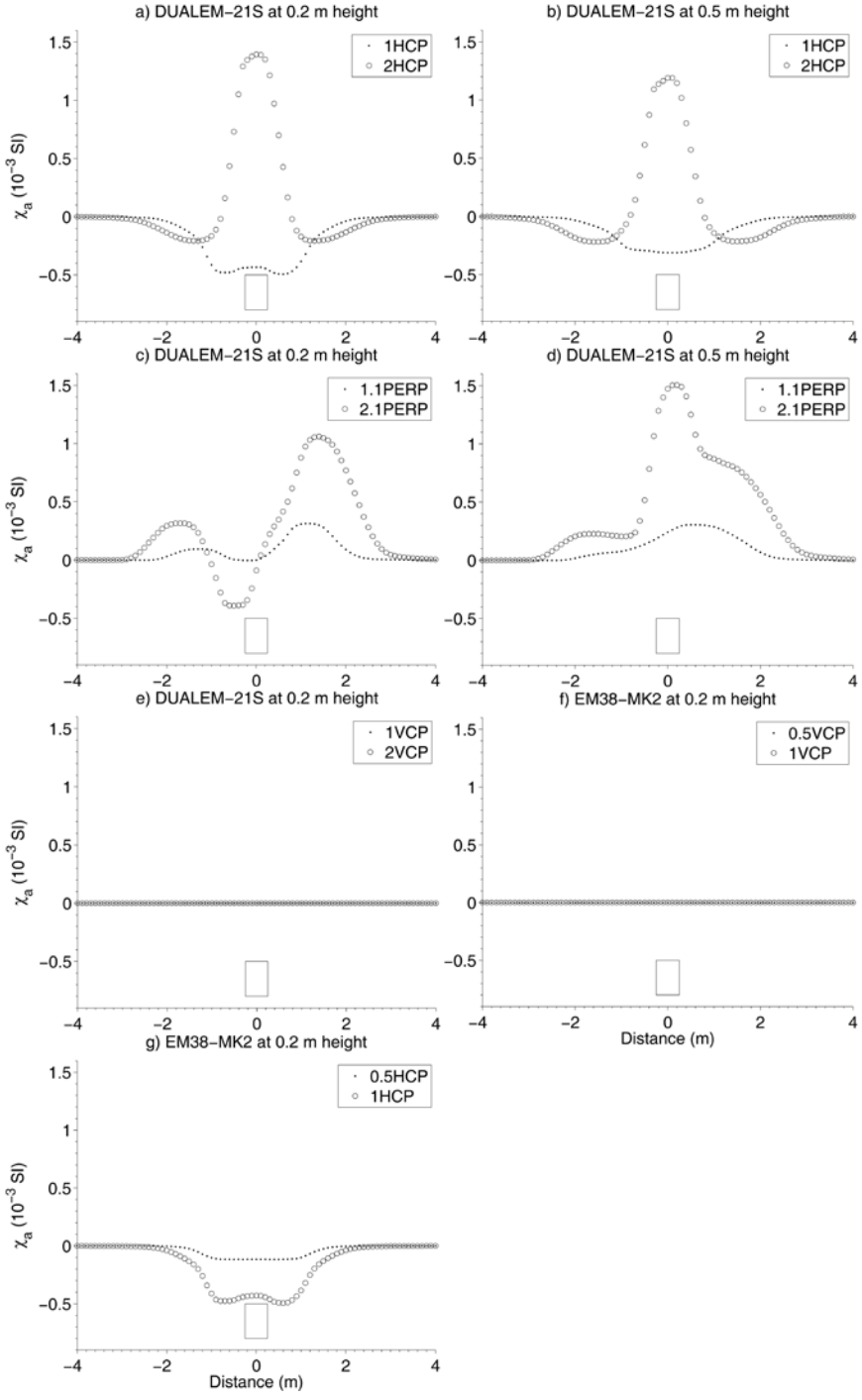

Figure A.1 Modelled anomalies of a transect through the basalt wall. Plots e) and f) do not show actual data.

Appendix B

Inversion of electrical resistivity data

Inversion modelling is the opposite of forward modelling. The goal of inversion modelling of ER measurements is to estimate the true conductivities of the subsurface based on sensor measurements at the surface. The surface measurements give only one value of the apparent or bulk electrical conductivity of a certain soil volume, as if it would be homogeneous. Inversion modelling allows us to estimate the actual conductivities of different zones wthin the soil volume. Each electrode arrangement of the ER-array has a different spatial sensitivity. In general, if the electrodes are more separated, they will be influenced by larger soil volumes (and consequently by deeper layers). By using a variety of electrode separations, different zones of the soil volume will contribute more or less to each arrangement. Thus, if the soil conductivity varies with location (and consequently with depth), then the surface measurements give different values for different electrode arrangements. This information is used in the inversion modelling.

The basic principle of all inversion programs is as follows [116]. A subsurface distribution of soil conductivities is adjusted until the forward modelled values of this distribution matches the measured values as close as possible. Therefore, the inversion is an iterative process where the subsurface conductivity distribution is changed at each iteration and the difference between the modelled and measured values is evaluated. This difference can be evaluated with a criterium such as least squares minimzation. The conductivity model of the soil can be variable in depth, i.e. composed of homogeneous horizontal layers (1-D), it can also vary according to one horizontal direction (2-D) or vary in all directions (3-D). An increase of dimension gives a more accurate estimate of the soil conductivities, but also requires a lot more surface measurements to be taken.

A two-dimensional inversion is a good compromise between accuracy and survey effort and can be easily implemented for the electrical array of the Geophilus.

The inversion program used here was RES2DINV (3.55, 2008, Geotomo Software, Malaysia), using methods described in [117, 118]. The soil volume is divided in blocks with a homogeneous conductivity. The forward modelling uses the finite-difference method to calculate the response of the soil model. An important aspect of ER-inversion is that the resolution of the inversion model decreases with depth. This is a direct consequence of the fact that only large electrode separations can reach deep layers, but they also measure a larger volume. Therefore, the power to reconstruct small structures will decrease with depth. Consequently, small archaeological structures will be more accurately modelled at shallow depths. Before running the inversion, it is important to have an idea of the reliability of each modelled block value, by calculating the model sensitivities for the electrode array used. The higher the sensitivity, the more reliable the block conductivity will be after inversion. The sensitivities for the array of the Geophilus, measured along a track of 10 m, clearly showed a decrease in depth (Figure B.1, all model blocks have an equal size). Blocks at the edges at an increasing depth were also less sensitive, because here the larger electrode separations could not be recorded.

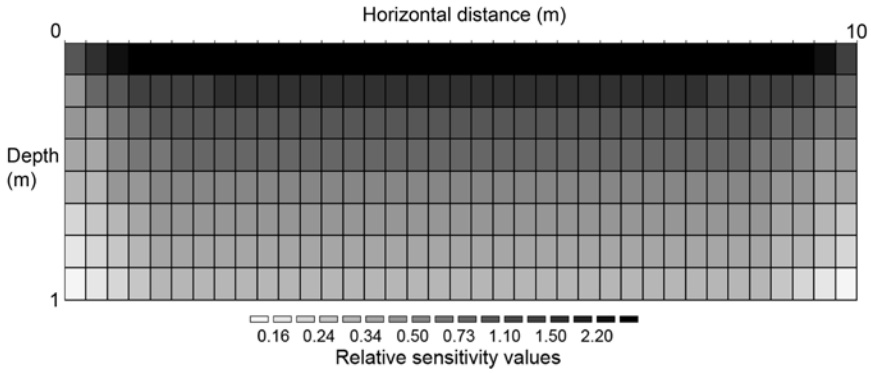

Figure B.1 Relative sensitivities in depth over a 10 m long transect, measured with the electrode array used by the Geophilus sensor.

Appendix C

Curriculum vitae

C.1 Personal data

Name:	David Simpson
Place of birth:	Beveren, Belgium
Date of birth:	August the 2nd, 1981
Nationality:	Belgian
E-mail:	davidgb.simpson@gmail.com

C.2 Education

2002-2005:	Master in Bioscience Engineering Option Soil and Water Management Ghent University
1999-2002:	Candidate Bio-engineer University of Antwerp
1993-1999:	Secondary education, Modern Languages-Mathematics Onze-Lieve-Vrouwecollege, Antwerp

C.3 Professional experience

2006-2009:	Doctoral researcher at the Research Group Soil Spatial Inventory Techniques of Prof. dr. ir. Marc Van Meirvenne, in the frame of a project of the Fund for Scientific Research-Flanders (FWO).
2005:	Researcher IWT-TETRA project University College Ghent

C.4 Scientific publications

C.4.1 Publications in international journals with peer review and in the Science Citation Index (A1)

[1] Cockx L, Van Meirvenne M, Vitharana UWA, Verbeke LPC, Simpson D, Saey T, Van Coillie FMB 2009. Extracting topsoil information from EM38DD sensors data using a neural network approach. Soil Science Society of America Journal 73, 1-8.

[2] Saey T, Simpson D, Vermeersch H, Cockx L, Van Meirvenne M 2009. Comparing the EM38DD and the DUALEM-21S sensors for depth-to-clay mapping. *Soil Science Society of America Journal* 73, 7-12.

[3] Simpson D, Lehouck A, Verdonck L, Vermeersch H, Van Meirvenne M, Bourgeois J, Thoen E, Docter R 2009. Comparison between electromagnetic induction and Fluxgate Gradiometer measurements on the buried remains of a 17th century castle. *Journal of Applied Geophysics* 68, 294-300.

[4] Simpson D, Van Meirvenne M, Lück E, Bourgeois J, Rühlmann J 2009. Prospection of circular ditches surrounding former Bronze Age burial mounds with multi-receiver electrical conductivity sensors. *Journal of Archaeological Science*, submitted.

[5] Simpson D, Van Meirvenne M, Lück E, Rühlmann J, Saey T, Bourgeois J 2009. Sensitivity of multi-coil frequency-domain electromagnetic induction sensors to map soil magnetic susceptibility. *European Journal of Soil Science*, submitted.

[6] Simpson D, Van Meirvenne M, Saey T, Vermeersch H, Bourgeois J, Lehouck A, Cockx L, Vitharana UWA 2009. Evaluating the multiple coil configurations of the EM38DD and DUALEM-21S sensors to detect archaeological anomalies. *Archaeological Prospection* 16, 91-102.

[7] Verdonck L, Simpson D, Cornelis WM, Plyson A, Bourgeois J, Docter R, Van Meirvenne M 2009. Ground-penetrating radar survey over Bronze Age circular monuments on a sandy soil, complemented with electromagnetic induction and Fluxgate Gradiometer data. *Archaeological Prospection* 16, 193-202.

[8] Saey T, Simpson D, Vitharana UWA, Vermeersch H, Vermang J, Van Meirvenne M 2008. Reconstructing the paleotopography beneath the loess cover with the aid of an electromagnetic induction sensor. *Catena* 74, 58-64.

[9] Vitharana UWA, Saey T, Cockx L, Simpson D, Vermeersch H, Van Meirvenne M 2008. Upgrading a 1/20,000 soil map with an apparent electrical conductivity survey. *Geoderma* 148, 107-112.

[10] Vitharana UWA, Van Meirvenne M, Simpson D, Cockx L, De Baerdemaeker J 2008. Key soil and topographic properties to delineate potential management classes for precision agriculture in the European loess area. *Geoderma* 143, 206-215.

[11] Vitharana UWA, Van Meirvenne M, Simpson D, Cockx L, Hofman G 2008. Agronomic consequences of potential management zones delineated on the basis of EM38DD measurements. *Near Surface Geophysics* 6, 289-296.

[12] Simpson D, Lehouck A, Van Meirvenne M, Bourgeois J, Thoen E, Vervloet J 2007. Geoarchaeological prospection of a Medieval manor in the Dutch polders using an electromagnetic induction sensor in combination with soil augerings. *Geoarchaeology-an International Journal* 23, 305-319.

C.4.2 Publications in international journals with peer review (A2)

[1] Simpson D, Van Meirvenne M, Lück E, Rühlmann J, Bourgeois J 2009. Testing of multi-coil FDEM sensors on a field model with magnetic susceptibility contrast. *ArcheoSciences, revue d'archéométrie* suppl. 33, 357-359.

C.4.3 Publications in national journals without review (A4)

[1] Simpson D, Lehouck A, Van Meirvenne M, Bourgeois J 2007. Elektromagnetische inductiemetingen als prospectietechniek voor de reconstructie van middeleeuwse landschappen in het Vlaamse kustgebied. *Archaeologia Medievalis* 30, 200-204.

[2] Simpson D, Van Meirvenne M, De Baerdemaeker J, Vitharana UWA, Cockx L 2006. Soil-crop-landscape relationships within an agricultural field in the loess region of Belgium. Soil Science Society of Belgium, *Pedologie-Themata* 13, p. 50.

C.4.4 Publications in proceedings of scientific conferences (C1)

[1] Verdonck L, Simpson D, Cornelis W, Plyson A, Bourgeois J 2008. Analysing the velocity of ground-penetrating radar waves: a case study from Koekelare (Belgium). In *Proceedings of the 1st international EARSeL workshop 'Advances on remote sensing for archaeology and cultural heritage management'*, Lasaponara R, Masini N (Eds), 30th of September-4th of October 2008, Rome, pp. 143-146.

[2] Vitharana UWA, Van Meirvenne M, Simpson D, Cockx L, De Baerdemaeker J 2006. Influence of the topography on the within-field soil variability in the loess region in Belgium. In *2nd Global Workshop on Digital Soil Mapping : book of abstracts*, Mendonça-Santos M. et al. (Eds), Brazil, 4th-7th of July 2006, Rio de Janeiro, p. 56.

C.4.5 Abstracts of conference or poster presentations (C3)

[1] Saey T, Simpson D, Vitharana UWA, Vermeersch H, Vermang J, Van Meirvenne M 2008. Reconstructing the paleotopography at the beginning of the Weichselian glacial stage using electromagnetic induction. Geophysical Research Abstracts 10, file: EGU2008-A-00121. *EGU General Assembly13*, 18th of April 2008, Vienna.

[2] Simpson D, Van Meirvenne M, Saey T, Vermeersch H, Bourgeois J, Lehouck A, Cockx L, Vitharana UWA 2008. Simultaneous detection of soil electrical and magnetic anomalies with multi-coil electromagnetic induction sensors. *Recent work in archaeological geophysics, Workshop International Society for Archaeological Prospection*, 16th of December 2008, London.

[3] Vitharana UWA, Van Meirvenne M, Amakor XNC, Saey T, Vermeersch H, Simpson D, Cockx L 2008. Use of proximal soil sensing to improve the thematic accuracy of a soil-polygon map. Geophysical Research Abstracts 10, file: EGU2008-A-09214. *EGU General Assembly 13*, 18th of April 2008, Vienna.

[4] Saey T, Simpson D, Vermeersch H, Vitharana UWA, Vermang J, Van Meirvenne M 2007. Reconstructing the paleotopography beneath the loess cover using high-resolution electromagnetic induction measurements. *Thematic Day 2007 of the Soil Science Society of Belgium: Soil resources in Belgium, current and future issues*, Brussels, p. 20.

[5] Simpson D, Lehouck A, Van Meirvenne M, Bourgeois J 2007. Suitability of a mobile electromagnetic induction sensor for archaeological prospection. *Near Surface 2007, the 13th European Meeting of Environmental and Engineering Geophysics of the Near Surface Geoscience Division of EAGE*, 3rd-5th of September 2007, Istanbul.

[6] Simpson D, Lehouck A, Van Meirvenne M, Bourgeois J 2007. Mobiele, niet-invasieve EMI-bodemsensor: een nieuw instrument voor archeologische prospectie. *Archeologisch Forum 2007*, 30th of April 2007, Mechelen.

[7] Vitharana UWA, Van Meirvenne M, Amakor XNC, Simpson D, Cockx L 2007. Evaluating two scales of polygon soil maps and an electrical conductivity survey in characterizing within-field soil textural variability. *Pedometrics 2007*, 27th-30th of August 2007. Tübingen, p.41.

[8] Vitharana UWA, Van Meirvenne M, Amakor XNC, Saey T, Simpson D 2007. Potency of proximal soil sensing to upgrade the soil map of Belgium: test case UGent experimental farm at Melle. *Thematic Day 2007 of the Soil Science Society of Belgium: Soil resources in Belgium, current and future issues*, 6th of December 2007, Brussels, p. 10.[71]

References

[1] English Heritage 2004. *Geoarchaeology-Using earth sciences to understand the archaeological record*. English Heritage Publishing, Swindon.

[2] Rapp G, Hill CL 2005. *Geoarchaeology-The earth science approach to archaeological interpretation*. Yale University Press, New Haven.

[3] English Heritage 2008. *Geophysical survey in archaeological field evaluation*. English Heritage Publishing, Swindon.

[4] Tabbagh A 1986. What is the best coil orientation in the Slingram electromagnetic prospecting method? *Archaeometry* 28**,** 185-196.

[5] Linford NT 1998. Geophysical survey at Boden Vean, Cornwall, including an assessment of the microgravity technique for the location of suspected archaeological void features. *Archaeometry* 40**,** 187-216.

[6] McNeill JD 1980. Electrical conductivity of soils and rocks. *Technical Note TN-5*, Geonics Limited, Mississauga.

[7] Samouëlian A, Cousin I, Tabbagh A, Bruand A, Richard G 2005. Electrical resistivity survey in soil science: a review. *Soil & Tillage Research* 83**,** 173-193.

[8] Telford WM, Geldart LP, Sheriff RE 1990. *Applied geophysics, 2nd edition*. Cambridge University Press, Cambridge.

[9] Brady NC, Weil RR 1999. *The nature and properties of soils, 12th edition*. Prentice Hall, New Jersey.

[10] Lück E, Rühlmann J, Spangenberg U 2005. Physical background of soil EC mapping: laboratory, theoretical and field studies. In: *Precision Agriculture '05*, Stafford JV (ed.). Wageningen Academic Publishers, Wageningen.

[11] Besson A, Cousin I, Dorigny A, Dabas M, King D 2008. The temperature correction for the electrical resistivity measurements in undisturbed soil samples: analysis of the existing conversion models and proposal of a new model. *Soil Science* 173**,** 707-720.

[12] Sheets KR, Hendrickx JMH 1995. Noninvasive soil-water content measurement using electromagnetic induction. *Water Resources Research* 31**,** 2401-2409.

[13] Domsch H, Giebel A 2004. Estimation of soil textural features from soil electrical conductivity recorded using the EM38. *Precision Agriculture* 5**,** 389-409.

[14] Hesse A 1990. Resistivity prospecting. In: *Archaeological prospecting and remote sensing*, Scollar I (ed.). Cambridge University Press, Cambridge. pp. 307-421.

[15] Scollar I 1990. Magnetic properties of soils. In: *Archaeological prospecting and remote sensing*, Scollar I (ed.). Cambridge University Press, Cambridge. pp. 375-421.

[16] Dearing JA 1999. Environmental magnetic susceptibility. *Using the Bartington MS2 system*, Bartington Instruments Limited, Oxford.

[17] Dearing JA, Hay KL, Baban SMJ, Huddleston AS, Wellington EMH, Loveland PJ 1996. Magnetic susceptibility of soil: an evaluation of conflicting theories using a national data set. *Geophysical Journal International* 127**,** 728-734.

[18] Hus JJ, Geeraerts R 1986. Palaeomagnetic and rock-magnetic investigation of late-Pleistocene loess deposits in Belgium. *Physics of the Earth and Planetary Interiors* 44**,** 21-40.

[19] Dalan RA 2006. A geophysical approach to buried site detection using down-hole susceptibility and soil magnetic techniques. *Archaeological Prospection* 13**,** 182-206.

[20] Linford NT, Canti MG 2001. Geophysical evidence for fires in antiquity: preliminary results from an experimental study. *Archaeological Prospection* 8**,** 211-225.

[21] Marmet E, Bina M, Fedoroff N, Tabbagh A 1999. Relationships between human activity and the magnetic properties of soils: a case study in the medieval site of Roissy-en-France. *Archaeological Prospection* 6**,** 161-170.

[22] Bevan BW 1994. The magnetic anomaly of a brick foundation. *Archaeological Prospection* 1**,** 93-104.

[23] Jordanova N, Petrovsky E, Kovacheva M, Jordanova D 2001. Factors determining magnetic enhancement of burnt clay from archaeological sites. *Journal of Archaeological Science* 28**,** 1137-1148.

[24] Scollar I, Tabbagh A, Hesse A, Herzog I 1990. *Archaeological Prospecting and remote sensing*. Cambridge University Press, Cambridge.

[25] Clark A 1990. *Seeing beneath the soil-prospecting methods in archaeology*. Routledge, Oxon.

[26] Gaffney C, Gater J 2003. *Revealing the buried past-Geophysics for archaeologists*. Tempus Publishing Ltd, Stroud.

[27] Conyers LB 2004. *Ground-penetrating radar for archaeology*. AltaMira Press, Lanham.

[28] Howell MI 1966. A soil conductivity meter. *Archaeometry* 9**,** 20-23.

[29] Tite MS, Mullins C 1970. Electromagnetic prospecting on archaeological sites using a soil conductivity meter. *Archaeometry* 12**,** 97-104.

[30] Tabbagh A 1984. On the comparison between magnetic and electromagnetic prospection methods for magnetic features detection. *Archaeometry* 26**,** 171-182.

[31] Tabbagh A 1985. The response of a 3-dimensional magnetic and conductive body in shallow depth electromagnetic prospecting. *Geophysical Journal of the Royal Astronomical Society* 81**,** 215-230.

[32] Tabbagh A 1986. Applications and advantages of the Slingram electromagnetic method for archaeological prospecting. *Geophysics* 51**,** 576-584.

[33] Tabbagh A, Bossuet G, Becker H 1988. A comparison between magnetic and electromagnetic prospection of a Neolithic ring ditch in Bavaria. *Archaeometry* 30**,** 132-144.

[34] McNeill JD 1980. Electromagnetic terrain conductivity at low induction numbers. *Technical Note TN-6*, Geonics Limited, Mississauga.

[35] Fröhlich B, Lancaster WJ 1986. Electromagnetic surveying in current Middle-Eastern archaeology - application and evaluation. *Geophysics* 51**,** 1414-1425.

[36] Dalan RA 1991. Defining archaeological features with electromagnetic surveys at the Cahokia Mounds state historic site. *Geophysics* 56**,** 1280-1287.

[37] Bevan BW 1991. The search for graves. *Geophysics* 56**,** 1310-1319.

[38] Desvignes G, Tabbagh A 1995. Simultaneous interpretation of magnetic and electromagnetic prospecting for characterization of magnetic features. *Archaeological Prospection* 2**,** 129-139.

[39] Kvamme KL 2003. Multidimensional prospecting in North American Great Plains village sites. *Archaeological Prospection* 10**,** 131-142.

[40] Linford NT 2006. The application of geophysical methods to archaeological prospection. *Reports on Progress in Physics* 69**,** 2205-2257.

[41] Rhoades JD, Corwin DL 1981. Determining soil electrical-conductivity depth relations using an inductive electromagnetic soil conductivity meter. *Soil Science Society of America Journal* 45**,** 255-260.

[42] Corwin DL, Rhoades JD 1982. An improved technique for determining soil electrical conductivity-depth relations from above-ground electromagnetic measurements. *Soil Science Society of America Journal* 46**,** 517-520.

[43] Sudduth KA, Drummond ST, Kitchen NR 2001. Accuracy issues in electromagnetic induction sensing of soil electrical conductivity for precision agriculture. *Computers and Electronics in Agriculture* 31**,** 239-264.

[44] Hill I, Grossey T, Leech C 2004. High-resolution multisensor geophysical surveys for near-surface applications can be rapid and cost-effective. *The Leading Edge* 23**,** 684-688.

[45] Rabbel W, Stuempel H, Woelz S 2004. Archaeological prospecting with magnetic and shear-wave surveys at the ancient city of Miletos (western Turkey). *The Leading Edge* 23**,** 690-703.

[46] Ohanian HC 1989. *Physics*. Norton, New York.

[47] Tabbagh A 1990. Electromagnetic prospecting. In: *Archaeological prospecting and remote sensing*, Scollar I (ed.). Cambridge University Press, Cambridge. pp. 520-590.

[48] Keller GV, Frischknecht FC 1966. *Electrical methods in geophysical prospecting*. Pergamon Press, Oxford.

[49] Frischknecht FC, Labson VF, Spies BR, Anderson WL 1987. Profiling methods using small sources. In: *Electromagnetic methods in applied geophysics 2, application, parts A and B*, Nabighian MN (ed.). Society of Exploration Geophysicists, Tulsa. pp. 105-270.

[50] Wait JR 1955. Mutual electromagnetic coupling of loops over a homogeneous ground. *Geophysics* 20**,** 630-637.

[51] Spies BR, Frischknecht FC 1987. Electromagnetic sounding. In: *Electromagnetic methods in applied geophysics 2, application, parts A and B*, Nabighian MN (ed.). Society of Exploration Geophysicists, Tulsa. pp. 285-426.

[52] Wait JR 1962. A note on the electromagnetic response of a stratified earth. *Geophysics* 27**,** 382-385.

[53] Callegary JB, Ferre TPA, Groom RW 2007. Vertical spatial sensitivity and exploration depth of low-induction-number electromagnetic-induction instruments. *Vadose Zone Journal* 6**,** 158-167.

[54] Geonics Limited 1999. Application of “dipole-dipole” electromagnetic systems for geological depth sounding. *Technical Note TN-31*, Geonics Limited, Mississauga.

[55] Dabas M, Jolivet A, Tabbagh A 1992. Magnetic susceptibility and viscosity of soils in a weak time-varying field. *Geophysical Journal International* 108**,** 101-109.

[56] McNeill JD 1996. Why doesn't Geonics Limited build a multi-frequency EM31 or EM38? *Technical Note TN-30*, Geonics Limited, Mississauga.

[57] Saey T, Simpson D, Vitharana UWA, Vermeersch H, Vermang J, Van Meirvenne M 2008. Reconstructing the paleotopography beneath the loess cover with the aid of an electromagnetic induction sensor. *Catena* 74**,** 58-64.

[58] Saey T, Simpson D, Vermeersch H, Cockx L, Van Meirvenne M 2009. Comparing the EM38DD and DUALEM-21S sensors for depth-to-clay mapping. *Soil Science Society of America Journal* 73**,** 7-12.

[59] Borchers B, Uram T, Hendrickx JMH 1997. Tikhonov regularization of electrical conductivity depth profiles in field soils. *Soil Science Society of America Journal* 61**,** 1004-1009.

[60] Farquharson CG, Oldenburg DW 2003. Simultaneous one-dimensional inversion of electromagnetic loop-loop data for both magnetic susceptibility and electrical conductivity. *Geophysics* 68**,** 1857-1869.

[61] Guérin R, Meheni Y, Rakotondrasoa G, Tabbagh A 1996. Interpretation of slingram conductivity mapping in near-surface geophysics: using a single parameter fitting with 1D model. *Geophysical Prospecting* 44**,** 233-249.

[62] Bowers RJ, Bidwell BA 1999. Geophysics and UXO detection. *The Leading Edge* 18**,** 1389-1391.

[63] McNeill JD, Bosnar M 2000. Application of TDEM techniques to metal detection and discrimination: a case history with the new Geonics EM-63 fully time-domain metal detector. *Technical Note TN-32*, Geonics Limited, Mississauga.

[64] Geonics Limited 1992. *EM38 operating manual*. Geonics Limited, Mississauga.

[65] Dabas M, Tabbagh A 2003. A comparison of EMI and DC methods used in soil mapping - theoretical considerations for precision agriculture. In: *Precision Agriculture '05*, Stafford JV (ed.). Wageningen Academic Publishers, Wageningen.

[66] Holladay JS, Lee JLC 2003. Modular electromagnetic sensing apparatus having improved calibration. *U.S. patent 6534985 B2*, 18 March 2003.

[67] Dualem Inc. 2007. *DUALEM-21S user's manual*. Dualem Inc., Milton.

[68] Robinson DA, Lebron I, Lesch SM, Shouse P 2004. Minimizing drift in electrical conductivity measurements in high temperature environments using the EM-38. *Soil Science Society of America Journal* 68**,** 339-345.

[69] Dalan RA 2008. A review of the role of magnetic susceptibility in archaeogeophysical studies in the USA: recent developments and prospects. *Archaeological Prospection* 15**,** 1-31.

[70] Goovaerts P 1997. *Geostatistics for natural resources evaluation*. Oxford University Press, New York.

[71] Atkinson PM, Lloyd CD 2007. Non-stationary variogram models for geostatistical sampling optimisation: An empirical investigation using elevation data. *Computers & Geosciences* 33**,** 1285-1300.

[72] Haas TC 1990. Kriging and automated variogram modeling within a moving window. *Atmospheric Environment Part A-General Topics* 24**,** 1759-1769.

[73] Walter C, McBratney AB, Douaoui A, Minasny B 2001. Spatial prediction of topsoil salinity in the Chelif Valley, Algeria, using local ordinary kriging with local variograms versus whole-area variogram. *Australian Journal of Soil Research* 39**,** 259-272.

[74] Dalan RA, Bevan BW 2002. Geophysical indicators of culturally emplaced soils and sediments. *Geoarchaeology - an International Journal* 17**,** 779-810.

[75] Hendrickx JMH, Borchers B, Corwin DL, Lesch LM, Hilgendorf AC, Schlue J 2002. Inversion of soil conductivity profiles from electromagnetic induction measurements: theory and experimental verification. *Soil Science Society of America Journal* 66**,** 673-685.

[76] Benech C, Marmet E 1999. Optimum depth of investigation and conductivity response rejection of the different electromagnetic devices measuring apparent magnetic susceptibility. *Archaeological Prospection* 6**,** 31-45.

[77] Lück E, Callmer J, Skanberg T 2003. The house of Baillif of Sövestad, Sweden - a multi-method geophysical case-study. *Archaeological Prospection* 10**,** 143-151.

[78] Maillol JM, Ciobotaru DL, Moravetz I 2004. Electrical and magnetic response of archaeological features at the early Neolithic site of Movila lui Deciov, Western Romania. *Archaeological Prospection* 11**,** 213-226.

[79] Vafidis A, Economou N, Ganiatsos Y, Manakou M, Poulioudis G, Sourlas G, Vrontaki E, Sarris A, Guy M, Kalpaxis T 2005. Integrated geophysical studies at ancient Itanos (Greece). *Journal of Archaeological Science* 32**,** 1023-1036.

[80] Fowler WR, Estrada-Belli F, Bales JR, Reynolds MD, Kvamme K 2007. Landscape archaeology and remote sensing of a Spanish-conquest town: Ciudad Vieja, El Salvador. In: *Remote sensing in archaeology*, Wiseman J, El-Baz F (eds). Springer Science, New York. pp. 395-421.

[81] T'Jonck G, Moormann FR 1962. Verklarende tekst bij het kaartblad 50E. *Bodemkaart van België*, IWONL, Gent.

[82] Lehouck A, Simpson D, Vermeersch H, Van Meirvenne M 2007. *Geoarcheologisch onderzoek naar (post)middeleeuwse nederzettingstructuren in de ruilverkaveling Sint-Rijkers. Locatie Vinkem: Kasteel 'de Moucheron'*. Archaeological Reports Ghent University, Gent.

[83] Lambrecht T 2002. *Een grote hoeve in een klein dorp: relaties van arbeid en pacht op het Vlaamse platteland tijdens de 18de eeuw*. Belgisch Centrum voor Landelijke Geschiedenis, Gent.

[84] Jordanova N 2001. Factors determining magnetic enhancement of burnt clay from archaeological sites. *Journal of Archaeological Science* 28**,** 1137-1148.

[85] Reynolds JM 1997. *An introduction to applied and environmental geophysics*. John Wiley & Sons, Chichester.

[86] Tassis GA, Hansen RO, Tsokas GN, Papazachos CB, Tsourlos PT 2008. Two-dimensional inverse filtering for the rectification of the magnetic gradiometry signal. *Near Surface Geophysics* 6**,** 113-122.

[87] Benech C, Tabbagh A, Desvignes G 2002. Joint inversion of EM and magnetic data for near-surface feature studies. *Geophysics* 67**,** 1729-1739.

[88] Bates MR, Bates CR 2000. Multidisciplinary approaches to the geoarchaeological evaluation of deeply stratified sedimentary sequences: examples from Pleistocene and Holocene deposits in southern England, United Kingdom. *Journal of Archaeological Science* 27**,** 845-858.

[89] Mikkelsen JH, Langohr R, Macphail RI 2007. Soilscape and land-use evolution related to drift sand movements since the bronze age in Eastern Jutland, Denmark. *Geoarchaeology-an International Journal* 22**,** 155-179.

[90] Tolksdorf JF, Kaiser K, Veil S, Klasen N, Bruckner H 2009. The Early Mesolithic Haverbeck site, Northwest Germany: evidence for Preboreal settlement in the Western and Central European Plain. *Journal of Archaeological Science* 36**,** 1466-1476.

[91] Cherretté B, Bourgeois J 2005. Circles for the dead. From aerial photography to excavation of a Bronze Age cemetery in Oedelem (West-Flanders, Belgium). In: *Aerial photography and archaeology 2003. A century of information*, Bourgeois J, Meganck M (eds). Archaeological Reports Ghent University, Gent.

[92] Thiesson J, Dabas M, Flageul S 2009. Detection of resistive features using towed Slingram electromagnetic induction instruments. *Archaeological Prospection* 16**,** 103-109.

[93] Panissod C, Dabas M, Jolivet A, Tabbagh A 1997. A novel mobile multipole system (MUCEP) for shallow (0-3m) geoelectrical investigation: the 'Vol-de-canards' array. *Geophysical Prospecting* 45**,** 983-1002.

[94] Lück E, Rühlmann J 2008. Electrical conductivity mapping with geophilus electricus. In: *Near Surface 2008, the 14th European Meeting of Environmental and Engineering Geophysics*. European Association of Geoscientists & Engineers, Kraków.

[95] Simpson D, Van Meirvenne M, Saey T, Vermeersch H, Bourgeois J, Lehouck A, Cockx L, Vitharana UWA 2009. Evaluating the multiple coil configurations of the EM38DD and DUALEM-21S sensors to detect archaeological anomalies. *Archaeological Prospection* 16**,** 91-102.

[96] Panissod C, Dabas M, Hesse A, Jolivet A, Tabbagh J, Tabbagh A 1998. Recent developments in shallow-depth electrical and electrostatic prospecting using mobile arrays. *Geophysics* 63**,** 1542-1550.

[97] Roy A, Apparao A 1971. Depth of investigation in direct current methods. *Geophysics* 36**,** 943-959.

[98] Germis A 1986. Geomorfologische studie van het bekken van de Molenbeek (Melle). *Master Thesis*, Geological Institute, Ghent University, Gent.

[99] Kvamme KL 2006. Integrating multidimensional geophysical data. *Archaeological Prospection* 13**,** 57-72.

[100] Fröhlich B, Gugler AIM, Gex P 1996. Electromagnetic survey of a Celtic tumulus. *Journal of Applied Geophysics* 35**,** 15-25.

[101] Conyers LB, Ernenwein EG, Grealy M, Lowe KM 2008. Electromagnetic conductivity mapping for site prediction in meandering river floodplains. *Archaeological Prospection* 15**,** 81-91.

[102] Cockx L, Ghysels G, Van Meirvenne M, Heyse I 2006. Prospecting frost-wedge pseudomorphs and their polygonal network using the electromagnetic induction sensor EM38DD. *Permafrost and Periglacial Processes* 17**,** 163-168.

[103] Simpson D, Lehouck A, Van Meirvenne M, Bourgeois J, Thoen E, Vervloet J 2008. Geoarchaeological prospection of a Medieval manor in the Dutch polders using an electromagnetic induction sensor in combination with soil augerings. *Geoarchaeology-an International Journal* 23**,** 305-319.

[104] Gee GW, Bauder JW 1986. Particle-size analysis. In: *Methods of soil analysis. Part 1: Physical and mineralogical methods*, Klute A (ed.). Soil Science Society of America, Madison. pp. 383-411.

[105] Roskams S 2001. *Excavation*. Cambridge University Press, Cambridge.

[106] Vos PC, van Heeringen RM 1997. Holocene geology and occupation history of the province of Zeeland. In: *TNO 59: Holocene evolution of Zeeland (SW Netherlands)*, Fischer MM (ed.). Nederlands Instituut voor Toegepaste Geowetenschappen TNO, Haarlem.

[107] De Mulder EJ, Geluk MC, Ritsema I, Westerhoff WE, Wong TE 2003. *De ondergrond van Nederland*. Nederlands Instituut voor Toegepaste Geowetenschappen TNO, Utrecht.

[108] Ovaa I 1957. De bodemgesteldheid van westelijk Zeeuws-Vlaanderen. *Stiboka Rapport 455*, University of Wageningen, Wageningen.

[109] Van der Sluys P, Ovaa I 1967. Toelichting bij de kaartbladen 53 Sluis en 54 West Terneuzen. *Bodemkaart van Nederland, schaal 1:50 000*, University of Wageningen, Wageningen.

[110] Brus DJ 1987. Toelichting op het kaartblad Zeeuws-Vlaanderen. *Geomorfologische kaart van Nederland, 1:50 000*, University of Wageningen-Rijks Geologische Dienst, Haarlem.

[111] Vanslembrouck N, Lehouck A, Thoen E 2005. Past landscapes and present-day techniques: reconstructing submerged medieval landscapes in the western part of Sealand Flanders. *Landscape History* 27**,** 51-64.

[112] Gottschalk MKE 1955. *Historische geografie van Westelijk Zeeuws Vlaanderen-Deel 1: Tot de St-Elisabethsvloed van 1404*. Van Gorcum, Assen.

[113] de Bakker H, Schelling J 1989. *Systeem van bodemclassificatie voor Nederland*. University of Wageningen, Wageningen.

[114] ten Cate JAM, Van Holst AF, Kleijer H, Stolp J 1995. *Handleiding bodemgeografisch onderzoek. Richtlijnen en voorschriften. Deel A: Bodem. Technisch Document 19A*. University of Wageningen, Wageningen.

[115] Groom R, Alvarez C 2002. 3D EM modelling-application of the localized non-linear approximator to near surface applications. In: *Proceedings of the Symposium on the Application of Geophysics to Environmental and Engineering Problems (SAGEEP)*, Las Vegas.

[116] Loke MH 2004. Tutorial: 2-D and 3-D electrical imaging surveys. www.geoelectrical.com.

[117] Loke MH, Barker RD 1996. Rapid least-squares inversion of apparent resistivity pseudosections by a quasi-Newton method. *Geophysical Prospecting* 44**,** 131-152.

[118] deGroot-Hedlin C, Constable S 1990. Occam's inversion to generate smooth, two-dimensional models from magnetotelluric data. *Geophysics* 55**,** 1613-1624.